Carnegie Mellon University

CARNEGIE INSTITUTE OF TECHNOLOGY

THESIS

SUBMITTED IN PARTIAL FULFILLMENT OF THE REQUIREMENTS

FOR THE DEGREE OF Doctor of Philosophy

TITLE Probing Collective Migration Of A 3-D Embryonic Tissue Through Microfluidics With 3-D Bio-Etching

PRESENTED BY Melis Hazar

ACCEPTED BY THE DEPARTMENT OF

Mechanical Engineering

_____ _____

ADVISOR, MAJOR PROFESSOR DATE

_____ _____

DEPARTMENT HEAD DATE

APPROVED BY THE COLLEGE COUNCIL

_____ _____

DEAN DATE

Probing Collective Migration of a 3-D Embryonic Tissue through Microfluidics with 3-D Bio-etching

Submitted in partial fulfillment of the requirements for

the degree of

Doctor of Philosophy

in

Department of Mechanical Engineering

Melis Hazar

B.S., Mechanical Engineering, Gazi University Ankara, TURKEY

Carnegie Mellon University
Pittsburgh, PA

January, 2015

Keywords: Cell Mechanics, Microfluidics, *Xenopus laevis,* Developmental Biology, Laminar Flow, Multicellular migration, Mesenchymal layer, Epithelial Layer, Tissue Etching, 3D microfluidic

To my mother who encouraged me for to dream bigger

To my father who generated my love for science

To my brother whom I love unconditionally

Acknowledgements

This work would not have been possible without the help and support of many individuals.

First, I would like to thank my advisors Philip R. LeDuc, Lance A. Davidson, William C. Messner for guidance, support, motivation, enthusiasm, ideas, and for the opportunity to work in an exciting multi-disciplinary lab on a variety of interesting projects. Their positive attidutes, approach to problem solving, and focus on the "big picture" have all been inspirations throughout my time at Carnegie Mellon University. I could not have imagined having better advisors and mentors for my Ph.D study. They have all set examples of excellence as researchers, mentors, instructors, and role models for me. I am not sure if many graduate students are given the opportunity to develop their own individuality and self-sufficiency by being allowed to work with such independence but they encourage me to grow as an independent thinker. I never wanted to miss my individual meetings with Phil since that where I obtained my inspiration and encouragement for the week. I would not have made it without his extensive knowledge, his laugh, positive energy and support. Lance is one and only person I know who knows everything, and I mean everything. Lance taught me how to be a scientist, how to think like a scientist and how to ask questions like a scientist. He was always there to teach me anytime and wasn't afraid to get his hands dirty in the process. And I want to thank Bill for not abandoning me after his move to Tufts. My PhD would not have been the same without his brilliant ideas and his support.

I also want to thank my committee member Shawn Litster for being a part of my committee, for his valuable comments and suggestions.

During my graduate program, I have had the good fortune of working closely with many truly gifted and dedicated individuals: From Dr. LeDuc's lab, Dr. Messner's lab, and Dr. Davidson's lab: Dr. YongTae Kim, Dr. Holley E. Lynch, Kyle B. Justus, Dr. Lina Gonzalez, Dr, Jiho Song, Dr. Robert Steward, Deepthi Vijayraghavan, Joseph Shawky, Natee Johnson,

Dr. Yukai Zeng, Dr. Mary Beth Wilson, Dr. Carsten Stuckenholz, Dr. Callie Johnson Miller, Dr. Warren Ruder, Kristin Warren, Dr. HyeYoung Kim, Dr. John Kang.

I want to Thank Chris Hertz, Michael Scampone and Virginia Barry for their assistance in administrative issues and Ed Wojciechowski for practical guideness.

I was also fortunate to have had the support and friendship of many people outside the lab over the years. First I want to thank Dan Fiore's valuable time to edit my thesis. Thanks especially to Bilge Yumer, Ersin Yumer, Tugce Yuksel, Bekir Bediz, Arda Gozen. But most importantly to Cagla who is beyond a friend and who always tries to show me the half full side of the glass even when it is half empty. And lastly to Kevin who has kept me sane.

This research was supported in part by the financial support of the National Science Foundation and National Institutes of Health.

Abstract

Most embryonic development and tissue self-assembly requires the integration of cell movements within multiple cell layers composed of different cell types, which are integrated with the signaling networks in these 3D environments. Although the role of cell mechanics in tissue self-assembly has been demonstrated, little is known about the mechanical responses of 3D multi-layer tissues to chemical cues. To investigate the collective movements within multilayered tissues, I developed a novel microfluidic technique capable of removing desired height or width of tissue from a composite tissue. I call this technique "3D tissue-etching" because it is analogous to techniques used in the microelectromechanics (MEMS) field where complex 3D structures are built by successively removing material from a monolithic solid through subtractive manufacturing. I used a custom-designed microfluidic control system to deliver a range of tissue etching reagents (detergents, chelators, proteases, etc.) to specific regions of multilayered tissues microsurgically isolated from embryos of the African Clawtoed frog, *Xenopus laevis*. *Xenopus* embryos and explanted tissues have long been used to elucidate signaling and other cellular processes during development and here provide an ideal model 3D tissue etching. Long exposure to a narrow etchant stream cuts completely through cell-cell layers to expose the substrate. By reducing the exposure time a single layer may be removed. By controlling the width of the etchant and the exposure time a broader swath of the surface layer may be removed. For more refined etching, after removal of a broad swath the resistance circuits can be switched and a second narrow stream can remove only a single narrow band within the swath exposed cells. I developed tissue-etching techniques that allow me to shape complex multi-layered embryonic tissues. The ability to control 3D stimulation and the form of multicellular tissues will provide extend the tools of tissue engineering to synthesize highly complex 3D integrated multicellular biosystems. Integration of tissue etching in my custom microfluidic system provides a "test-bed" where a range of

hypotheses concerning the control and regulation of development and cell differentiation can be implemented and tested.

Contents

List of Figures

Chapter 1

Introduction

All animals develop from a fertilized egg with very dynamic and complex spatiotemporal events. During the development process, this single-celled fertilized egg continuously divides and differentiates into different types of cells in an organized and precise manner [17]. For example, during development, chemical patterning of cell identity and guided cell movements are essential for vertebrate development. These features are critical to forming and elongating the prospective dorsal axial tissues including muscle and the central nervous system [18]. Without this integrated response, vertebrates cannot develop. Specific external signals such as chemical and mechanical stimulation guide movement of cells to specific locations and direct their differentiation. For instance, cells can migrate toward a source of a chemical using "chemotaxis". Chemotaxis guides cells of the blood and lymphoid system during late morphogenetic processes that shape the cardiovascular system [19, 20], thus the lack of this coordinated biological control would cause the vertebrate to lack a functioning heart. To understand these complex processes researchers employ early stages of developing embryos of several model organisms such as *Xenopus laevis* [21], *Drosophila melanogaster* [22], *Danio rerio* [23]. These model organisms allow one to learn about role of chemical and mechanical processes in development without having to experiment on human embryos.

Embryonic development involves complex series of cell signaling, cell migration and cell

differentiation processes that are coordinated spatiotemporally throughout morphogenesis. The word morphogenesis itself is Greek and the literal translation is "beginning of the shape". Morphogenesis is one of the fundamental processes in the embryo that gives the final shape of an organism. This process involves specification of cells, tissues, and organs, control collective or individual cell migration and organization of spatial distribution of various cell types to form the structure of various part of the body. [19]. Hence, processes that guide embryonic development are crucial to an organism's fate. Starting from fertilization until the whole organism is shaped, every morphogen and response needs to take place very precisely in order for the organism to eventually reach programmed shape. The fate of a tissue and its ultimate physiological function relies on integrating genetic programs and processing external cues to provide positional information to guide cell migration and induce cell differentiation [24]. Coordination of this complex mechanism is achieved through spatiotemporal cues in the microenvironment such as localized presentation of growth factors and gradients of substrate stiffness [25]. Starting at the very early stage of the embryo, cells and tissues receive spatiotemporal stimulation from chemical growth factors and respond to these factors by triggering changes in gene expression as well as changes in the cytoskeleton depending on morphogen concentration in the microenvironment [26]. These responses result in observable phenotypes such as the production of cell protrusions, altered cell shape or changes to motility. Over the decades, many molecule pathways have been identified that initiate, maintain and guide moving cells during embryonic development but now the question is the underlying mechanisms by which cell monolayers respond to growth factors, sense directional signals, induce motility, and coordinate individual cell movements in such a precise, timely manner [27].

Coordinated collective migration is central to embryonic morphogenesis, wound repair, cancer invasion and homeostasis. In such migration, individual cells do not move on their own, instead they are physically and molecularly connected and and move as clusters or sheets. They remodel their ECM and migration tracks guided by chemical and physical

signals [?]. Cells preserve cell-cell cohesion while tissues rearrange. They can carry immobile cells via mobile ones. Also, cells coordinate cytoskeletal dynamics to function as a single unit and jointly generate force. This collectiveness influences every cell to ensure the effective movement and robust decisions [28]. Although studies describe cell adhesion, cell structure and cellular mechanisms, how they affect cellular architecture during collective migration remains unknown.

There are several models to study collective cell migration *in vitro*. The most common way to study collective cell migration is 2D scratch wound assays [29]. Experimental models of these movements have focused on the collective behaviors of coherent epithelial monolayers of cultured cells such as Madin-Darby canine kidney (MDCK) cells [30, 31]. Although traditional 2D cell cultures on flat surfaces are not very representative of the native 3D environments that cells experience, these models allows us to define major principles of single layer epithelial sheet migration that are revealed in parameters such as speed of wound closure, cohesiveness of the cell-cell junctions and individual or collective cell polarization, and migration can be assessed. By contrast, embryonic development and tissue-self-assembly require the integration of cell movements within multiple cell layers composed of different cell types.

Considering the important role cell mechanics plays in tissue self-assembly it is surprising that little is known about the mechanical response of the multi-layer tissues to chemical cues. One of the reasons for this knowledge gap is the lack of the technologies allowing us to both stimulate and analyze the individual responses of cells within multi cell layer tissues. New tools are needed to investigate collective movements of multi-layered tissues. The lack of techniques to provide inputs and measure biological responses with sufficient temporal and spatial resolution has hampered the advancement of quantitative approaches to understanding development and tissue engineering. The objective of this thesis is to propose development of new 3D tools that will allows us to study cellular and molecular mechanisms of collective cell movements in multilayer tissues.

Studies have shown that cells cultured in 2D or 3D *in vitro* environments have differences in terms of their cell shape, cell-matrix adhesions and migratory behavior and much more compared to *in vivo* environments. *In vivo* studies using vertebrate or invertebrate organisms engage *in vitro* information on migration mechanism to embryonic development [**?**].

Embryonic tissues isolated from developing embryos provide an excellent model system to study coordinated collective migration in a controlled environment. The embryo of *Xenopus laevis* is particularly well suited for these studies because it can be integrated with microscopic methods as well as gene and protein expression analysis for long term studies of organism development. African Claw-toed frog, *Xenopus laevis*, embryos have been used as a model system since the 1930s because of its advantages over other model organisms [32].Therefore, its development is very well characterized (Figure 1.1). *Xenopus laevis* has relatively large eggs, 1-1.4 mm in diameter, which is advantageous for classical microsurgical manipulations, modern molecular-genetic techniques, and imaging. This makes *Xenopus laevis* easier to work with than other vertebrate embryos. A single female frog can lay hundreds of eggs at a time with hormone-stimulated mating. Embryos develop external to the mother and can be regulated with temperature allowing researchers control over their environment. Furthermore, every embryo has their own yolk part which helps them to survive in simple salt solutions for several days. The ability to perform microsurgery to cut explants from *Xenopus* embryos makes this organism ideal for local stimulations. Another advantage of using *Xenopus* is that development is rapid compared to mammalian developmental models such as that of a mouse or rat. For instance, pre-cardiac *Xenopus* cells migrate to the correct position about a day after fertilization and a beating heart forms in the third day [**?**]. Also, frogs are vertebrates like humans and use many of the same genes during development [33]. These are a few reasons why *Xenopus* is a popular model system and these features of *Xenopus* embryos make them highly suitable for microfluidic studies.

Embryonic tissues develop using set of highly regulated signaling systems that organizes all the information from internal and external cues such as chemical gradients, growth factors,

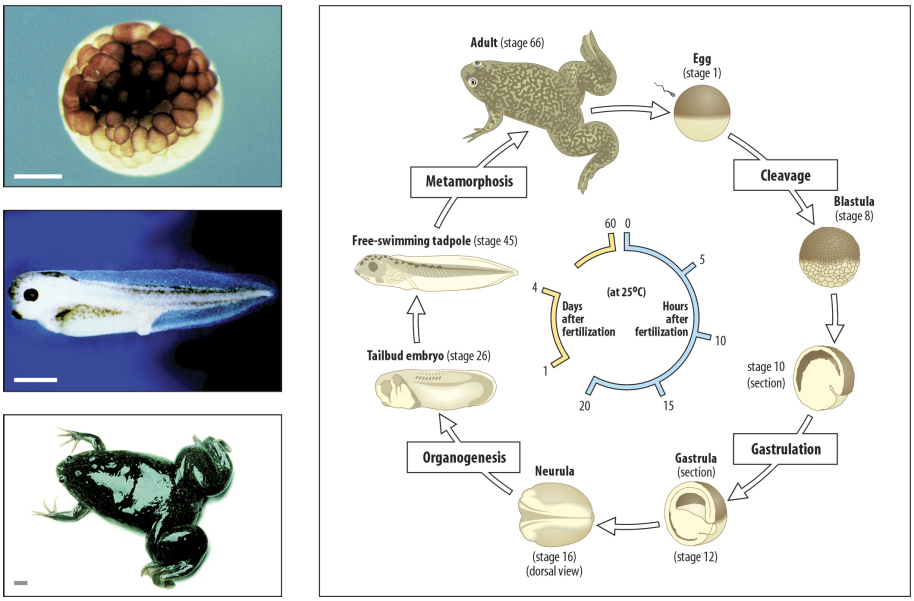

Figure 1.1: *Xenopus laevis* life cycle [1].

morphogens etc. Since external and internal chemical signals drive cells to specific locations, and manage cell differentiation into specific tissues, these chemicals play a fundamental role in the process of shaping the finalized animal or human [34]. It is assumed that congenital birth defects occur due to dysregulation of these chemical gradients or failure of the morphogenetic programs they are thought to regulate in early stages of embryonic development. Congenital birth defects such as neural tube and chronic heart defects are present in nearly one in 130 live births such defects and are principle causes of infant mortality in the first year of life [35,36]. Such defects cause immense personal suffering, and have a high cost to society [37]. A major aim of modern developmental biology is to understand the root causes of these defects and provide tools for genetic counseling. Systematic efforts are underway to identify mutations in mice that parallel human congenital birth defects [38].

While progress has been made toward understanding the role of cell mechanics in tissue self-assembly and the patterns that transduce chemical signals to cellular responses, little is known about the mechanical responses to chemical cues of the multi-layer tissues in coordinated cell rearrangements. However, being able to both discover the principles that guide self-assembly during embryonic development and apply those principles to direct or engineer

tissue by providing cues that guide cell fate decisions might lead to high-impact application in bioengineering and medical science especially within the fields of synthetic morphogenesis and organ regeneration. Characterizing the mechanical role of the cytoskeleton in controlling tissue mechanics and morphogenesis will provide valuable insights into biomechanical lesions that may be responsible for congenital birth defects and aid the identification of new factors that contribute to birth defects. Because of this potential, a variety of approaches have been made to simplify the complex, overlapping chemical stimuli functions operating within developing multicellular tissues to better understand the mechanisms driving cellular movements within multicellular sheets.To understand underlying mechanism of coordinated cell arrangements in response to chemical gradients, we need to control chemical microenvironment of a multicellular tissue. Although controlling these gradients may be the key to understanding and preventing birth defects, such control is difficult within multilayer tissue microenvironment of the embryo.

The effects of chemical control at an early stage significantly influences development of organs and other physiologically important tissues at later stages. Many different strategies have been used to deliver chemicals to cells in order to study the effects of chemical environment on embryonic development [39]. Externally provided soluble growth factors can manipulate cell differentiation programs during development. Methods of delivering these factors or modulating their activity include growth-factor-soaked heparin or agarose beads, gradient-leveling or saturating concentrations of growth factors, selective over-expression of genes encoding growth factors, activated receptors, or knock-out receptors in patches of cells [40, 41]. However, a major drawback of these approaches for investigating dynamics is that chemical activity is poorly regulated. Since spatiotemporal control is pivotal in studying and understanding embryonic development, microfluidics has become a preferred method for controlling microenvironment for local stimulation studies [**?**]. With microfluidic science, devices that are able to manipulate small volumes of fluids can be designed and manufactured. Laminar flow enables high throughput biological experiments from sub-cellular to

multi-cellular level with such precision and localization [**?**]. Laminar flow allows multiple different fluids to flow without mixing (except by diffusion), even though they are streamed parallel and adjacent to one another [42].This sharp concentration gradient offers differential treatments across the laminar flow interface [43]. Contrary to traditional methods, chemical gradients can be delivered very precisely while being spatiotemporally controlled even in very early embryonic stages with microfluidics. Thus, a number of technologies exist for spatiotemporal stimulation of biological systems including patch clamping, micropipetting, and laser microsurgery [44–48] and are useful for examining local domains. However these approaches cannot provide high bandwidth spatiotemporal control over chemical environments needed to work out the details of complex biochemical signaling pathways and the biophysical properties of multicellular tissues. In this study, I use microfluidics as a tool to locally and precisely control tissue environment as well as tissue architecture in order to study coordinated cell arrangements and migration.

The overarching objective of this thesis is to highlight development of a new 3D microfluidic methodology to enable studies of the principles of self-assembly during embryonic development and then to apply those principles to direct or engineer tissue assembly. This approach enables spatiotemporal regulation of chemical environments in and around tissue explants of *Xenopus laevis* embryos so I provide cues to guide cell fate decisions and investigate the processes that guide collective movements of multiple cell layers in response to these cues. I investigated the individual responses of individual cell sheets (epithelial and mesenchymal layer) to mechanical cues in a multi cell layer tissue. Developing a novel 3D microfluidic technique capable of producing complex patterns of laminar multicellular structures allows us to study the multi-layer coordination of epithelial and mesenchymal cell layers as well as the acute mechanical and behavioral response of these layers to removal of neighboring or overlying tissues.The intellectual merit of this thesis is the focus on developing a unique tool-kit for manipulating multicellular embryonic tissues, including embryoid bodies and progenitor cell aggregates, and direct their self-assembly into predictable struc-

tures. I aim to fill the technological gap in studying multi-layer collective migration with "3D tissue-etching" so one can analyze the dynamic collective responses of epithelial and mesenchymal cells in a single tissue with a microfluidic platform. I call this technique "3D tissue-etching" in analogy with the techniques used in the MEMS field. With this technique, I will have the opportunity to investigate the role of mesenchymal layer underneath the epithelial layer while also studying epithelial layer dynamic responses and collective multi-layer rearrangement in response to reorganization of tissue architecture on top of mesenchymal layers. This thesis provides a unique advance in the field microfluidics to probe the role of individual layers in 3D environments rather than 2D flat experiments. 3D tissue etching offers a unique way to study mechanical response and analyze collective cell sheet migration.

Spatial and temporal control over the chemical microenvironment at an early stage significantly influences development of organs and other physiologically important tissues at later stages. Fluidic devices have been implemented to manipulate cell attachment as well as deliver chemical reagents to specific cell populations [48–51]. Established microfluidic techniques are ideally suited to create and maintain stable chemical gradients in the environment of cells. These approaches become much more complicated when scaling up to larger scale studies such as at the tissue level. The ability to stimulate single cells and tissues with microfluidics has been mainly confined to 2D stimulation approaches, state-of-the-art is reviewed here [52]. Several standard approaches are currently used to study the effects of chemical environment on embryonic development. To analyze the mechanochemical response of multilayer tissue, I developed a 3D microfluidic system to control the local chemical microenvironment for imposing mechanical stimulation. However, a major drawback of these conventional approaches for investigating dynamics is that chemical activity is poorly regulated. My goal is to understand integrated mechanochemical responses of complex 3D tissues through novel 3D microfluidic approaches. I tested the hypothesis that complex tissues, composed of multiple cell types including both epithelial and mesenchymal cells, are mechanically coupled and that by locally inhibiting the mechanics of specific layers I am

able to control the collective migration of the integrated tissue. I developed "subtractive manufacturing" tools in contrast to the "additive manufacturing" by manipulation of complex tissues composed of multiple cell types including both epithelial and mesenchymal cells. I developed new 3D microfluidics tools to manipulate streams in complex patterns in the main chamber, but also to independently manipulate streams beneath the tissue nearer to the mesenchymal cell adhesion complexes. This study uses laminar flow through a three-dimensional channel formed by two microfluidic channel fabricated in layers that contact one another face-to-face at a 90° angle. I use 3D streams and complex 3D tissues to generate complex chemical and architectural microenvironments with the goal of controlling the tissue mechanics, cell motility, and wound healing. The ability to control 3D stimulation and the form of multicellular tissues will have high impact on tissue engineering and regeneration applications in bioengineering and medicine. It will also provide significant improvements in the synthesis of highly complex 3D integrated multicellular biosystems. Furthermore, my custom microfluidic system can be configured to test a range of hypotheses concerning the control and regulation of development and cell differentiation with additional applications in tissue engineering.

There are several ways to drive flow with pressure in microfluidics without miniaturization: commercially available syringe pumps and gravity-driven flow with differences in hydrostatic pressure. Conventional syringe pumps employing flow control regulate limit long-term use due to a small volume of syringes. In addition, a flow rate maintained by pressure differences using simple gravitational forces cannot be maintained for a long time since it changes as liquid volume decreases in the reservoirs. Pressure control is far better for controlling the flow rate into a microfluidic network [53], because the flow rate is proportional to the inlet pressure and pressure at the inlet is easily measured for high bandwidth feedback control. Prior work from our group developed an approach that enabled fine spatial precision and long term control of a flow rate in microfluidics [54]. This approach is based on the rate of volumetric flow of a fluid through a rigid microfluidic channel of uniform cross-section

being proportional to the pressure drop across the channel, and inversely proportional to the fluid resistance of the channel, itself dependent on the channel's cross-sectional area and length [48]. Since the total flow rate through the outlet channel is proportional to the sum of inlet pressures, changes in one pressure at one inlet require corresponding changes in forcing pressures at other inlets if a constant flow rate is required. Constant flow rate is desirable because the flow rate determines shear stress experienced by cells or tissues on the channel surfaces. Shear stress is even more important with multilayer tissues as the layers adhere to each other less strongly than the bottom layer adheres to the microfluidic channel. In addition, I now know that control of the shape of the cross section profile of the central stream requires control of the pressure at multiple inlets.

In this thesis, chapter 2 introduces the methodologies that have been used in this thesis. It includes an in-depth understanding of microfluidics and its application to biological studies as well as the advantages of using laminar flow velocity profiles and interface models as a tool to examine biological questions. Also, handling embryos and dissecting embryonic tissue from embryos are discussed. Chapter 3 is devoted to the 3D bioetching technique. Using three-inlet channel, I etched desired stripes of both layers to study their collective "healing" response to bio-etching. This system provides for us a 3D tissue environment to study each layers' response to etching and their collective response result in reorganized collective migration. Chapter 4 includes collective cell migration studies using 3D bioetching technique. Finally, in chapter 5, I conclude my thesis and touch on some possible future work of using 3D microfluidics to study embryonic bridges for a deeper understanding of tissue integrity in collective cell movements.

Chapter 2

Methodology

2.1 Microfludics

Microfluidic science is the process of designing and manufacturing systems that manipulate fluids with the use of channels at microliter and smaller volumes. Although laws of physics stay the same when scaling down, viscous forces dominate inertial forces within microfluidic channels so that the flow is laminar. In this regime, two fluids can flow adjacent to one another without convective mixing [42]. If the channels are small enough, a planar interface that forms between two adjacent solutions becomes the location of a sharp concentration gradient. Advantages of laminar flow are not only limited to the ability to use smaller volumes of chemicals and polydisperse chemical streams adjacent to each other without mixing except diffusion but also provides separations and point-of-care or in-the-field detection with high resolution and sensitivity at very low cost. Microfluidics have been used in many areas including chemical syntheses [55, 56], optofluidics [57, 58], fuel cell [59, 60], cell patterning [61], molecular interaction and diffusion analysis [62], embryo transporting [63], neutrophil chemotaxis through chemical gradient generation [64], embryonic development under localized temperature gradients [65], cell migration [12].

The interest in microfluidics for cellular studies has evolved because of the practical use of laminar flow interfaces. Laminar flow formation provides the ability to both control the cellular environment and maintain sharp interfaces to have polydispersive flow to address the specisfic cells or subcellular level locally. The co-flowing streams can then be used to differentially treat two adjacent regions of space inside the channel. By simply manipulating the fluids in micro-channels and using the advantage of laminar flow, microfluidics enable high-throughput biological experiments that offer new capabilities in controlling concentrations of molecules in space and time [66]. Microfluidics enable the local control of tissue to the subcellular scale in a dynamic and automatic manner so we can best study cell behavior [67]. Combining microfluidic techniques with dynamic and automated control with complex microfabrication enables a more precise regulation of experiments to reveal the complex chemical and mechanical signalling pathways within the cell to unwind the control mechanism within the entire organism. Thus, this technique has been used to concurrently treat distinct regions of cells, clusters of cells or embryos with multiple fluid environments that differ in temperature or chemical composition [67–70].

Composition of chemical and mechanical parameters together form the microenvironment of a cell. Chemical parameters include all molecules in the media around the cell and the mechanical environment is composed of the response to the topology and stiffness of substrate as well as deformations exerted by the adjacent cells and the extracellular matrix [71]. Overall, chemical and mechanical signals are thought to be strongly coupled [72]. Long-term studies of localized responses of cells and tissues to chemical and mechanical stimuli are critical in studying developmental biology systems like *Xenopus*. But, one of the important limitations in the area of tissue generation is the lack of techniques to provide inputs and measure biological responses with sufficient temporal and spatial resolution. Microfluidic technology provides an opportunity to control stimulation in both time and space in living systems within aqueous environments. Traditional cell culture study methods can change and control such parameters for a population of cells but lack the ability to control chemical

or mechanical parameters locally over a long time period. For instance, when the chemical environment is changed, signaling pathways trigger changes in gene expression as well as changes in the cytoskeleton. Changes in the cytoskeleton should result in observable phenotypes such as the production of cell protrusions, changes to motility, or altered cell shape. These changes can be remarkably rapid, occurring within minutes or even seconds. Contrary to traditional approaches that apply chemical compounds which fail to change parameters dynamically, live spatiotemporal control stimulation with microfulidics should be combined. Recently, our group used a novel live spatiotemporal microfluidic control with embryonic tissues [73]. In this paper, it has been shown that, spatiotemporally regulated cell contractility effects cell shape and eventually may result in changes in morphology and function of the organism.

2.1.1 Fabricating Microfluidic Mold and Channel

Microfluidic channels are composed of multiple or singular microchannels that are brought together to perform a desired function. These channels can be fabricated through additive (molding) or subtractive (etching) manufacturing into different materials such as glass, silicon or polymers. Before the most common way to fabricate microfluidic channels was photolithography on silicon substrates. Photolithography is the process that uses the light to replicate a microfluidic channel design from a photomask to a light sensitive photoresist on the substrate. The steps of fabricating a mold includes a design of the channels in a software program, printing this design onto a photomask, molding the design onto a silicon wafer using a photoresist with photolithography. First, desired microfluidic channel geometry is drawn in a software program (AutoCAD, SolidWorks, Illustrator etc.) and it is printed on a photomask by photomask manufacturer using UV opaque ink for plastic films. Later, photoresist (SU8 50,100,250 etc.) is poured on a silicon wafer and spread. Using spin coating at a specific speed for a specific time (changing with the channel height), height of the photoresist on the substrate is achieved the height of the designed channel. After spin

coating, soft baking for an hour is suggested. Photomask is placed on the photoresist coated silicon wafer and exposed to UV light and UV exposed areas are cured when using negative resist like SU8. There is also positive photoresists that are removed wherever UV light is exposed. When using SU8 photoresist, photomask enables the desired design to be cured only since the rest is prevented by the opaque mask, in other words: wherever it is exposed, stay. After UV treatment, silicon wafer needs to be hard baked to harden the photoresist. Etching process follows baking and for negative photoresistant like SU8 using SU8 solvent non-cured part of the photoresist is etched away leaving the negative mold for desired design. Silicon wafer then needs to be cleaned with DI water before use (Figure 2.2) . This process is highly effective, precise and cost effective but requires photoresistant, photomask, flat substrate like silicon wafer, spin coating, UV light and a hood or clean room. Although these molds are reusable for mass production, after roughly 100 uses, photoresistant comes off. Disadvantages include the need of a flat surface, fragility of silicon wafer, dimension limitation, inability to fabricate circular channels and limited amount of use. Although lithography provides the ability to fabricate precise, small channels it requires high tech tools and environments and harsh chemicals for etching steps. With the advancement of microludic technology towards 3D geometries, other fabrication methods have been started to be used for mold fabricating like 3D printing and micro-nano milling [2, 74] to overcome the limitations of lithography methods. Micro and nano miling technology have been used for organs-on-chips with the need of using circular channels especially for vascular engineering. Micro and nano milling enabled the fabrication of circular cross-sectioned microchannels. On the other hand, with the increase use of 3D printers the need to pholithography has been decreasing. 3D printers are not as time-consuming and do not require photomask or tedious steps like photolithography by providing flexible geometries (Figure 2.1). Instead of fabricating a monolithic 2D form, 3D printers even offer lego-like modular microfluidic systems [2]. Most 3D printers cannot go tiny dimensions except Nanoscribe but they definitely offer the ease of fabrication and unlimited amount of use.

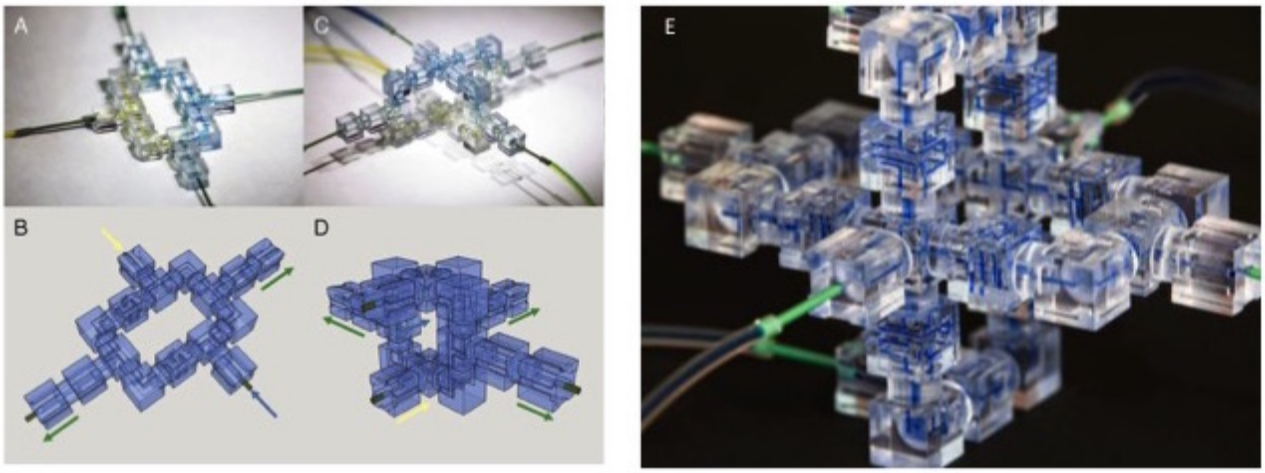

Figure 2.1: Microfluidic system assembled from 3D printed modular components. Single-outlet subcircuits were combined to parallelize operation of the tunable mixer to have (A and B) two, (C and D) three outlets. Each subcircuit is constructed identically and arranged around a single inlet splitter such that the mixing ratio at each outlet is independently controlled by corresponding choices of reference and select resistors. Adapted from [2]

Microfluidics technology rapidly evolved over the last two decades with the invention of soft lithography [3] . Soft lithography altered the traditional way of fabricating microfluidic devices on silicon substrates and enabled the use of polymer molding which is a lot cheaper and does not require strong know-how or clean room. Current technology uses an elastomer, poly-di-methyl siloxane (PDMS; SYLGARD 184, Dow Corning, MIDLAND, MI, USA) to fabricate microfluidic channels. PDMS is in liquid form at room temperature and it solidifies when it is mixed with its cross linking agent. In general a 1:10 ratio has been used for microfluidic channel fabrication. PDMS can be cured at room temperature or in the oven to shorten the time. After the PDMS hardens, the desired design of the micro channels is obtained. Using a needle appropriately sized to the future tubing, inlet and outlet holes are punched. The final step of microfluidic channel fabrication is placing the previously cleaned glass and PDMS replica in plasma cleaner for a minute. The oxygen plasma cleaner helps glass and replica to have a covalent bond to seal the PDMS-glass bonded channels. PDMS has many advantages for cellular studies such as the ability to fabricate by following relatively easy steps, biocompatibility, permeabliability to gas and transparency which makes

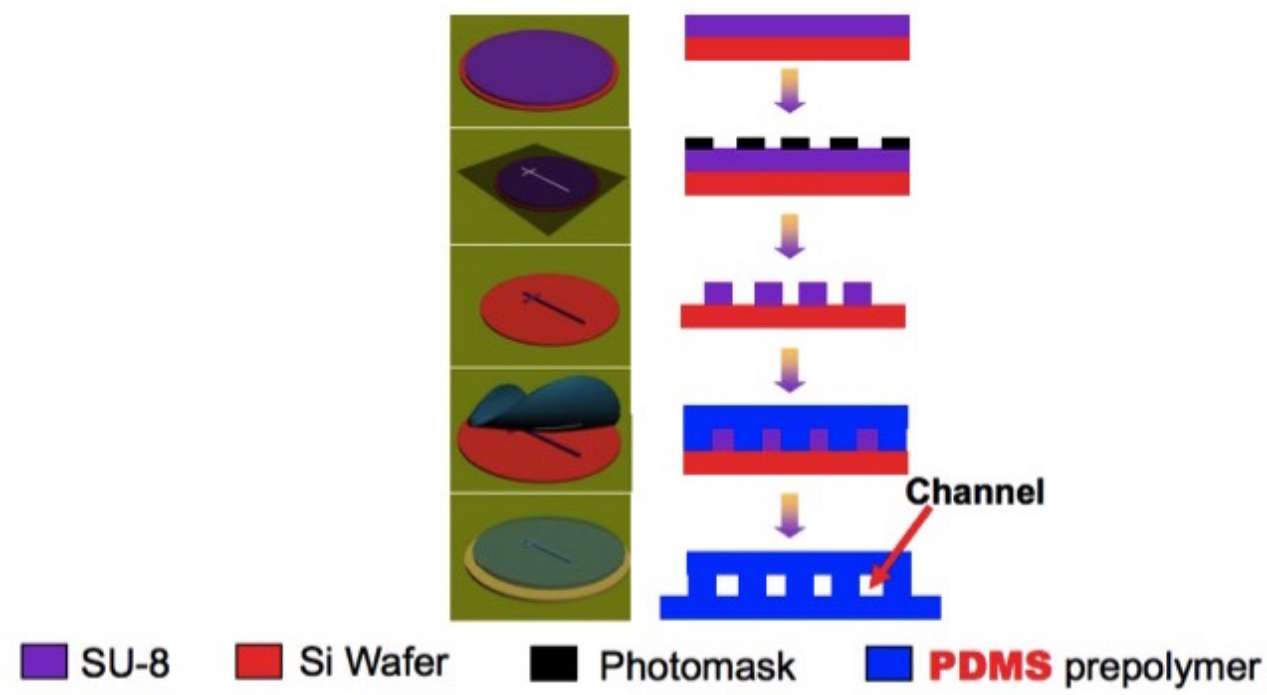

Figure 2.2: Soft Lithography Steps. Adapted from [3]

it perfect for imaging cellular biological studies.

In this thesis, modular fluidic resistances (R20-100x50) and (R60-100x50) were produced from microfluidic channels 20 and 60 mm long each and had cross sections that were 100μm wide and 50μm high [75]. The microfluidic channel for the tissue had three inlet channels that were rectangular cross sections with dimensions 500μm wide, 300μm high, and 5 mm long. These inlet channels converged to form a single outlet channel (rectangular cross section 1500μm wide, 300μm high, and 10 mm long). The reservoirs and pressure sensors were connected to the microfluidic device using polyethylene tubing (Intramedic, inner diameter of 0.78 mm).

2.1.2 Driving Flow in Microflluidic Channel

Over the time, various flow controllers have been developed as flow control is essential to any microfluidic application in order to accurately drive the fluids inside microfluidic de-

vices. Surface tension [76], acoustic wave [77], electrokinetic (electro osmotic pump) [78] and pressure driven controllers (syringe pump, pressure pump, peristaltic pump, etc) [75] are the main methods that have been used to drive flows in the microfluidic channels over few decades. The most common methods are pressure driven flow and electrokinetic flow but the latter method is not biocompatible and therefore not suitable for live biological experiments. As such, in this thesis, flow is driven by regularized pressure. The governing equation of for incompressible, Newtonian fluid motion in pressure-driven flow is derived by Navier-Stokes equation:

$$\rho(\frac{\partial u}{\partial t} + (u{\cdot}\nabla u) = \nabla p + \mu\nabla^2 u + \rho g \tag{2.1}$$

where ρ is the density of the fluid, u represents velocity, μ is the dynamic viscosity, p represents pressure, and g is gravitational acceleration.

Navier-Stokes equation (equation 2.1) can be simplified by making several assumptions like 1) incompressible (the incompressibility constraint ($u{\cdot}\nabla u = 0$) and the boundary conditions (u = 0 at the walls) and Newtonian fluid, 2) steady-state flow (i.e. no transient variation), 3) axial bulk flow to downstream for a channel with a uniform cross-section with no advection across streamlines that is formed by the bulk flow, and 4) gravitational effects are negligible leaves the equation as the fluid flow is determined entirely by the pressure [79]:

$$\mu\nabla^2 u = \nabla P \tag{2.2}$$

Pressure-driven flow profiles are based on macroscale Poiseuille flow theory [80]. J.L.M. Poiseuille studied this flow regime in the early 1800s, and it is well-studied characteristic flow in microfluidics. Poiseuille flow is characterized by a parabolic velocity profile, where velocity varies parabolically across the channel because of the so-called no-slip boundary condition, with a maximum velocity in the center of the channel and zero on all stationary boundaries like at the wall of the microfluidic chip. Despite the parabolic profiles in simple geometries with pressure-driven flows, for boundary forces induced flows (such as electro-osmotic-flow,

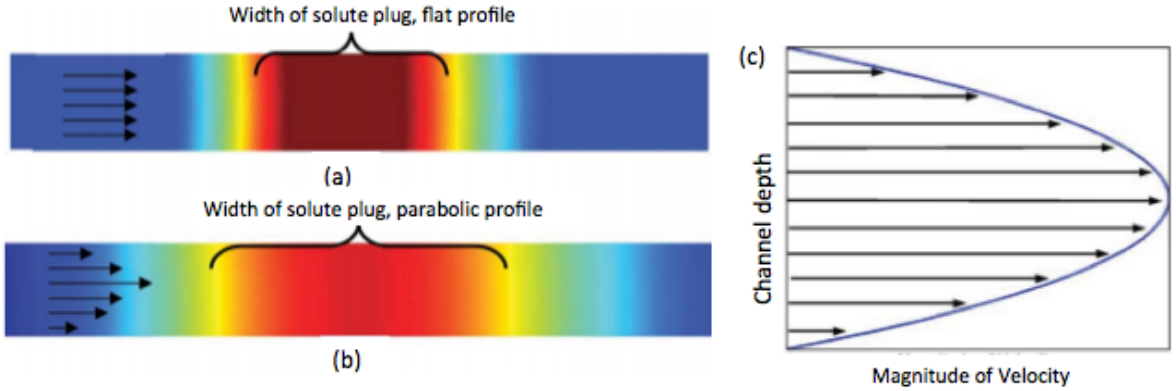

Figure 2.3: Hydrostatic dispersion effects in different flow profiles. Schematics showing the added dispersion of a solute due to flow profiles (a) The dispersion of a solute in a uniform velocity flow, red indicates region of high concentration and blue indicates regions of no concentration. Dispersion in this case is only due to pure molecular diffusion. (b) The dispersion of a solute in a microchannel with pressure-driven flow. Notice the broadening of the band due to the non-uniform flow profile. (c) The flow profile in Poiseuille flow. [4]

wall-shear-driven-flow, etc.) nearly uniform profiles can be expected [81]. Uniform velocity profiles provides minimized hydrostatic dispersion effect. On the other hand the nonlinearity in Poiseuille flow velocity profile causes a hydrostatic dispersion effect in the channel which might be undesirable for localized stimulations Figure2.3.

One way to use pressure-driven flow is using positive displacement pumps like commercially available syringe pumps to regulate flow through the inlets of channels. While this method enables to maintain fixed flow rates, one of the important drawbacks is syringe pump volume, which is relatively small. With this system, long-term studies cannot be conducted due to volume limitation. Another way is to utilize gravity force by using height difference between reservoirs. One of the important drawbacks of this method is to maintain the flow rate as its changes as fluid volume drops in the reservoir. Thus this system may not be as precise as desired. My experiments require the long-term, precise control of the laminar flow interface in microfluidic channels in order to manipulate the cellular chemical environments and architecture. Long-term studies are necessary for investigating cell responses, which are often take several hours to days. However, existing commercialized systems have limitations

for long-term studies because they use syringe pumps with relatively small volumes. In this thesis, I use a novel control system that was designed by a former member of LeDuc lab [75]. This system controls the pressure at the inlets of microfluidic channels by modulating the resistance of the fluidic network connecting the microchannels to supply reservoirs. This system controls and varies the position and the shape of the interface between the fluids with high precision and high bandwidth for long time periods. With this approach large fluid reservoirs may be used for long-term studies (hours to days) of cellular dynamics [82].

2.1.3 Laminar Flow: Moving Interface

Scaling down a system impacts the effects of inertia forces effect the most. At the micro-scale, surface area to volume ratio increases causing viscosity forces to take over the inertia resulting in laminar flow. Viscosity of a flow is the quantitative measurement of the fluid's ability to resist shear stresses. When viscosity is dominant in a flow, fluid moves in parallel layers (laminar flow) whereas when inertia (the tendency of the fluid to retain its initial motion unless an outside force acts on it) dominates flow can eventually result in turbulent flow. In contrast to the macro-scale, laminar flow in micro scales can be achieved with simple designs if the Reynolds number (Re), the ratio of viscous to inertial forces, is small. Re number is a dimensionless number that quantifies the flow characteristics for given flow conditions. The Re number can be calculated as follows:

$$Re = \frac{\rho U^2}{(\mu U)/L} = \frac{\rho U L}{\mu} \tag{2.3}$$

where Reynolds Number is non-dimensional, ρ is the density of the fluid(kg/m^3), U is the velocity based on the actual cross-section area of the duct or pipe (m/s), L is the characteristic length(m), and μ is the dynamic viscosity (Ns/m^2).

Reynols number is used to show if the flow regime is laminar or turbulent. The Re number has three ranges to characterize the flow. For low Reynolds numbers (Re$<$2300),

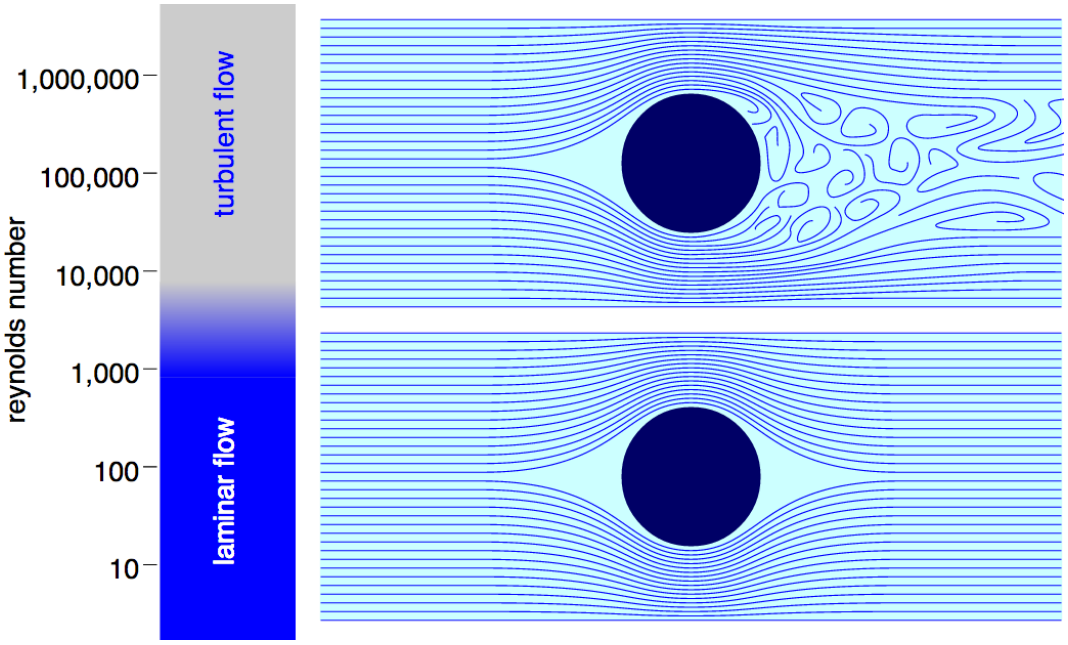

Figure 2.4: Fluid Flow Regimes as a Function of Reynolds Number [81]

flow behavior depends on flow viscosity, and the flow is mostly steady, smooth, viscous, or laminar. For high Reynolds numbers (Re>4000), behavior of flow is determined by the inertia more than the viscosity and the flow is unsteady, churning, roiling, or turbulent. For intermediate Reynolds numbers (2300<Re<4000) the flow is transitional-partly laminar and partly turbulent (Figure 2.4).However, in a straight channel, the value of $Re = 10^3$ is the limit for the transition from a laminar to turbulent flow [81].

However, low Reynolds numbers do not guarantee steady and smooth flow without any vortexes. At Re>10 local microvortices and flow separation occur due to the increase of inertial force which can cause complex flow patterns. Due to the high viscosity, Reynolds numbers in microfluidic channels are usually roughly 1, which is called Stokes flow or Creeping flow regime. In creeping flow, inertia terms become so small that they are negligible in the momentum equation, which makes the system linear. The most famous example of creeping flow that shows how smooth the flow is compared to other laminar conditions is that of a viscous fluid flowing over a stationary solid sphere with the axisymmetry about the flow direction (Figure 2.5). This property of flow is especially critical for my experiments,

High Reynolds number flow >>1)	Low Reynolds number flow (Re << 1)
Inertial forces dominate	Viscous forces dominate
Flow separation (e.g. vortex shedding)	No flow separation
May be turbulent	Always laminar
Not reversible	Reversible
Non-linear	Linear
Large momentum (vortices in wakes)	Small momentum (no vortices in wakes)
Coasting	No coasting

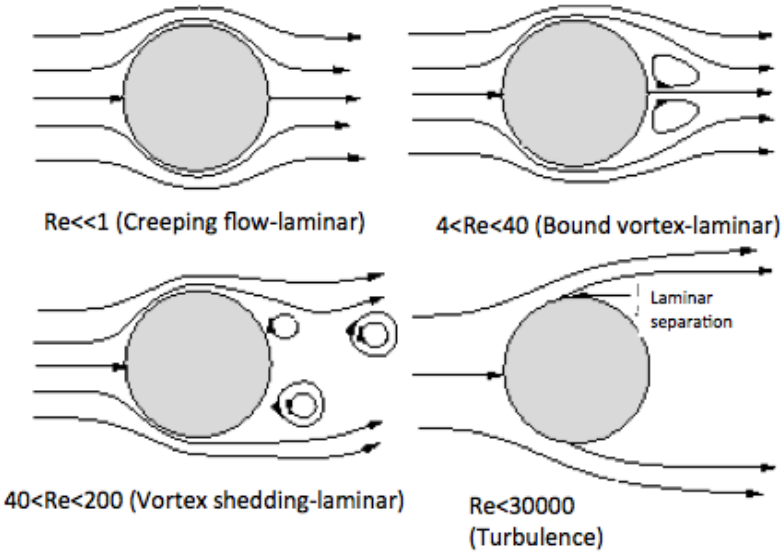

Figure 2.5: Different Low Reynolds Regimes flowing over a stationary solid

since the flow in microfluidic channel flows over *Xenopus* embryonic tissue which is multi layer thus not flat. With the advantage of using creeping flow by keeping Re number is smaller than 1, flow is not disturbed by a solid explant and still provides spatial regulation.

Microfluidics offer unique behavior such as creating and controlling the sharp interface and developing different uses for it. When miscible fluids interact, over the time they become a homogeneous solution. There will be no meniscus forming between two miscible fluids like alcohol and water. However, under laminar flow conditions, there will be a boundary between two flowing miscible fluids and mixing will only occur at a predictable rate by diffusion. This boundary is called as a dynamic or 'moving interface' [5] and this unique behavior can be used for temporally and spatially control within microfuidic channels. On the other hand, laminar flow provides another type of interface with two immiscible fluids (e.g. oil and water) where one liquid is dispersed in another called floating interfaces (Figure

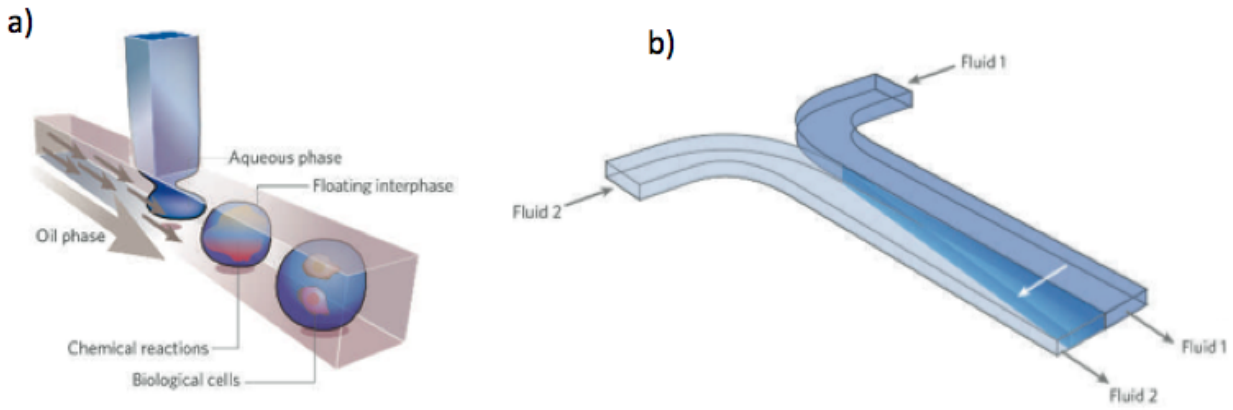

Figure 2.6: Microfluidic Interfaces with immiscible(a) and miscible fluids(b). [5]

2.6). Floating interfaces usually are used to produce droplets for microscale containers (i.e. capsules) and acts as permeable walls between two fluids, which is utilized for performing and analyzing reactions, creating custom magnetic or protein-coated vesicles, or transporting cargos [83–85]. Here in this thesis, I used the advantage of moving interfaces, where I moved two water-based solutions next to each other without mixing.

2.1.4 Diffusion Across the Moving Interface

A planar interface that forms between two adjacent fluids is the location of a sharp concentration gradient. Under laminar flow conditions, mixing between adjacent streams occurs only at a predictable rate of diffusion. Diffusion though causes the gradient to broaden as the flow advances down the channel. This diffusion can be controlled and width of the diffusion can be managed. As contact-time increases between miscible fluids with low velocity, diffusion broadens and, if contact-time is long enough two miscible fluids eventually mix despite laminar flow condition. To ensure efficient local stimulation, diffusion rate still should be controlled. To control the width of diffusion, another dimensionless number, Peclet number (Pe), added to the equation. Peclet number is given by the ratio of convective fluxes to

diffusive fluxes and changes for every species and fluids. At the conditions where Pe number is high enough, mixing is negligible because diffusion occurs slowly on flow time scales.

The Peclet number is defined as:

$$Pe = \frac{U_a L}{D} \tag{2.4}$$

where U_a is the average velocity of the flow, L is a characteristic length of the system perpendicular to the direction of the flow and D is the diffusion coefficient of the particle or molecule of interest [5].

In microfluidics, usually Re«1 due to laminar creeping flow, thus Pe number ends up being Pe»1 since average velocity and characteristic length are coming from Re equation and they are very small numbers. In laminar flow, under the conditions of Pe»1, mixing through diffusion is negligible [86]. In this case, diffusion does not broaden in the channel and change the interface. Interface stays sharp as contact time of these two miscible fluids is short.

Since this system is pressure-driven flow and velocity profile is parabolic, being the max velocity in the center and near zero velocity at the walls, diffusion at the interface changes in channel height and becomes more significant at the walls [87]. The diffusive dispersion grows more quickly and diffusion becomes broader as flow-rate becomes smaller at the same cross section [88]. Since my experiments are with live tissue, we needed to find the optimum flow rate to flow over the tissue without affecting its fate. The lowest possible flow rate for the experiments employing sharp concentration gradients of chemicals was determined by using computational fluid dynamics (CFD) simulations by former LeDuc lab member [82]. The simulation results showed that diffusive dispersion is more significant near the wall and grows more quickly than the center of the channel where the fluid velocity is relatively high. Diffusion thickness is determined based on a 10% threshold of mass fraction, which is normalized by the concentration across the interface. The simulation results showed that diffusion exponentially grows under a flow rate of 10μl/min in a microfluidic channel [89].

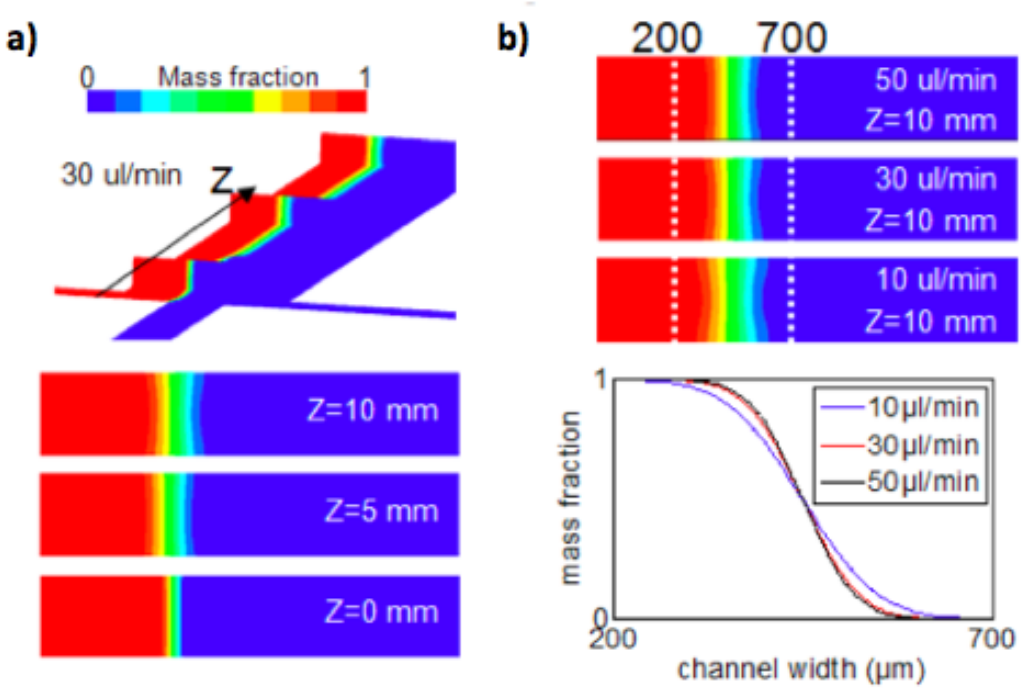

Figure 2.7: Diffusive dispersion across a laminar flow interface. a) Diffusive dispersion through the channel at a flow rate of 30 μl/min. b) Diffusion profile in the cross section to the downstream flow at flow rates of 10, 30, and 50 μl/min. [6]

2.1.5 Controlling Interface with Resistances

For a 2D multi-inlet and one outlet microfluidic device at a low Reynolds number, a position of the laminar flow interface between multi-inlet streams can be mathematically determined by the pressures at the channel inlets and the dimensions of the channel that determines fluidic resistances. As we can effectively ignore the inertial terms nonlinear partial differential equation (Navier-Stokes equation) into a simple linear one where the fluid flow is determined entirely by the pressure. Since there is no leakage through the channel assumed, the flow rate in the outlet channel should be equal to the sum of the inlet flow-rates due to mass conservation. Disregarding the differences of density and viscosity among the fluids at the inlets, it is true that the interfaces are planar and stable through the main channel and there is no mixing across the interfaces between the streams except by diffusive dispersion. With the assumption that there is no pressure difference in all the cross sections of the

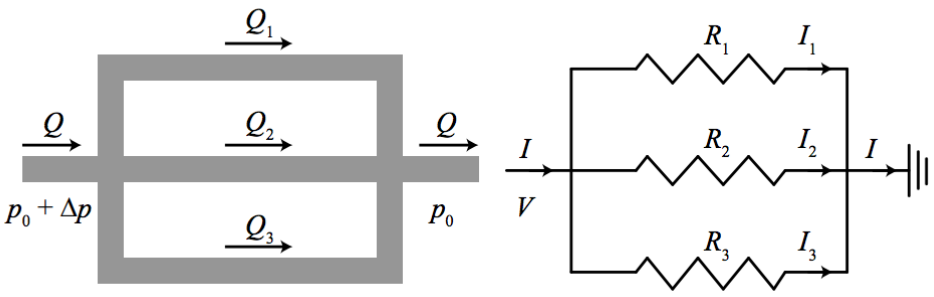

Figure 2.8: Schematic of pressure-driven flow in a network of parallel channels in the relation to electrical circuits [7]

microfluidic channel, regulation of the pressure at the channel inlets allows control of the interface positions and adjacent fluid volume will be determined by the relative inlet flow rate proportionally between each stream. In the case of square channels or low aspect ratio rectangular channels, a approximation of the relation between pressure and flow rate(Q) is given by:

$$\nabla P = \frac{12\mu LQ}{wh^3}/[1 - 0.63\tanh(\frac{h}{w})] \tag{2.5}$$

where w is the widest and h is the smallest dimension.

Due to continuity through fluid networks along the channel length, the flow rate must remain constant.

$$\nabla P = Q.R \tag{2.6}$$

where R is a fluidic resistance along the length of the channel.(Figure 2.8)

Since the total flow rate through the outlet channel is proportional to the sum of inlet pressures, changes in one pressure at one inlet require corresponding changes in forcing pressures at other inlets if a constant flow-rate is required. Constant flow-rate is desirable because the flow rate determines shear stress experienced by cells or tissues on the channel surfaces. Shear stress is even more important with multilayer tissues as the layers adhere to each other less strongly than the bottom layer adheres to the microfluidic channel.

In a microfluidic device whose inlet channels have equal fluid resistance, the volumetric flow-rate through the outlet channel is proportional to the sum of the pressures at the inlets [90]. Under laminar flow conditions, the two fluids will enter the outlet channel side-by-side in volumetric proportion according to their relative flow-rates. These flow-rates depend only on the pressure drop across the inlet channels. Consequently, the position of the interface between the streams can be controlled by modulating fluid pressure at the inlets when the interfaces are planar [91, 92]. The width fraction has been believed to be linearly correlated with the pressure fraction so the interface position between three streams in the 3-inlet microfluidic channel can be readily determined by the pressure fraction [92]. Here, in this research, I use fluidic channels with different dimension as rresistances to change the inlet pressure individually. By using resistances, the pressure that is the same at the three reservoirs can be manipulated, thereby allowing flow rates to be altered individually in every inlet [93].

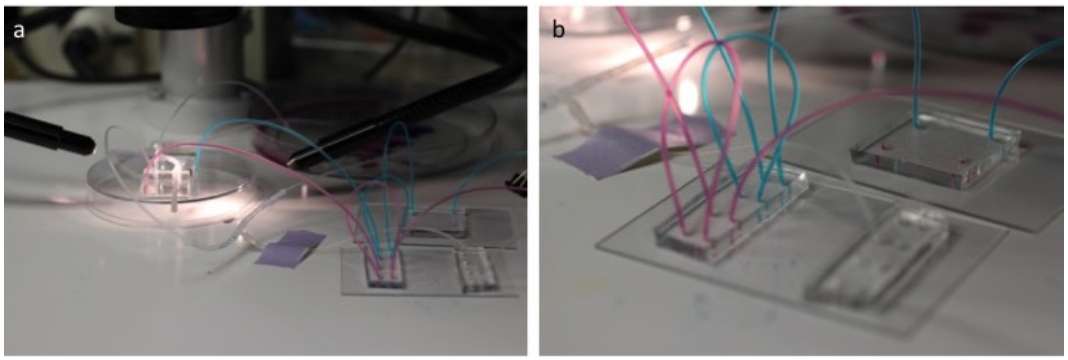

Figure 2.9: Modular fluidic resistances

.

The relation between pressure-drop along the channel downstream and the flow-rate Q is analogous to Ohm's Law for electrical circuits with fluid pressure-drop for electrical potential difference (i.e. voltage, V) and fluid flow for electric current, i.

$$V = i.R \tag{2.7}$$

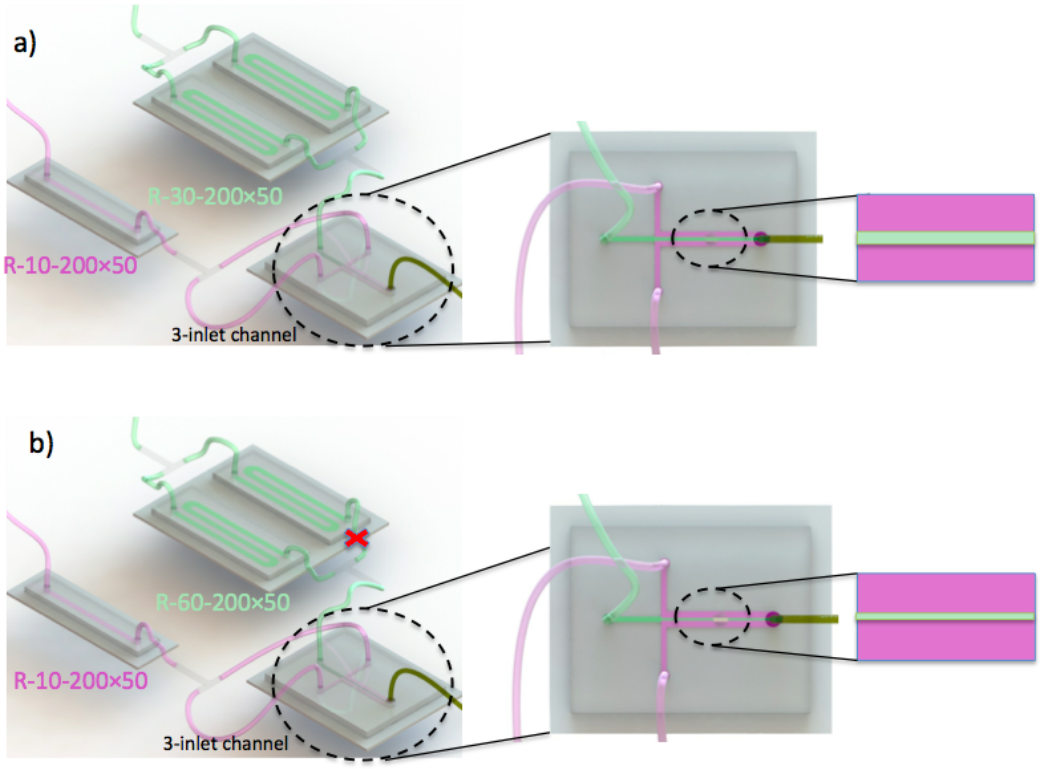

Figure 2.10: Interface control with resistances in 3-inlet microfluidic channel. The width of each inlet fluid in the main channel changes due to their flow rate. a) Resistance-10 is at the two side inlets shown in pink, Resistance-30 is on the center inlet shown in green. b) Resistance-10 is at the two side inlets shown in pink, Resistance-60 is on the center inlet shown in green. Modular resistances are also microfludic channels 200μm wide and 50μm high

.

To modulate inlet pressures, three resistances and three chamber sizes (R10-200x50, R20-200x50, R60-200x50) (have been designed as modular microfluidic devices in this study (Figure 2.9).Smallest modular resistance (R10-200x50) is 10 mm long, and the rectangular cross-section is 200μm wide and 50μm high. In figure 2.10, three parallel streams in volumetric proportion to different resistances have been depicted in a three-inlet channel. This figure represents the notion the more the resistances, the narrower the width of the central stream in the main channel. This opportunity allows us to change the interface in the main channel spatiotemporally without any complicated set-up thus allowing us to test different controlled conditions.

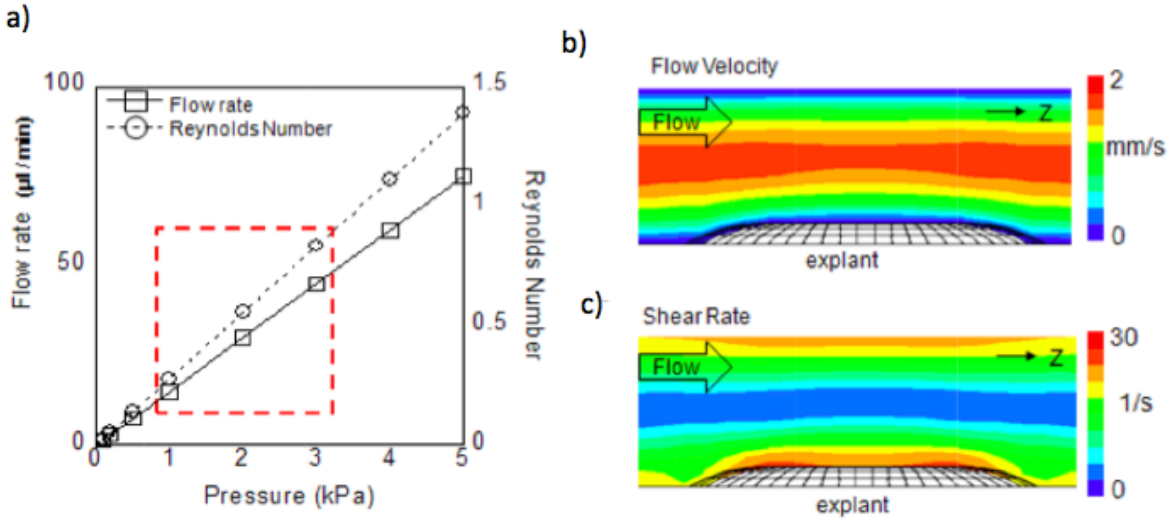

Figure 2.11: CFD simulation of flow properties around the explant. a)Relative effects for flow-rates, pressures, and Reynolds number. The red dashed box represents a useable range of the pressure in the experiment to prevent high diffusion and high shear stress based on the simulations. b) Flow velocity c) Shear rate around the explant at 30μl/min flow-rate [**?**].

2.1.6 Flow Characteristic Around a 3D Explant

One important issue to consider when delivering chemical factors to multicellular tissues using microfluidics is the effect of the shape of a three-dimensional (3D) tissue on flow patterns around the tissue, which is critical for a precise stimulation performance of the system. Several factors such as the size and shape of the tissue, the size of the channel, and flow conditions can change the localized pattern of stimulation since larger microscale channels may have higher sensitivity to the chemical patterns even at relatively lower Reynolds number [94]. Former lab member run computational fluid dynamics (CFD) simulations to explore the effect of these factors on the flow conditions, all CFD work in this section is belong to YongTae Kim [82]. Optimum numbers were obtained by considering the diffusion broadening issue at low flow-rates and the high shear stress on the explant at high flow-rates. CFD results showed that flow conditions are not disrupted around the explant for some range of Reynolds numbers, flow rates, and the optimum shear stress range that explants can handle without detaching is also obtained. The determination of the diffusion thickness was based

on a 10% threshold of mass fraction, and diffusion thickness at the end of the channel kept at 20μ on the bottom plane. When Re number is kept under 1, optimum flow rate range is between 10μl/min and 50 μl/min (Figure2.11 a). From these CFD result, I selected a flow rate of 30μl/min for experiments which corresponded to a inlet pressure of 2 kPa. This flow-rate is equal to a fluid velocity around the explant of less than 1.0 mm/s and a shear rate of less than 30 s^{-}1 (Figure2.11 b and c); this is small relative to the reported biological shear rate for other embryos [65]. The shear stress was 0.04 Pa (0.4 dynes/cm^2), which is approximately 2.7% of the shear stress that leads to physiological responses approximately 1.5 Pa (15 dynes/cm^2) [89].

2.2 Handling *Xenopus leaves* Embryos and Explant Preparation

Eggs were collected from hormonally stimulated female *Xenopus laevis* frogs. Eggs were fertilized *in vitro* [95], dejellied in 2% Cysteine solution (pH 8) [96] and cultured in 1/3 X Modified Barth's Solution (MBS) until stage 10 [97]. At stage 10 embryos were transferred into Danilchik's For Amy solution (DFA) and forceps were used to remove viteline membranes. I used hair-loops and hair-knives to micro surgically isolate Animal cap explants. Microfluidic channels were coated with fibronection at 4°C overnight. Micro surgically isolated explants were positioned in the channels using negative pressure.

2.3 Positioning living Animal Cap Explants into microfluidic channels

Animal cap tissue needs to be positioned in the center of the microfluidic channel for our experiments. After coating the substrate of the microfluidic network with fibronectin, I

position 100 μm thick micro surgically isolated tissue explants in the microfluidic chamber. I close all the inlets with microscale tubes and valves, and open one inlet and one outlet in the large main chamber. Using negative pressure in the inlet connected to a syringe, the tissue explant that is located on the top nearby the outlet of the microfluidic device is positioned inside the chamber. Carefully adjusting the syringe, I position the tissue into the desired location(center of the outlet channel) in the chamber. After positioning, I close the inlet and outlet with valves in order to close the entire network closed so that there is no pressure differential around the tissue. This enables the tissue stably attached to the substrate without any disruption. Otherwise, the tissue will not be firmly attached to the substrate or might need more time for the attachment and spreading. I allow the explant to adhere the glass substrate for 4 hours prior to flow studies.

2.4 Microscopy and image analysis

To capture images of animal cap bio-etching in microfluidic channels, a digital charge-coupled device (CCD) camera (The Imaging Source Europe GmbH) mounted on a stereomicroscope (SZX12, Olympus Corp., Waltham, MA) was used to acquire images at room temperature. A laser scanning confocal scanner (Leica TCS SP5; Leica Microsystems) mounted on an inverted compound microscope (DMI6000, Leica Microsystems) was used to collect high-resolution time-lapese confocal images. The image acquisition and subsequent analysis of time-lapses sequences used custom-written macros and plug-ins, and image analysis software (Fiji). As the visualization of the streams was very important, two drops of food coloring (McCormick, green) were added to a 20 mL central reservoir as previously described [75]

Chapter 3

Probing a Complex Multi-Layer Embryonic Tissue Through Novel 3D Bio-ethching

Morphogenesis consists of a complex series of cell signaling, migration and differentiation events that are coordinated as tissues self-assemble during embryonic development. Studies of collective cell movements have typically been studied in 2D with single layers of cultured cells adhering to rigid substrates such as glass or plastic. *In vivo*, the intricacies of the 3D microenvironment and complex 3D responses are thought to play critical roles in the formation of functional tissues. To study such processes as collective cell movements within 3D multilayered tissues, we developed a microfluidic technique capable of producing complex 3D laminar multicellular structures. We call this technique "3D tissue-etching" because it is analogous to techniques used in the microelectromechanics (MEMS) field where complex 3D structures are built by successively removing material from a monolithic solid through subtractive manufacturing. We use a custom-designed microfluidic control system to deliver a range of tissue etching reagents (detergents, chelators, proteases, etc.) to specific regions of multilayered tissues. These tissues were previously isolated by microsurgical excision from

embryos of the African Claw-toed frog, *Xenopus laevis*. The ability to shape the 3D form of multicellular tissues and to control 3D stimulation will have a high impact on tissue engineering and regeneration applications in bioengineering and medicine as well as provide significant improvements in the synthesis of highly complex 3D integrated multicellular biosystems.

3.1 Microfluidics in Cell Biology

Microfluidics have been used in numerous cell biology applications where there is a need to control temporal or spatial stimuli in a microenvironment. Microfluidics have become a commomplace tool with the development of soft-lithography methods which allow the easy fabrication of channels in which laminar flows can be combined with minimal mixing [3, 98]. Microfluidic technology enables spatiotemporal control over living cells [99] and allows for high-throughput manipulation of the microenviorenment from subcellular to multicellular scales. Microfluidics offer high molecular selectivity micron scale spatial accuracy to spatially control sub-cellular processes; a level of control that is extremely challenging without laminar flow, since small molecules diffuse across the distance of a cell diameters within seconds [100]. Spatiotemporal control offered by microfluidics allows long-term studies of localized responses of cells and tissues to chemical stimuli, which are critical in numerous areas including developmental biology [89, 101, 102].

Tissue engineers have recently turned to decellularization techniques to isolate signaling factors embedded in tissues and to use those factors for regenerative medicine. Intriguing examples of these include decellularization techniques with the ability to decellularize 3D heart matrix to engineer bioartificial heart, to decellularize a liver to recellularized liver graft and to decellularize the human vein for vascular tissue-engineering scaffold [103–105]. In contrast to these bulk, or whole tissue decellularization approaches where all the cells are removed from a tissue we present a microfluidic etching technique for localized removal of targeted

cells. We use this approach with a composite tissue consisting of epithelial and mesenchymal cell layers to expose interactions between layers in a 3D tissue. Microfluidics has been used to control the environment of developmental biology systems such as mechanochemical sensing in *Xenopus* [89, 106] and developmental changes in Drosophila melanogaster embryos [70]. Microfluidics applied in developmental biology provides the opportunity to study the coordination of cell behaviors in a 3D environment.

3.2 Advantages of 3D Tissue Systems Versus 2D Cell Culture Systems

One of the most important properties of 3D tissues during development is the structure and interactions between cells in the tissue. Cells during development and regeneration must orchestrate numerous signaling events; cells coordinate inputs from 3D cell-cell interactions mediated by receptors and cell-matrix adhesion to regulate cell fate [107, 108]. To understand these processes requires tools to control 3D cell-cell interactions; however, conventional approaches are mainly limited to 2D monolayer systems and do not allow manipulation of complex multilayer tissues [109–111]. For example in controlling tissue structure and 3D cell-cell interactions, studies have been conducted on the behavior of epithelial monolayers of cultured cells such as such as human umbilical vein endothelial cells (HUVEC) or Madin-Darby canine kidney (MDCK) cells [112] in response to laser cuts or scratch assays but these methods are restricted to monolayers [113, 114]. One limitation of current cell-based approaches is that tissues and organs are 3D, and thus traditional 2D cell culture studies (e.g. Petri dishes or flasks) lack important features necessary to accurately replicate cell function and formation [115]. Cells that are grown on 2D substrates may respond and differentiate differently than those in more physiologically relevant 3D environments [72, 116–118].

Here, we demonstrate a novel microfluidic application to etch spatially multi-level mul-

ticellular structures while altering the structure and 3D cell-cell interactions in tissues. We manipulate the complex tissues in the *Xenopus laevis* animal cap (AC), which is composed of stratified layers of epithelial and mesenchymal cells. We first demonstrate that we can make a full cut in a local region through the entire multi-layered AC. We then show that we can cut a similar local region but only removing the top layer of cells of the tissue. Finally we show that we can cut a different widths of cells away from defined layers of cells allowing us step-wise spatial precision in cell layer removal for examining in the future 3D cell interactions in tissues. We implemented different etching protocols including the chemicals sodium dodecyl sulfate (SDS), triton X-100, trypsin and sodium hydroxide (NaOH) to alter and shape these 3D tissues. We believe our results will provide an approach that will greatly enhance the understanding of tissue remodeling events, which will impact fields such as cancer, embryonic morphogenesis and wound repair.

3.3 Result/Conclusion

3.3.1 Experimental Technique to etch a composite tissue through 3D Bio-etching

To etch 3D tissues, we used our custom-designed microfluidic control system to deliver of a range of tissue etching reagents adopted from decellularization protocols over microsurgically isolated early stage embryonic tissue (Figure3.1a). Controlling the flow rate at the inner microchannel inlets individually enables precise and dynamic chemical control over the 3D tissue [94]. Our system implemented a pressure-driven (nitrogen gas) approach and included two variable-volume fluid reservoirs with etchants and culture media (Danilchik's For Amy solution-DFA), two microfluidic resistances and a 3-inlet converging microfluidic channel (Figure 3.1b). The main microfluidic channels and fluidic resistance modules were fabricated with conventional soft lithography techniques from polydimethylsiloxane (PDMS). After

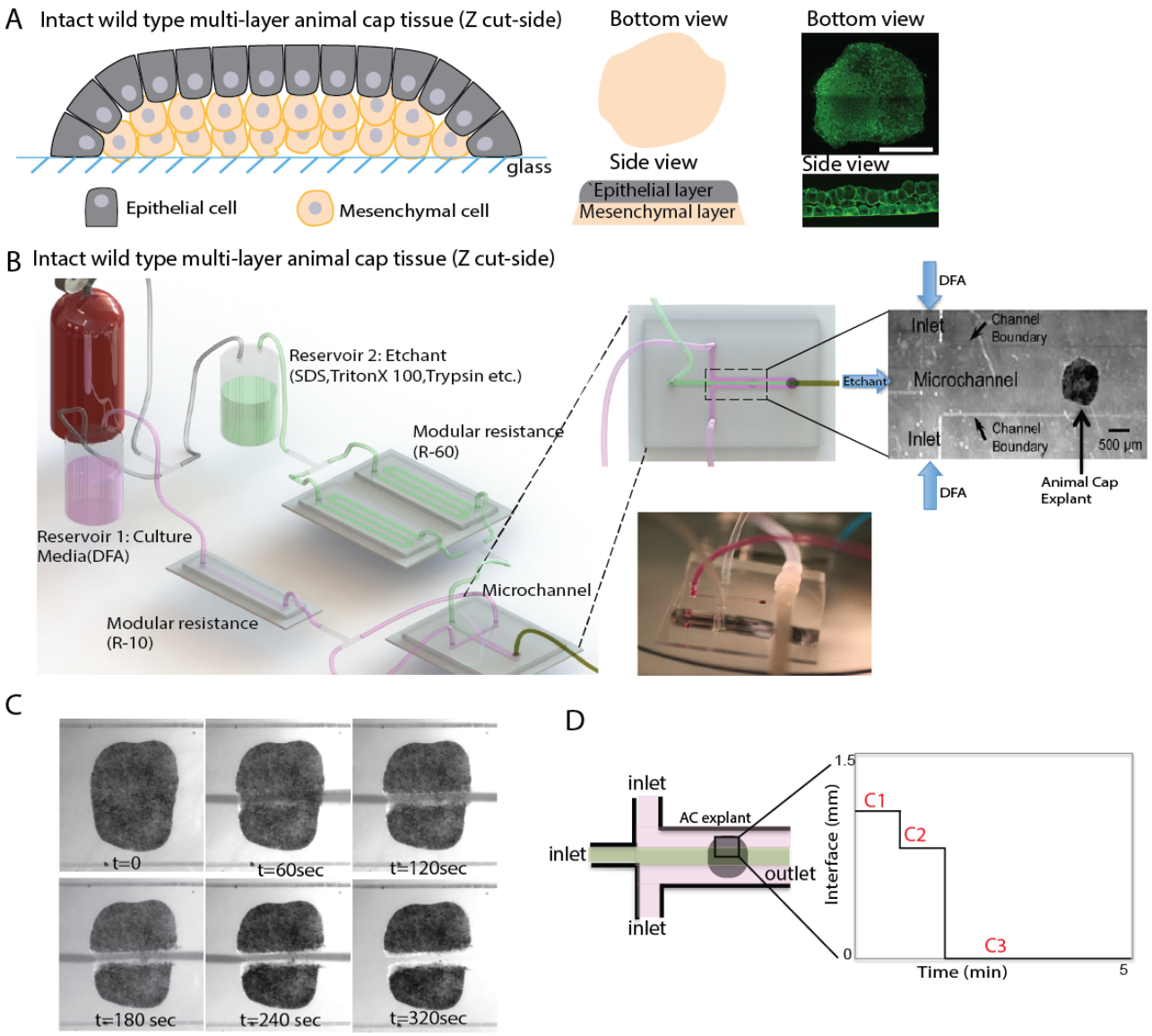

Figure 3.1: Probing a complex multi-layer embryonic tissue through novel 3D bio-etching. a) Schematics and images of two layer animal cap tissue with bottom and side view. b) Experimental set up for 3D tissue etching and real pictures of microfluidic channel c) Long exposure of AC to a narrow stream of etchant creates a deep through cut of the AC. d) 3-inlet microfluidic channel schematic and interface control over the time. Green center interface changes over the time with resistances. Side pink resistances stay the same but interface changes according to resistance change in green. Center inlet is set to Case 1 (C1): lower resistance, Case 2 (C2): Higher resistance, Case 3 (C3): shut off.

fabrication the main channels were coated with fibronection. In the main T-shaped, 3-inlet microfluidic channel, the two side inlets had the identical high-flow rate flows, which were controlled by microfluidic resistances [75] with the center inlet having a lower flow rate

(Figure 3.1 c). These fluidic resistances altered the flow rates that defined the width of the etching streams in the main microfluidic channel and thus the width of the areas exposed to the etchants over the apical surface of the tissue (Figure 3.1b). Inlet pressures can be dynamically changed to deliver etchant to any location over the apical surface and width of the tissue. The tissue used in these experiments was microsurgically isolated from gastrula stage *Xenopus laevis* embryo and positioned inside of the outlet of the main channel. The tissue was first allowed to adhere to the fibronection coated glass surface for 4 hours. Once adhered, we collected time-lapse sequences of the process of etching and the response of the remaining tissues. Decellularization of organs through using etchants has been used to create ECM for a variety of reconstructive surgical applications and regenerative medicine strategies for tissue and organ replacement [119]. However, current decellularization aproaches remove all cells to produce foundational scaffold ECM to regenerate an organ. In our approach, the goal as to remove only select cells in controlled areas to understand how collective 3D cell responses react. Our tissue etching technique allowed the removal of specific layers of tissue through exposure to a narrow etchant stream, which removed layers of cells to expose lower layers of cells or even to the supporting substrate such as glass (Figure 3.1 d).

Here, contrary to decellularization techniques, cells exposed to etchants were removed by culture media not by the etchant. We used Sodium dodecyl sulfate (SDS) as etchant. After the microsurgically cut tissue is positioned and adhered in the microfluidic channel, center inlet is connected to SDS reservoir. Using modular resistances, a narrow center stream delivers the etchant on top of multi layer animal cap tissue. With long exposure time, we get deep etch that has multi-layer height (Figure 3.1 d). By reducing the exposure time a single layer of epithelial cells may be removed(Figure 3.2). By controlling the width of the etchant and the exposure time a broader swath of the surface layer may be removed (Figure 3.4). After removal of a broad swath the resistance circuits can be switched and a second narrow stream can remove only a single narrow band within the swath-exposed cells. With this novel 3D bio-etching, depending on the exposure time of the etchant, single or multiple

layers can be removed.

3.4 Width and depth of the tissue etching regulated by microfluidic positioning and duration of detergent stream.

As a first step we removed all of the layers in a spatially controlled region of the 3D *Xenopus* AC. To accomplish this, we first used sodium dodecyl sulfate (SDS) as an etchant. After positioning and adhering the microsurgically excised in the microfluidic channel, the center inlet was connected to the SDS reservoir. We started the pressure driven flow and opened the valves of the side inlets. After the DFA was in the entire main channel and the flow equilibrated, the center inlet's valve was opened to start the etching process. Using modular fluidic resistance modules, a narrow center stream delivered the etchant to the apical layer of the multi layer animal cap tissue. By controlling the width of the etchant and the exposure time a broader swath of cells may be removed. We also used this methodology to remove multiple layers of cells through the entire AC so that the interacting substrate was exposed, but only in the specified regions where cells were previously removed; we call this a "through cut" approach (Figure3.1 d).

To create more complex structures we limited the amount of time the tissue was exposed to SDS. By reducing the exposure time a single layer of epithelial cells was removed (Figure 3.2), which we called a "single cut". For the single cut, after the first layer was etched, the middle inlet of the microfluidic system containing the etchant was closed to stop the flow of the etchant. This approach created a discontinuous region of epithelial cells (EL) over a mesenchymal cell layer (ML) (Figure 3.2). Where the EL is continuous it remains in contact with the deeper mesenchymal layer. The width of the etched gap in the epithelium was controlled by modulating the central inlet flow rate by changing microfluidic resistance

modules (Figure 3.2c). With this approach we controlled the etching depth and width of the epithelial layer in a spatiotemporally controlled manner. The single cut approach created a free margin in the epithelial cell layer that remains in contact with deep mesenchymal cells. The viability of the cells in the tissue were directly related to their exposure to the etchant (Figure 3.3).

3.5 Multi-step etching can create novel 3D tissues

By repositioning the microfluidic stream after a single cut we created a 3D 'tiered' tissue. After the removal of a broad swath of epithelial cells we switched resistance modules to produce a more focused stream and create another free edge in the mesenchymal cell layer (Figure 3.4a). To create the step like spatially etched structures requires sequential steps (Figure 3.4 b and c). As before the DFA reservoir was connected to a lower resistance and then connected to two side inlets. The width of etchant was based on the ratio of resistance modules in the side inlets compared to the middle inlet. In the first step, two higher fluidic resistance modules, namely the R-60 length of the channel, were connected in parallel to each other with the same resistance of an R-10 module. The etchant reservoir was connected to two of the same resistance modules with a T connector (Figure 3.4b). This configuration with etchant inlet:side inlet resistance modules in the ratio 1:3 cut a defined region of the EL with a relatively wide stream in the main channel. In step two, one of the resistance modules leading to the etchant channel was closed off to create an etchant:side ratio of 1:6. The increase in the resistance to the etchant flow caused the middle stream to narrow (Figure 3.4c). The narrow stream of etchant then acts on the ML without contacting the EL since the EL was already removed in step 1 (Figure 3.4d). Resistances can be manually changed in a few seconds so that a narrow cut with the ML can be made within a wider region that cut through the EL (Figure 3.4e). With spatiotemporal control of the etchant our microfluidic technique enables multiple rounds of etching, which we have used to create "step" shaped

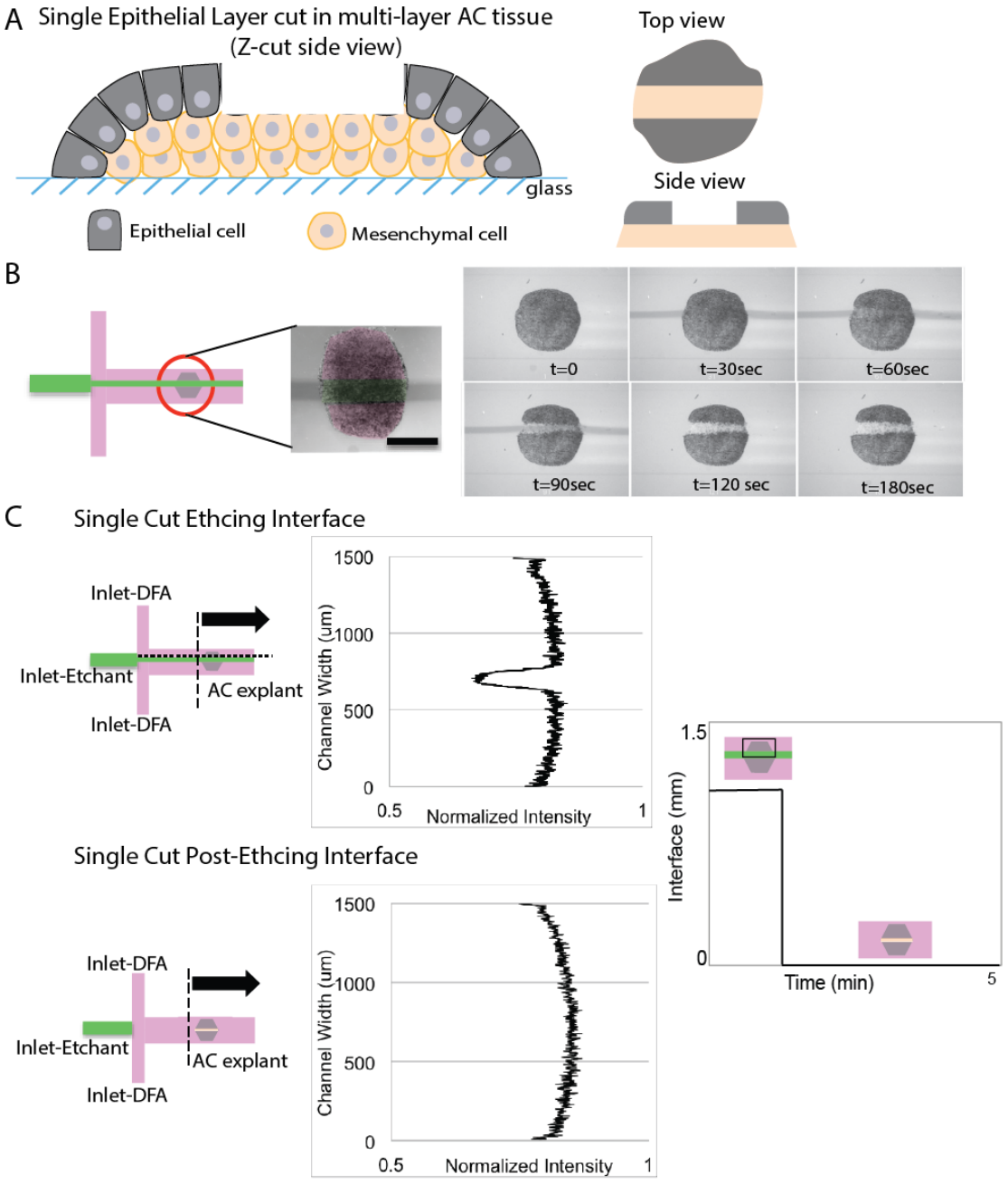

Figure 3.2: Single layer etching of a 3D AC tissue. a) Schematics of a single epithelial layer etched animal cap tissue with top and side views. b) Experimental time sequence of a single cut embryonic tissue undergoing bioetching over 180 seconds. %0.3 SDS was used as etching chemical. c) Interface control over the time with intensity profile over the time during etching. Green center interface is set by R-30 during etching. After the epithelial layer was etched, the center inlet was closed off so that the etchant was no longer on the AC. Side pink interfaces are set by R-10.

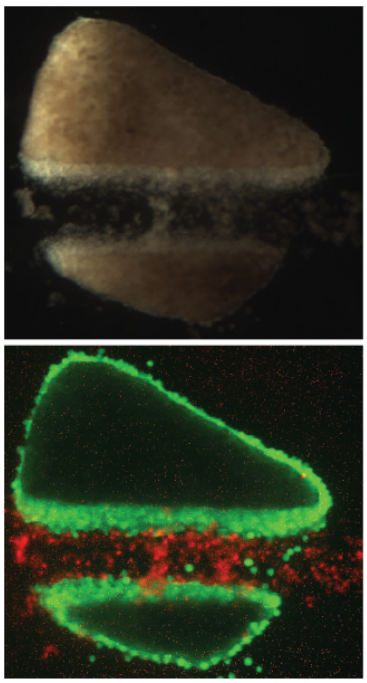

Figure 3.3: Explant viability test. Live/Dead Cell viability assays were used to highlight the viability of the cells after the detergent treatment. This assay confirms that most cells were alive after the detergent treatment. Green: Live cell Red: dead cell

margins within 3D animal cap tissue. The removal of the etchant was also analyzed when the inlet channels was closed (Figure 3.5).

3.6 Alternative etchants

In addition to SDS we tested other detergents, enzymes, and bases for their ability to remove cells from tissues. Detergents have been extensively used to decellularize tissues and organs by solubilizing cell membranes and dissociate DNA from proteins [119]. Sodium dodecyl sulfate (SDS), which is anionic detergent, is effective in solubilizing numerous proteins by disrupting non-covalent bonds within and between proteins. However, detergents can disrupt or dissociate desired proteins from the ECM. Furthermore, SDS may also denature ECM proteins resulting in the potential loss of their native conformation and function. Non-ionic detergents, often called non-denaturing detergents, like Triton X-100 are potentially useful

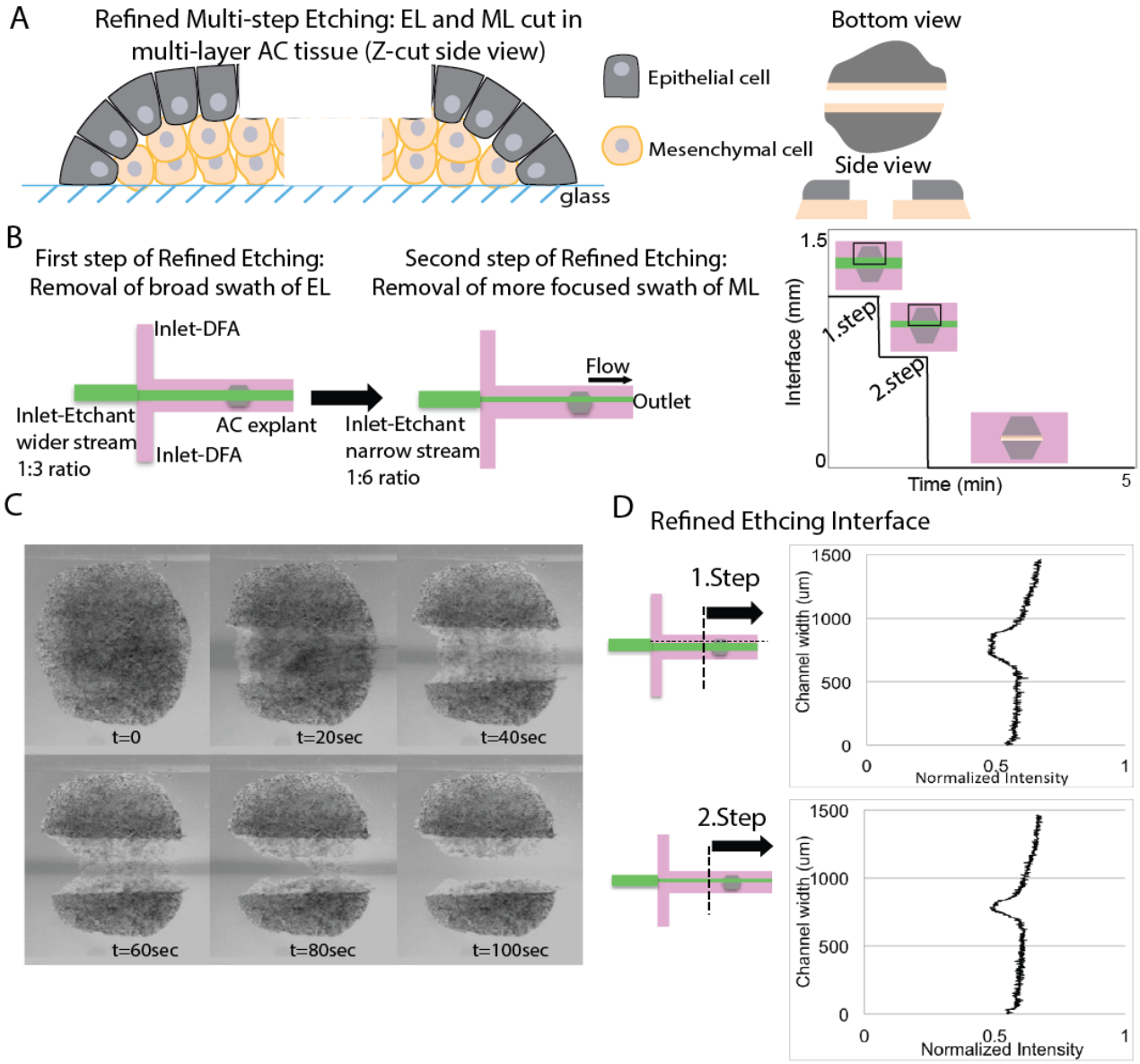

Figure 3.4: Refined etching. a) Schematics of double layer subtractive manufactured animal cap tissue with top and side view. % 0.3 SDS was used as the etching chemical. b) The AC is first exposed using a wider stream to remove a width of the top cell layers. The center inlet resistance is lower to create a wider interface. Second step of experimental technique for double cut embryonic tissue bioetching. Center inlet resistance is higher thus interface is thinner. c) Time lapse images of double etching showing the removal of the top layer and then the bottom layers of cells over 100 seconds. d) Interface control over the time with intensity profile over the time during etching. Center interface (green) is set by R-30 and switched to R-60 during etching. After epithelial layer followed by mesenchymal layer is etched, center inlet was shut down. Side pink interfaces are set by R-10.

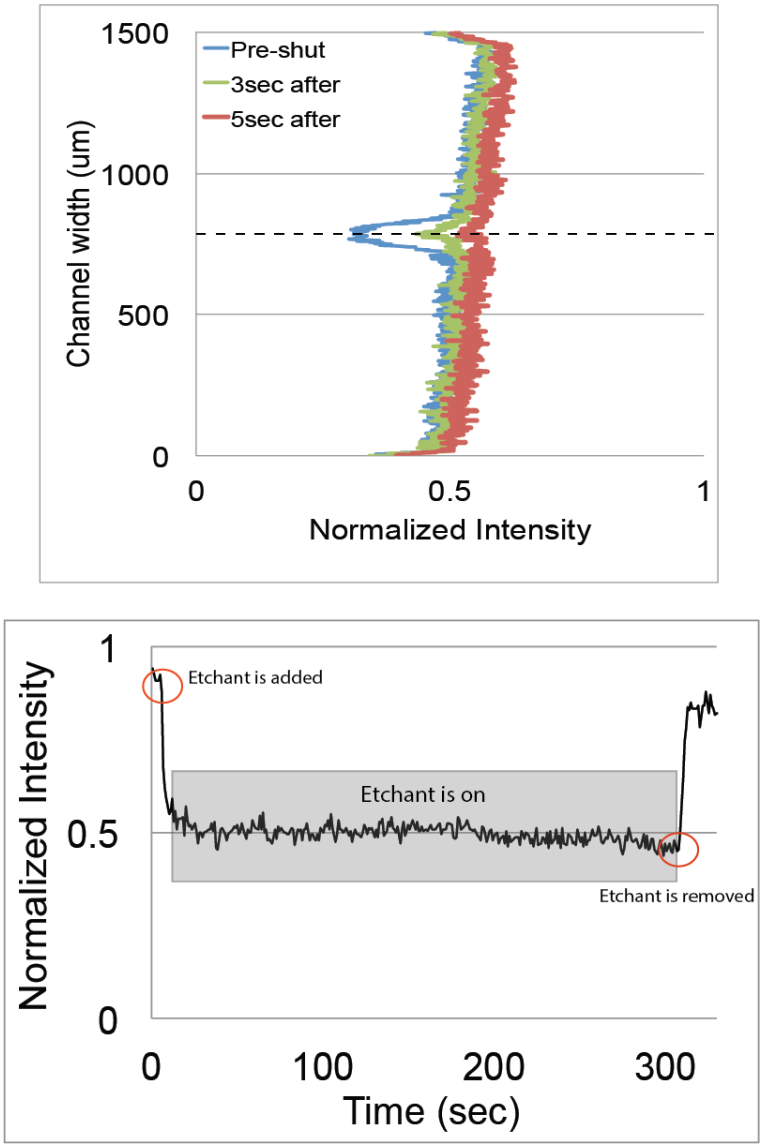

Figure 3.5: Channel kymograph showing the speed of the detergent removal. The intensity profile in the channel was plotted to show how quickly the detergent stream was removed. In 5 seconds, the detergent stream was completely removed. The intensity profile at 760um was plotted versus time to analyze the intensity changes when the detergent stream was turned on and off. Since the detergent was mixed with the dye, the detergent stream intensity profile showed the stream location in the channel.

since they break lipid-lipid and lipid-protein interactions and leave more protein-protein interactions intact. For this reason, Triton X-100 is often used to isolate biologically active membrane proteins. Following our work with SDS, we examined the effects of Triton X-100. We used 3% Triton X-100 as an etchant to create single cuts in the epithelium to expose a

broad swath of mesenchymal cells (Figure 3.6 a). Triton X-100 did not appear to remove the epithelial layer as well as SDS. We noticed that the removal of epithelial and mesenchymal cells within the etched regions took much longer than with SDS..

Next, we used base sodium hydroxide (NaOH) as an etchant, since strong bases can affect ECM mechanical properties and NaOH is known to disrupt tissue architecture [Gall and Pardue, 1969]. Using 0.1M NaOH with the previously described approach for single-cut etching removed a single cell layer within 80 seconds (Figure 3.6 b). Other potential etchants are proteolytic enzymes such as trypsin, which provide high specificity for removal of cell residues and undesirable ECM constituents. Complete cell removal by enzymatic treatment alone is difficult, however, and residual enzymes and partially denatured proteins as well as highly charged nucleic acids may impair recellularization [120]. We used the proteolytic enzyme trypsin as an etchant. Trypsin is commonly used in cell culture protocols to dissociate cell monolayers from substrates, but the ability of trypsin to etch cells locally from a substrate was not known. We found that trypsin did not remove cell layers even when the tissue was exposed for much longer time periods (15+ minutes) (Figure 3.6 c).

3.7 Conclusion

We demonstrated the ability to create and shape 3D tissues with subtractive manufacturing or "tissue-etching" using a microfluidics based approach. While many approaches use 2D environments with monolayers, our unique microfluidic technique provided the ability to control the 3D environment and study the interactions of individual epithelial and mesenchymal layers. We used the animal cap ectoderm of the *Xenopus laevis* embryo as a model system for the study of tissue bio-etching in embryonic cell layers as they are multi-layered with both an epithelial and a mesenchymal layer, and are well suited to microscopy analysis. The cells of the animal cap are considered to have similarities to mammalian embryonic stem cells, which may provide insight into stem cell response in the future as well. Since our

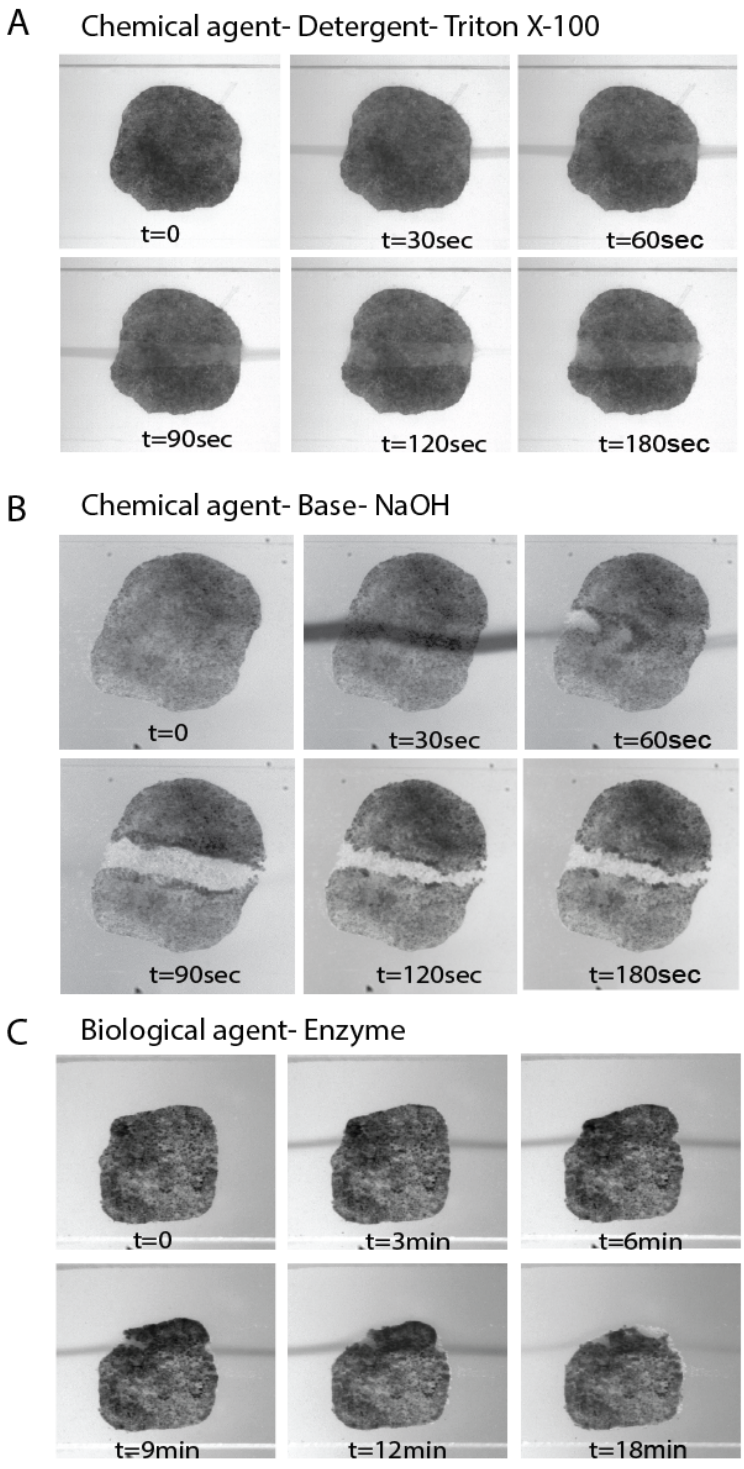

Figure 3.6: Etching of the AC 3D tissue under the application of different etchants. The single cut approach was used and the etchant was applied to the apical side of the AC over time. The deteregents that were used were a) nonionic detergent, %3 Triton X-100, b) base, 0.1N NaOH, and c) biological agent, trypsin.

method introduced a new chemical bio-etching method with a precise spatial and temporal control of the etched area, this precise positioning allowed us to construct novel epithelial and mesenchymal tissue architectures. We are able to induce through single cuts and double cuts tremendous precision in shaping 3D tissues. The deep cells below the EL removed by etchants were not exposed unless the stream remained after the cells dissociated and were removed by flow. Also, short exposures to etchants were quickly washed away with fresh media, which replaced the etchant in the microfluidic chamber. Unlike decellularization approaches, this technique leaves most cells viable. Thus, this 3D tissue-etching assay will be useful in the future to study mechanical responses, collective cell sheet migration, and explore processes that are used to coordinate composite tissues during morphogenesis. The ability to control the form of multicellular 3D tissues will have high impact in the allied fields of tissue engineering and regeneration medicine as well as insight into cancer and stem cell biology.

Chapter 4

Studying Collective Cell Migration of Multi-layer Embryonic Tissue Using 3D Bio-etching

4.1 Collective Cell Migration

The coordinated cell migration is critical to embryonic development, homeostasis, complex organs systems, and diseases such as cancer [111]. Therefore, studying collective cell migration to understand these important topics, several model organisms such as *Xenopus laevis* [21], *Drosophila melanogaster* [22], *Danio rerio* [23] are used to determine what molecules are important in initiating, maintaining and guiding moving cells. In such migration, cells move collectively as sheets, strands or clusters by using the guidance of numerous chemical and mechanical signals [121]. In single cell migration, cells move individually and change their location from one place to another in response to the cues that exist in the environment [122]. Collective migration, though, is different from single cell migration in that collections of individual cells function as a single unit and stay adhered to each other as they move, which results in migrating cohorts that varies degrees of tissue organization [123–125].

Collective cell sheet migration is an important process that sculpts the shape of an organism and its internal tissues during early development [26]. Hence, failure of collective cell migration during development causes fatal consequences like immunosuppresion, autoimmune diseases, defective wound repair, or tumor dissemination.

Morphogenesis consists of a complex series of cell signaling, migration and differentiation that are coordinated during both embryo development and cases of tissue self-assembly [125]. Developmental model systems such as *Xenopus laevis*, a carnivorous claw-toed frog native to Africa, have been widely used to study intricate development processes such as patterning and morphogenesis during gastrulation. *Xenopus* embryogenesis consists of serial important processes starting within the first 90-minute cell cycle at 21°C. After the first division, cell proliferation is rather fast with 20 to 30 minute intervals. About seven hours after fertilization, when there are 4096 cells (after 12 cleavages), the embryo begins to change dramatically. Cell division intervals increase to four hours, and cells start to change their shape to become more elongated and bottle-like [**?**,**?**]. At the mid-blastula stage, the embryos have three regions– the animal cap (AC), marginal zone and vegetal mass (Figure4.1) [8].

After mid-blastula transition is completed, cells at the surface start relocating to more interior locations. This orchestrated movement is defined as gastrulation where a ball of cells turns into multi-layer tissue. Convergent extension of these bottle-shaped cells creates a dorsal lip of blastopore which is an indicator of the beginning of gastrulation [126]. During gastrulation, the embryo is dramatically restructured by processes such as cell migration [20].

Gastrulation is crucial to the proper development of all multicellular animals, especially those with complex tissues (Figure4.2). Collective movements *in vivo* are key to the gastrulation where single embryonic layer blastula is rearranged to form three layer structure (ectoderm,mesoderm,endoderm). Each layer gives rise to specific tissues and organs in developing embryo.

Formation of the ectoderm is essential for establishment of the epidermis and nervous

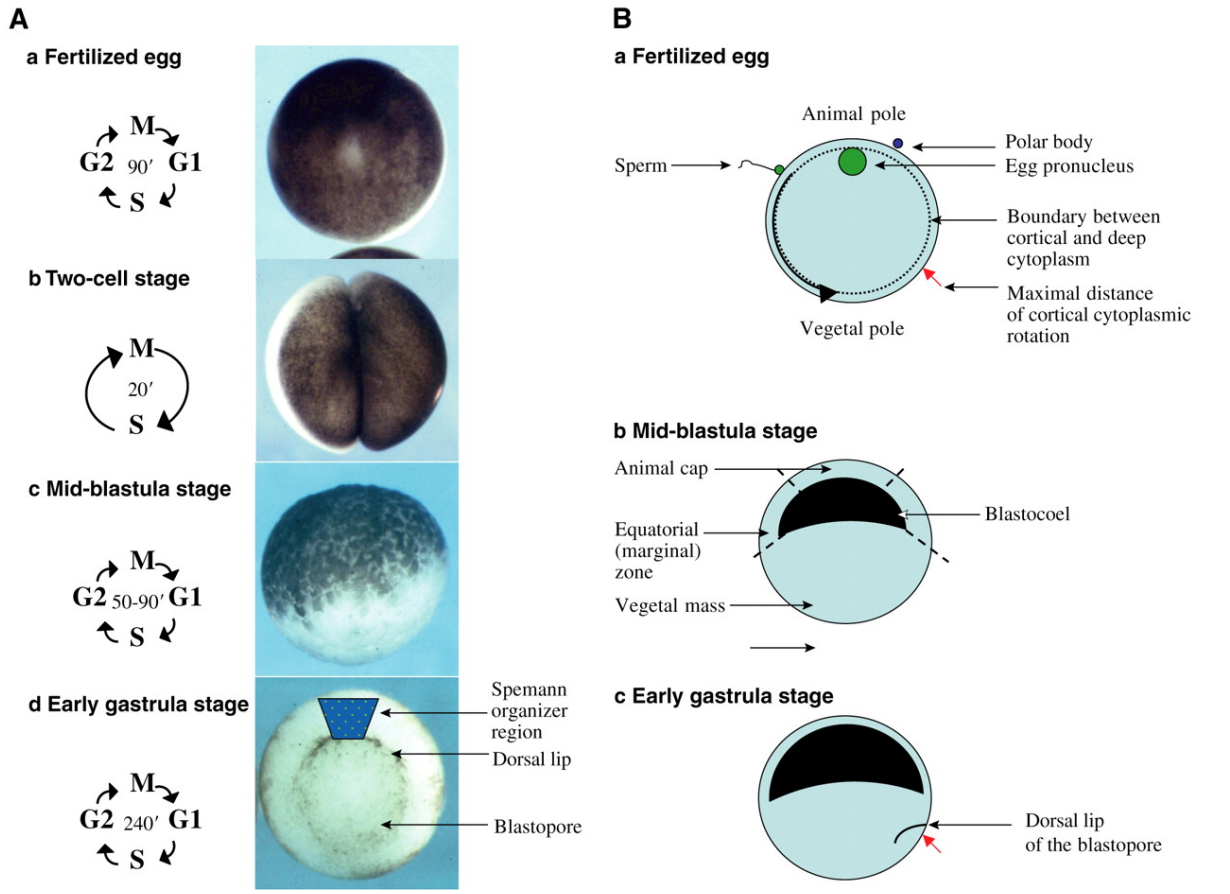

Figure 4.1: Characteristic of *Xenopus laevis* early development. **A)**Different stages of *Xenopus laevis* embryos. **B)**Schematics of sliced sections from different stages. [8]

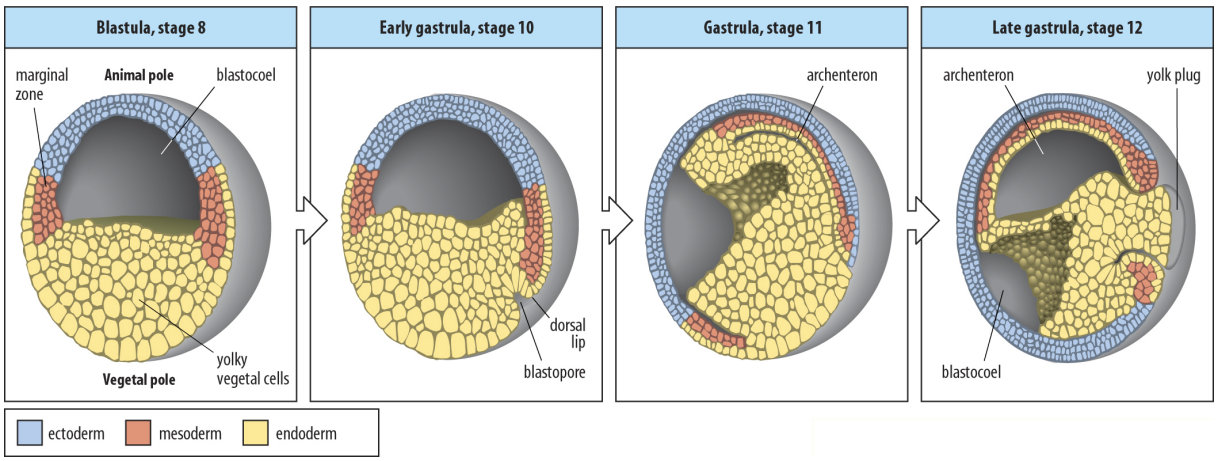

Figure 4.2: *Xenopus laevis* blastula stage fate map showing primary germ layers: Ectoderm, Mesoderm, Endoderm. [9]

system. In this thesis, I used tissues microsurgically isolated from embryos of *Xenopus*, the animal cap, which are fated to be ectoderm later in normal development. *Xenopus* embryos are used to elucidate genes important in morphogenesis and here provide a model for collective migration of a complex tissue.

The animal cap tissue is a composite tissue with two layers: epithelial (pigmented cells, facing external media) and mesenchymal (non-pigmented cells, lower tissue facing interstitial media) layers. These layers can be dissected from the embryo (dashed lines; Figure 4.1). Dissected animal cap tissue survive and continue to develop its pre-programmed fate as it would in an embryo in a simple salt solution for several hours. Importantly, the *Xenopus* animal cap does not respond to nonspecific biological perturbation but respond differentially to molecules that are active in the environment and can differentiate into specific types of neural, mesodermal, and endodermal tissues (Figure 4.3). Hence, the cells of the animal cap are equivalent to mammalian embryonic stem cells. Finding from *Xenopus laevis* AC studies underlie many recent advances in stem cell biology [10]. Animal cap tissues (AC) are an excellent model to investigate the coordinated cell movements within multilayered tissues since it is multi-layered. In contrast to the studies of collective cell movements in epithelial monolayers of cultured cells, multi layered animal cap tissue can reveal information about collective cell migration and tissue self-assembly in composite tissues.

Animal cap tissue has always been popular model for understanding cellular activities from the one-cell stage to organ level as animal cap tissue goes through massive cell rearrangements that are crucial for the animal's fate during gastrulation. During epiboly, which occurs at the same time as gastrulation, cell layers start to spread and thin. Animal cap tissues begin five to six cells thick and thins to two cell layers by the end of gastrulation [11]. Studies showed no evidence of death but rather showed that deep cells rearrange their shapes, thin and extend from thick multilayers to one thin layer [127]. Though individual cell movements have been described [127, 128], the cellular mechanisms behind these movements have not been revealed. Conventional studies target the functions of certain signaling pathways of

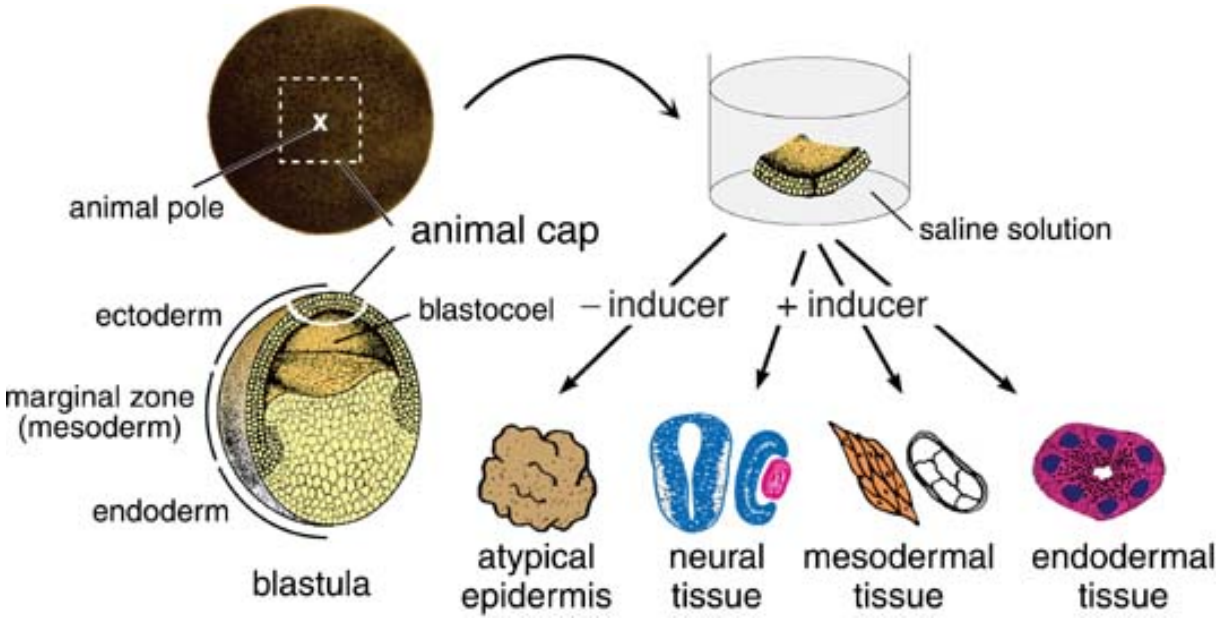

Figure 4.3: Animal Cap Assay [10]

an individual cell layer to be able to understand the multilayer mechanism of thinning. Multi-layer mechanisms might be challenging to anticipate from single layer studies, since multiple signals plays role in a spatiotemporal manner. However, understanding multi-layer coordinated movement is also important in the areas of biotechnology to engineer artificial tissues and develop new techniques to control tumor cells.

Similarly, wound healing is a critical part of human physiology that involves numerous synchronized events including inflammation, tissue formation and remodeling [?, ?]. While wound healing is common across many organisms, the ability to reestablish tissue integrity involves many events including chemical and mechanical processes [?, 129] . The chemical and mechanical components are an integrated response with 3D features that enable repair to occur. In embryos, wounds heal faster and without a leaving scar, and thus there is an interest in understanding wound healing in embryonic level to improve the adult wound healing [129, 130]. Understanding the 3D nature of this process would provide advances on numerous fronts including developmental biology and regenerative medicine. Most wound healing studies are carried out in 2D with single layers of cultured epithelial cells adhering to

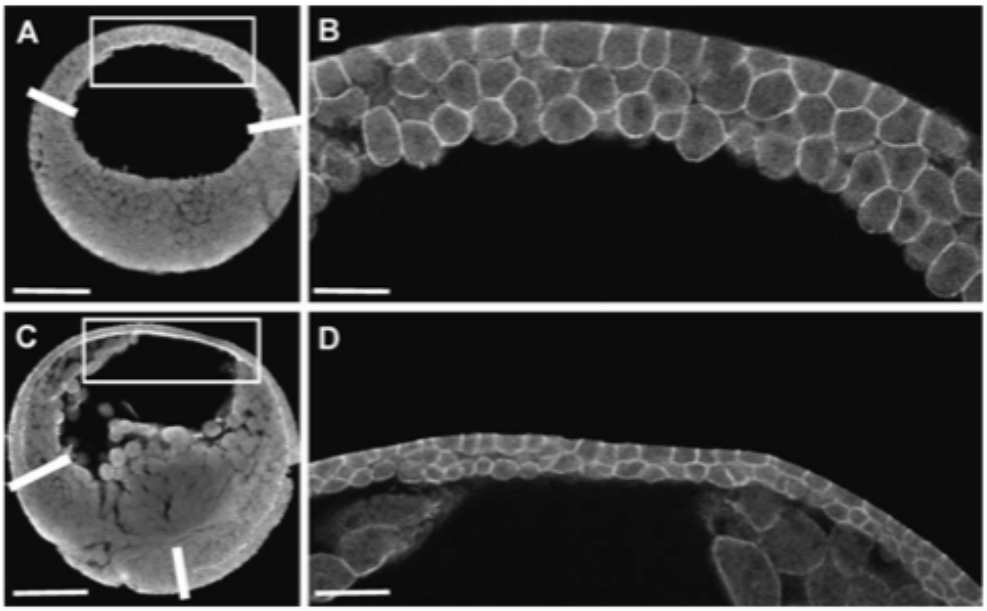

Figure 4.4: Animal Cap thins during gastrulation. A and B shows the beginning of the gastrulation (stage 9) and C and D shows the end of the gastrulation. Cell outlines visualized using antisera to C-cadherin (scale bars = 300 μm in A and C; scale bars = 75 μm in B and D) [11]

rigid substrates such as glass or plastic. But in real tissues, the intricacies of the 3D microenvironment and complex 3D responses are extremely important to more fully understand and address wound healing.

A recent study revealed complex interactions between a heterogeneously patterned substrate and the cell mechanics that guides collective migration. These interactions resulted in the formation of multicellular "bridges" [14]. Studies of these collective cell movements have focused on the behavior of epithelial monolayers of cultured cells such as Madin Darby canine kidney MDCK cells. By contrast, most embryonic development and tissue self-assembly requires the integration of cell movements within multiple cell layers composed of different cell types. Although the role of cell mechanics in tissue self-assembly has been demonstrated, little is known about the mechanical response of the multi-layer tissues to environmental cues. One of the reasons for this knowledge gap is the lack of the technologies to analyze the individual responses of epithelial and mesenchymal cell sheets in a multi-cell layer tissue.

4.2 Studying Collective Cell Migration Using Microfluidics

Microfluidics provide highly controlled spatial and temporal chemical patterns to overcome the complications of traditional methods. Understanding the underlying signaling pathways of collective cell functions requires highly regulated control mechanisms. Since scale of size is well matched to physical dimensions of biological studies, microfluidics have been used in cellular biology to utilize laminar flow benefits of delivering precise chemicals. However, these studies are mostly limited to either single cells or monolayer sheets. Cells must communicate to combine into networks, such as tissue and organs. Thus higher levels of organization is required to make assumptions for a 3D animal models. Bio-etching technique gives the opportunity to study collective cell arrangements in 3D fashion. I used unique 3D microfluidics approach to examine integrated 3D responses of cell mechanics and cell-cell interactions in a more realistic system using *Xenopus*. My experiments suggest the hypothesis that complex tissues, composed of multiple cell types including both epithelial and mesenchymal cells are mechanically coupled and that by locally inhibiting the mechanics of specific layers I was able to expose novel features of collective migration within the integrated tissue.

Using a custom-designed microfluidic control system to deliver a range of tissue etching reagents (detergents, chelators, proteases, etc.), I etched the desired width and depth of the superficial epithelial and deep mesenchymal layers using different types of etchants as described in Chapter 3. Bio-etching allows me to produce different classes of wounds and analyze coordinated responses of the remaining tissue.

4.3 Collective Multi-layer Response to "Subtractive Manufacturing" of Single Layer Bio-etching

Removing select cells from the epithelial layer left a discontinuous region of epithelial layer(EL) being intact with mesenchymal cell layer(ML). Previously, laminar flow of trypsin solution in microfluidic channels has been shown as an example of wound healing assay (Figure 4.5). 2D scratch wound assays are used to asses the following parameters: speed of wound closure, width of the defect, cohesiveness of the cell-cell junctions and individual or collective cell polarization and migration [29]. Contrary to these 2D studies, this system provides well-controlled cell removal of a portion of 3D integrated tissue as opposed to monolayer examples.

I specifically focused on the cell migration in the top layer, as the epithelial cells move to "heal" over the mesenchymal cell layer (Figure4.6b). To track the movement, I had options such as the replaying time lapse movies, creating kymographs and strain maps. I used the kymograph to see the dynamics by using ImageJ (Figure4.6c). Kymographs of the vertical line(dotted) in the center of the tissues were used to show the dynamic responses effectively. This kymograph clearly showed that in the process of epithelial layer healing the center of the tissue edge of the explant stopped spreading and involved to wound healing. This shows the distance of signal transmission within the tissue or strain equilibrium in response to closing the gap in the middle. I also noticed from kymographs that speed of closure was higher than normal speed of AC spreading. To examine further, I looked at the area decrease of etched area over the time to quantify cell movements (Figure 4.6d). It is clear from Figure 4.6 d that more than half of the closure of the etched area was completed in first 20 minutes. For the first few minutes, the speed of closure seemed to be higher than the rest. Additionally, I plotted the intensity profile over time to examine the behavior of epithelial cells in first 20 minutes compared to the rest (Figure 4.6e). Since epithelial layer dark pigmented and mesenchymal layer is non-pigmented, intensity profile pictures the etched area as etched

areas intensity is lower compared to non-etched areas. Intensity graph also indicated the differences in speed of cells within first 20 minutes.

I used custom written macros to calculate the velocity and displacement values from time lapse movies that are acquired with steremicroscope (Figure 4.7). Images are collected every second for bio-etching stacks and every minutes for healing stacks. First, I used segmentation to generate masks for every image from left over EL. Segmentation creates binary stack for macros. Macros written by Dr. Holley E. Lynch used the mask to find the centroids, and then draw a line at given angle from the centroid to linearly calculate the edge movement from centroid. This macro tracks the edge for every image that are given and calculates the velocity and displacement for every pixel on the line. I used linear displacement macro to analyze free edge of two layers and EL movement. Velocities are presented in microns per minute. Velocity graph (Figure 4.7 a) highlighted a peak in the velocity in first few minutes of healing. Although the fastest known cell speed is 600 microns per hour by keratocytes [131], this peak is equal to 1000 micron per hour. Displacement graph (Figure 4.7) shows that free edge of two cell layer,the other edge of remaining EL also stopped spreading and contributed the healing process although the speed of that edge is not as high as free edge of EL. A potential explanation for outer edge being not as fast is the distance from the removal area. The difference in displacement values indicates that explant is experiencing high strain. Overall, this single layer bio-etching provided us free edge of epithelial layer to study the response of removing neighboring cells on mesenchymal cells in more 3D relevant environment.

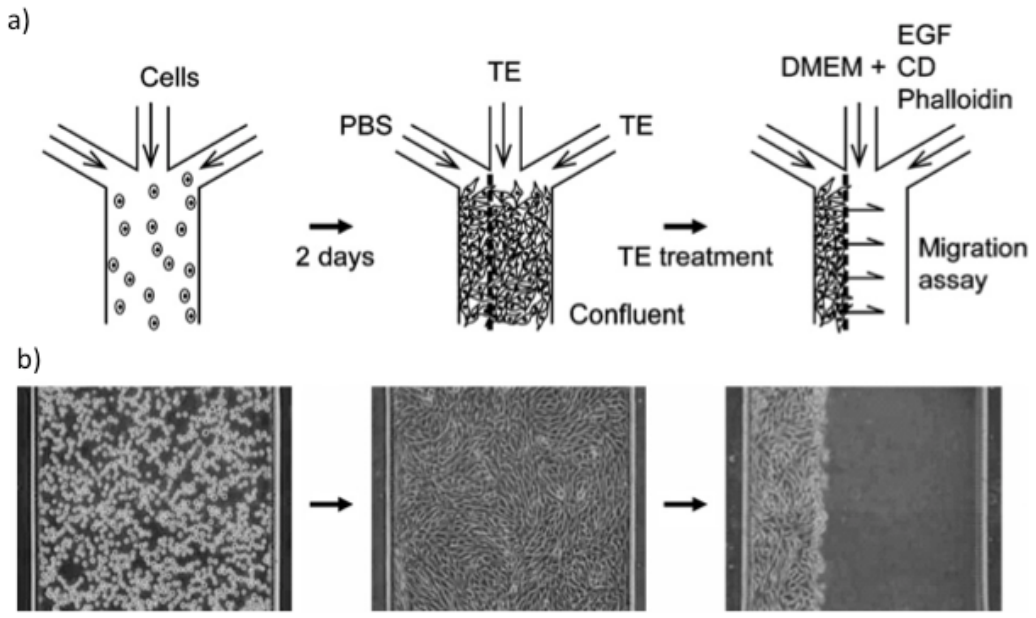

Figure 4.5: On-chip monolayer cell migration assay using microfluidic channels [12]

4.4 Collective Multilayer Response to "Subtractive Manufacturing"

I then used multi-step subtractive manufacturing to remove a desired part of the epithelial and mesenchymal layer to further test if these two layers are mechanically connected in complex tissues, and if superficial layers provide cues that coordinate collective migration in deep cells. Deep cells contribution to collective cell migration is often ignored because of the lack of the technology to study the layer under another. Davidson *et. al.* studied the excision wounds in whole embryo [13]. In this paper, mesenchymal and epithelial and mesenchymal layer behavior were studied in response to microsurgical wounds. They showed that deep cell contraction and ingression was responsible for wound healing in *Xenopus laevis* animal caps (Figure 4.8).

Here, I connected the fluidic resistances in parallel to be able to increase the resistances simultaneously at desired time during experiment. The relation between pressure drop along the channel downstream and the flow rate Q is analogous to Ohm's Law for electrical circuits

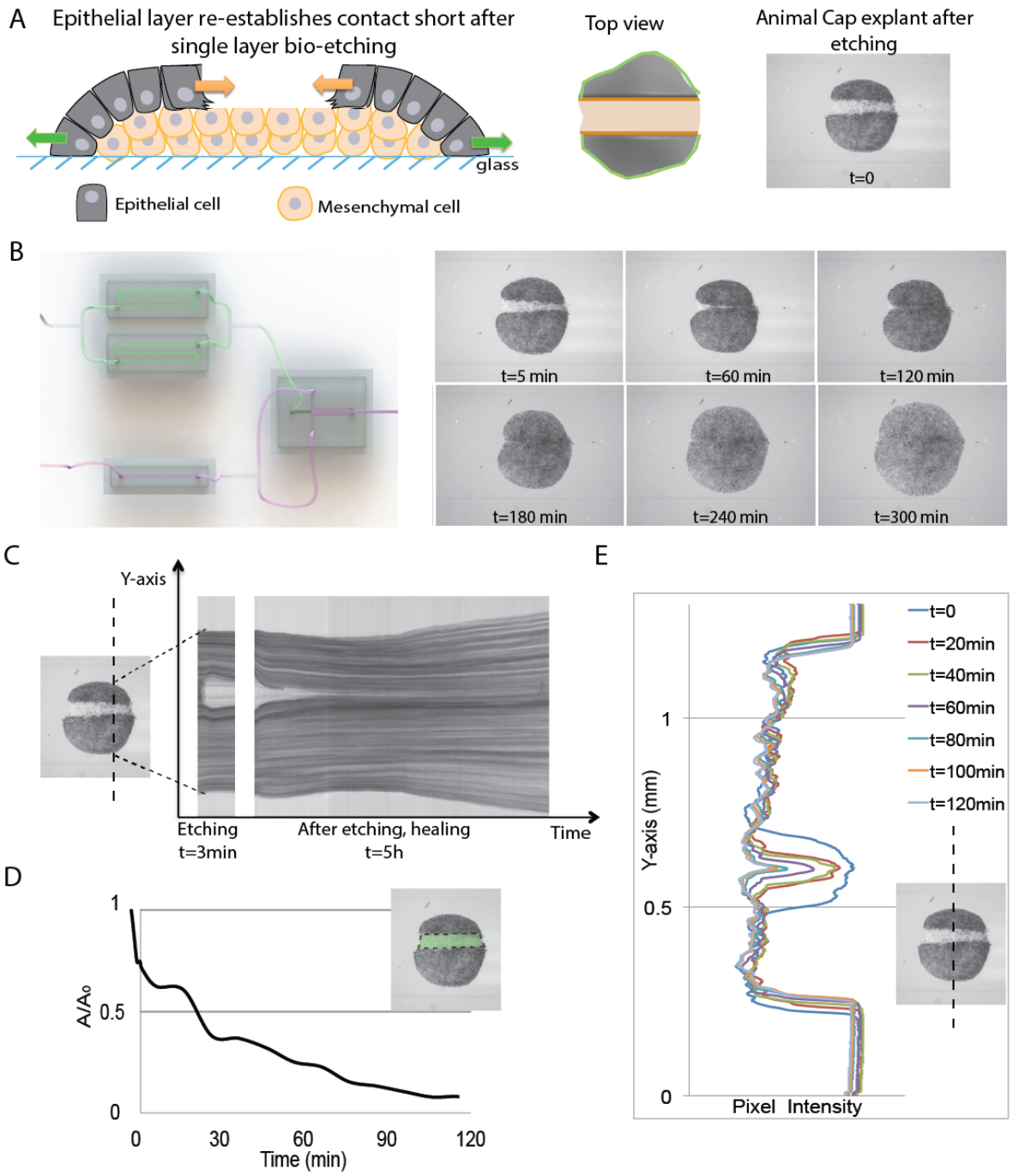

Figure 4.6: Single Cut Healing a)Schematic of single layer etched tissue with Z-cut side view and top view. Real picture of AC explant in the tissue right after etching is stopped. Green represents free edge of two cell layer. Orange represents free edge of EL. b) Schematic of microfluidic setting for single layer etching and time lapse of healing AC for 5hours. c) Kymograph of the etching and healing. Vertical dotted line shows where the data collected. d) Healing of etched area. A0 is initial green area. e)Intensity profile of healing over time. Vertical dotted line shows where data is collected.

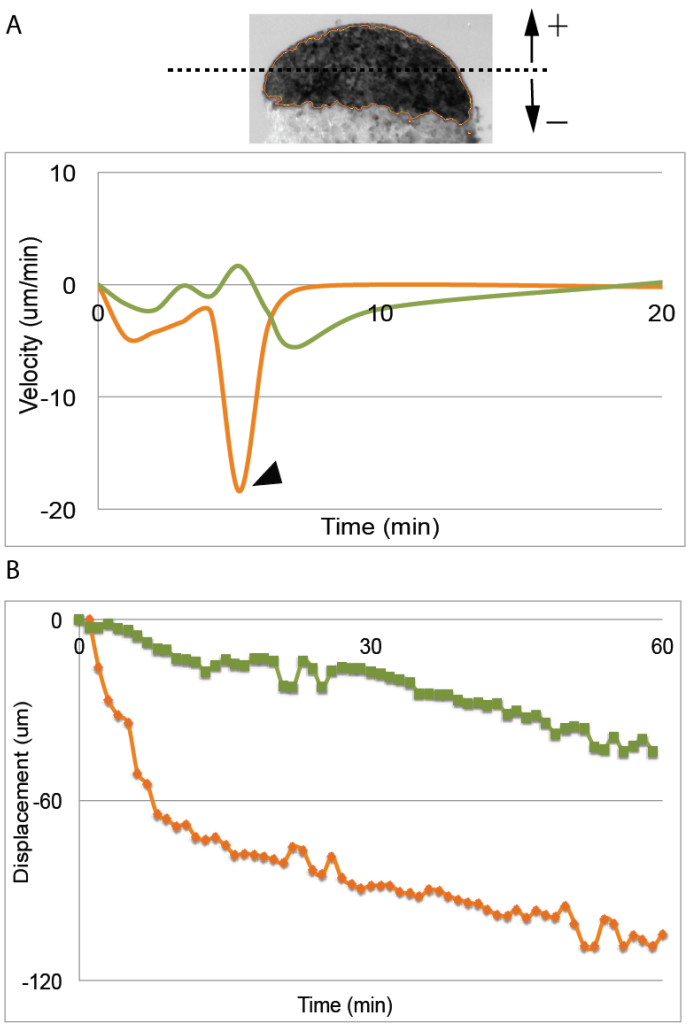

Figure 4.7: Velocity and displacement graph of single layer bio-etching healing a)Velocity values of remaining EL layer over first 20 minute. Free edge of EL shows a drastic velocity peak in first few minutes. It is equlivant to 1000μm/h(arrow head). Free edge velocity peak is followed by free edge of two cell layer immediately. b) Free edge of EL and two-cell layer displacement over 60 minutes. Velocity and displacement are calculated from the distance from the centroid of remaining EL (dotted line) to edges.Green:free edge of two-cell layer Orange: Free edge of EL

with fluid pressure drop for electrical potential difference. Considering N element with individual resistances R_m, m= 1,...,N, there are two simple situations the resistances are either in series or in parallel, as is familiar from elementary courses: When the elements are

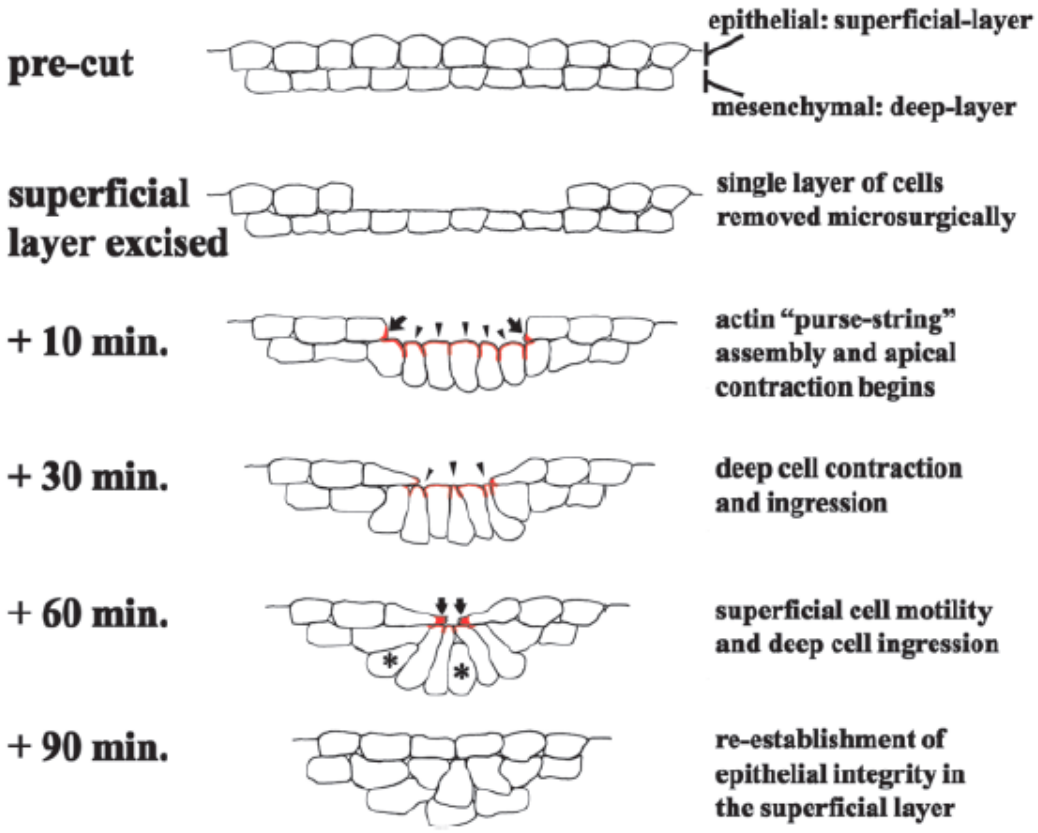

Figure 4.8: Steps in embryonic wound healing in the *Xenopus laevis* animal cap ectoderm in response micro surgically removal of epithelial cell layer [13]
.

placed in series, the effective resistance R_eff of the combination is:

$$Reff = \sum_{m=1}^{N} R_m \tag{4.1}$$

In contrast, when elements are placed parallel, the effective resistance R_eff is:

$$Reff = \frac{1}{\sum_{m=1}^{N} R_m^{-1}} \tag{4.2}$$

Using this notion, I used a microfluidic system in which pressure is regulated by resistances that were placed in parallel(Figure 4.9). This configuration helped me to change the interface in the channel during the experiment in seconds. With this design, the width of the center

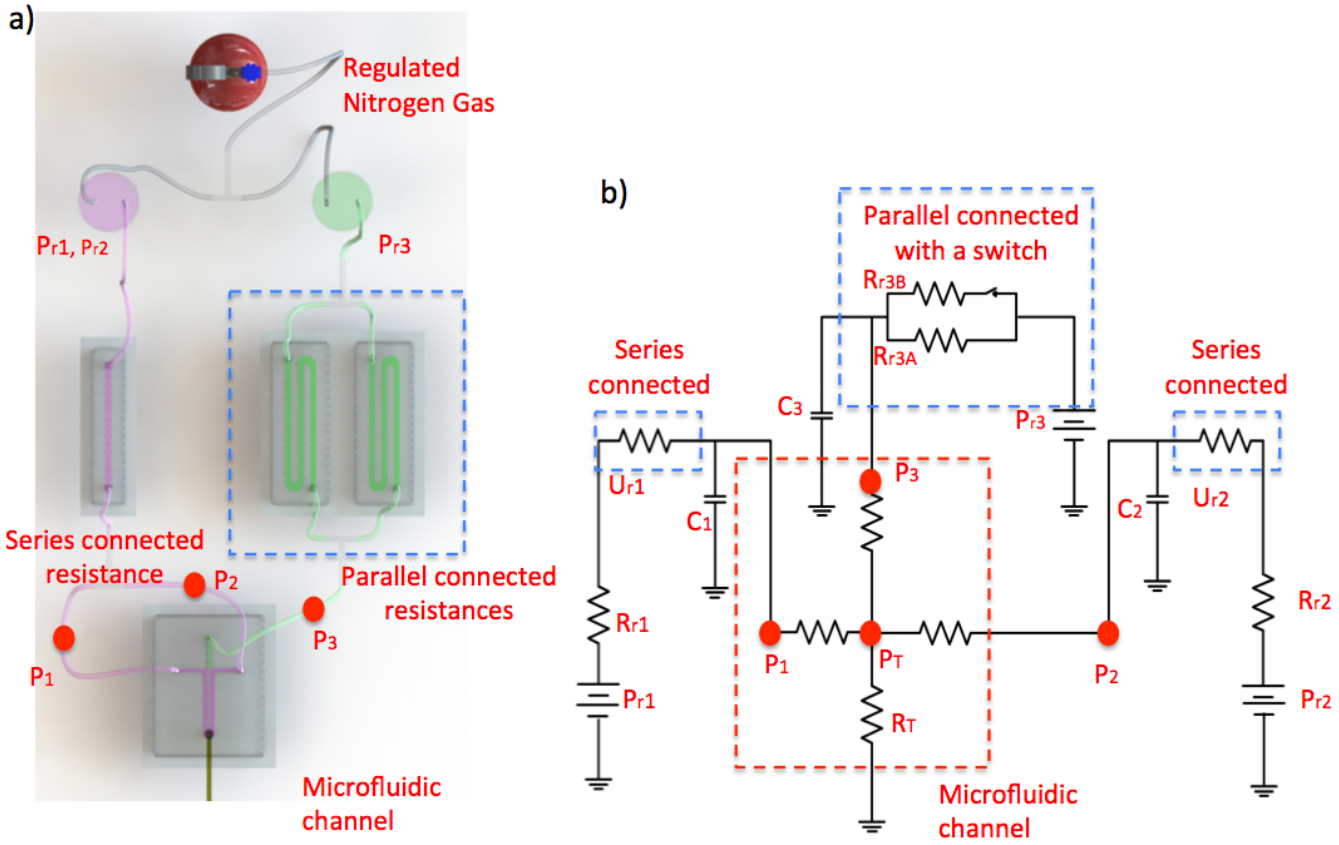

Figure 4.9: Interface control for refined etching a) Schematic of pressure regulation system. b) Fluidic circuit diagram of the system for refined etching.To change the interface, at the first step, switch is on(both valves are open), at the second step, switch is off (one of the valve is closed) in the third modular mechanism.

inlet is regulated and manipulated without any need to stop experiment. Simply changing the resistances from R-30 to R-60 provided me a wide and then a narrow stream(half width), and so I used these two different widths of detergent stream to etch the EL and ML layer, respectively.

Here, I used refined bio-etching technique in two steps. First, I connected the resistances parallel which makes the total resistances and thus the flow rate lower (Figure 4.9b). With this interface, I first etched the desired epithelial layer. I collected time lapse sequences every second. Once the epithelial layer was cleaved, I closed one of the R-60 resistance valve resulting in a higher resistance in the center inlet. Because of the drop in flow-rate in the

middle channel, middle interface becomes narrow. In the second step, desired (half width of epithelial etched) mesenchymal stripe was cleaved. Carefully looking at the movies whenever the desired mesenchymal layer is etched, middle inlet valve is closed off and I collected time-lapse movies every minute for 10 hours to capture the response of AC to refined bio-etching (Figure 4.10).

Refined etching technique is a great way to study mechanical coupling between layers since this double step subtractive manufacturing provides a 3D environment to study multicellular interactions. After multi step refined etching, epithelial and mesenchymal layer both have etched areas leaving two "islands" behind. At this point, animal cap is not intact but etched three-dimensionally (Figure 4.10a). The epithelial layer and the mesenchymal layer show behavior resembling wound healing to close the etched area. Mesenchymal cell layer contracts immediately and keep contracting until EL spreads back again. There seems to be a communication and "help" between these two cell layer that has not been shown before. That makes the system a very unique tool to study collective reorganization and migration in response to removal of their neighbors. Explant attachment experiments were imaged with a digital charge-coupled device (CCD) camera mounted on a stereoscope. Computer-controlled acquisition software was used to collect time-lapse sequences to collect the data for long hours until the explant completely "heals" and start spreading again (Figure 4.10b). Time-lapse movies are analyzed using ImageJ. First I looked at the information about cell movements with kymographs (Figure 4.10c). Kymographs are very powerful to highlight the cell movement within the explant. Kymograph graph data is collected from the dotted line shown Figure 4.10a. The kymograph shows the same peak velocity that was observed with single layer etching within first minutes. Hence, I plotted the velocity differences in two types of free edges in response to refined multi step etching (Figure4.10d) to depict the peak velocity. Velocity analysis showed that epithelial cells moves much faster than they normally do especially right after the etching. Animal cap cells migrate with a speed of 50μm per hour, but here within the first few minutes, their speed goes up more than 1500μm per hour

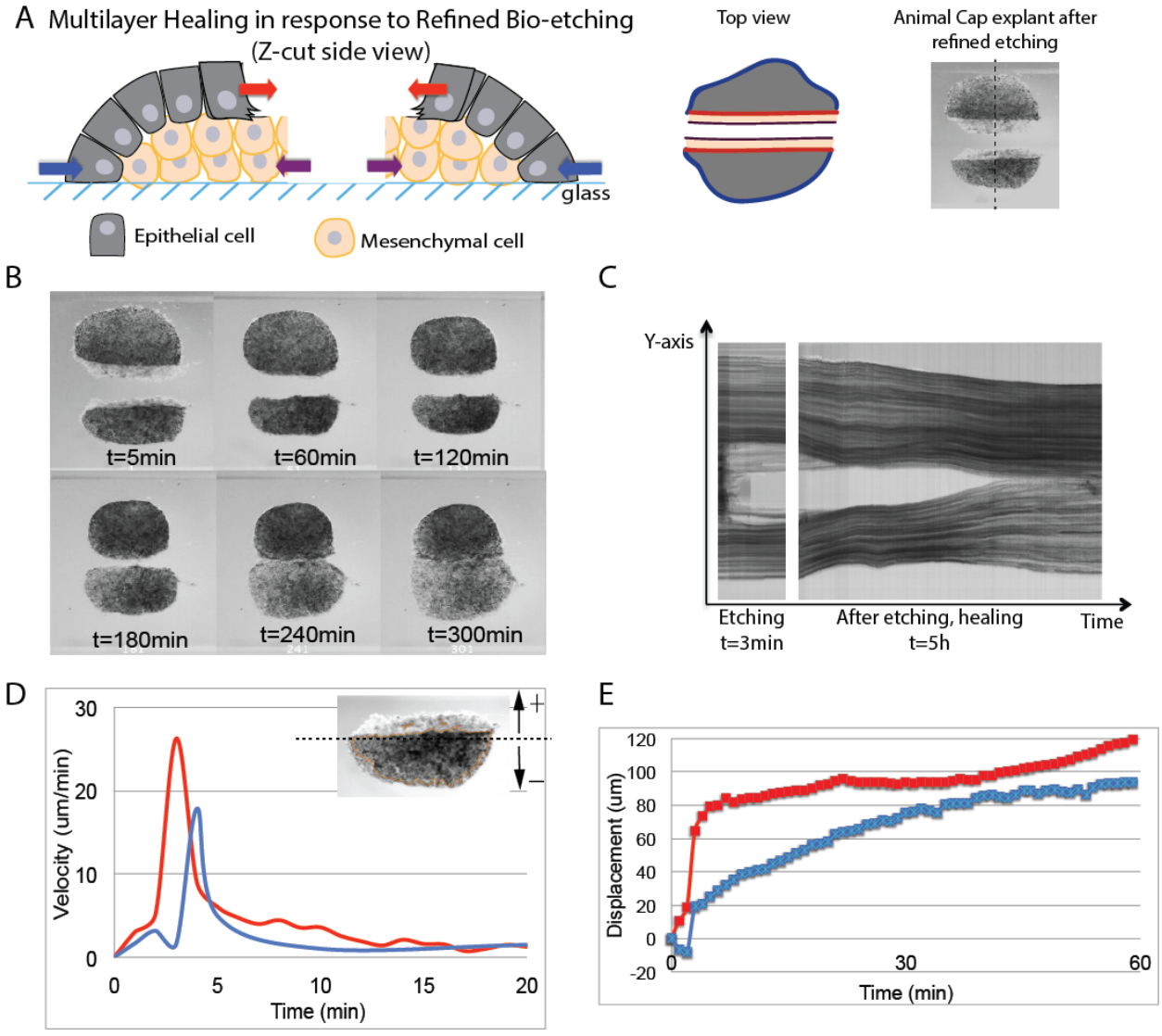

Figure 4.10: Refined Bio-etching Healing a) Schematic of refined etched multilayer animal cap. Red:free edge of EL. Blue: free edge of two cell layers. Purple: Free edge of ML. Real picture shows where the etchant is turned off thus where the healing starts. b) Time lapse images of refined-etched healing animal cap tissue using stereomicroscopy. c) Kymograph of multilayer etching and healing response. Dotted line above indicates where the data is collected. d) Velocity differences of free edge of the EL and free edge of two-cell layer. The free edge of the EL peaks up to 1500um in an hour. e) Differences in displacement at the two different edges when layers are moving to reestablish their contact.

which is even more than any known speed of any type of cell and faster than single layer etching. My hypothesis is because of the mesenchymal cell layer contribution. I hypothesize that mesenchymal cells attach to the leading epithelial cell and pull it while they ingress and

contracts as it is shown (Figure 4.8).

It was shown that healing is driven by deep cell contraction and ingression. On the other hand, refined multi-layer etching causes explant to lose contact with the other half of the explant. The data shows that the epithelial layer moves towards the etched area of mesenchymal layer first to regain the missed contact with etching. During this time, the mesenchymal layer stops its own fated behavior of spreading and rather contracts until the epithelial layer completely covers the mesenchymal layer. Then they start spreading together (Figure 4.10 b t=180-300min). After second step, ML etching especially, cells have no way of communicating because of the flow in between. However, two pieces of remaining cell layers seemed to migrate back and reestablish their contact with the other piece before they start spreading again. I suspect the fibrils that might be left over from the cells that have been etched that cells prefer to spread that area. Additionally, judging from the physical connectivity of the outer edge-free edge of the two cell layer- and the inner edge velocity-free edge of epithelial cell layer-, I believed that there is a mechanical coupling between these two cell layers (Figure 4.10 e). Also, one easily can see the strain that explant is experiencing during this migration by looking at the displacement differences between two edges.

I also expressed live cell reporters such as plasma membrane targeted GFP, histone labeled H2B, and use real time inverted confocal microscopy to reveal fine scale cellular responses to micro-environmental features. To express live cell reposters, messenger RNAs (mRNAs) are injected at one cell stage within 90 minutes after fertilization(before first division) to have a even distribution of fluorescence in the embryo. To inject, sharp micro needle are prepared using micropipette puller. Pulled needles are kept sterile and should not be touched without gloves. Embryos that are transferred to Ficoll solution are injected using micro-manipulator. The micro-manipulator applies certain amount of pressure to push out certain amount of liquid out from needle. This pressure is determined by the amount that is being injected. Oil can be used to make bubbles thus measure the right amount before injecting the embryo. Using the manipulator, I usually inject 3 times from animal side of the embryo

and embryos are cultured as usual. First I injected 70K dextran as cytoplasm marker. I etched as described above and fixed the explant. Fixing explant preserves the shape of the cells and provides valuable information about cellular architecture right after etching. Then, I injected live reporters of GFP and H2B to reveal the mechanism in the mesenchymal side in high resolution. GFP (magenta) was used to label the cell membrane where H2B (yellow) was used for nucleus. For confocal movies, microfluidic chambers with explants housed inside were placed on an x-y position controlled stage, and time-lapse sequences for translocation experiments were recorded using a confocal scanning head (Leica TCS SP5: Leica Microsystems, Bannockburn IL) mounted on an inverted compound microscope. Confocal images with fluorescing explants give more detailed information at cell size level from the mesenchymal layer side whereas stereoscope gives more collective migration info from the epithelial layer side(Figure 4.11a). Etched explants were moved to confocal and I acquired time lapse movies for healing to study the dynamic cellular mechanism with high resolution confocal imaging for 5 hours (Figure 4.11 b).

Time-lapse sequences were analyzed either manually or with custom-image processing macros (ImageJ). This confocal lime lapse movies indicated that the EL immediately to migrate toward etched area with very high speed. In the mean time the ML contracts and shrinks in size (Figure 4.11 c). This graph depicts the mechanical coupling and collective movement in response to removal of neighboring cells. Retraction of ML usually last an hour and within this hour EL covers ML and they start migrating towards etched area in cohorts. Free edge of two-cell layer also moves towards etched area as a result of transit chemical signals. When continuous tissue is broken, chemical signal from wounded edge enhances forces towards free surface in result of large lamelipodia. Every cells contributes and generates traction forces in the order of the distance to wounded edge [132]. In results of this arrangements in tissue, two cell layer outer edge migrates in a slower rate (Figure 4.11 d).

I showed the synchronized cellular behavior in response to removal of neighboring cell

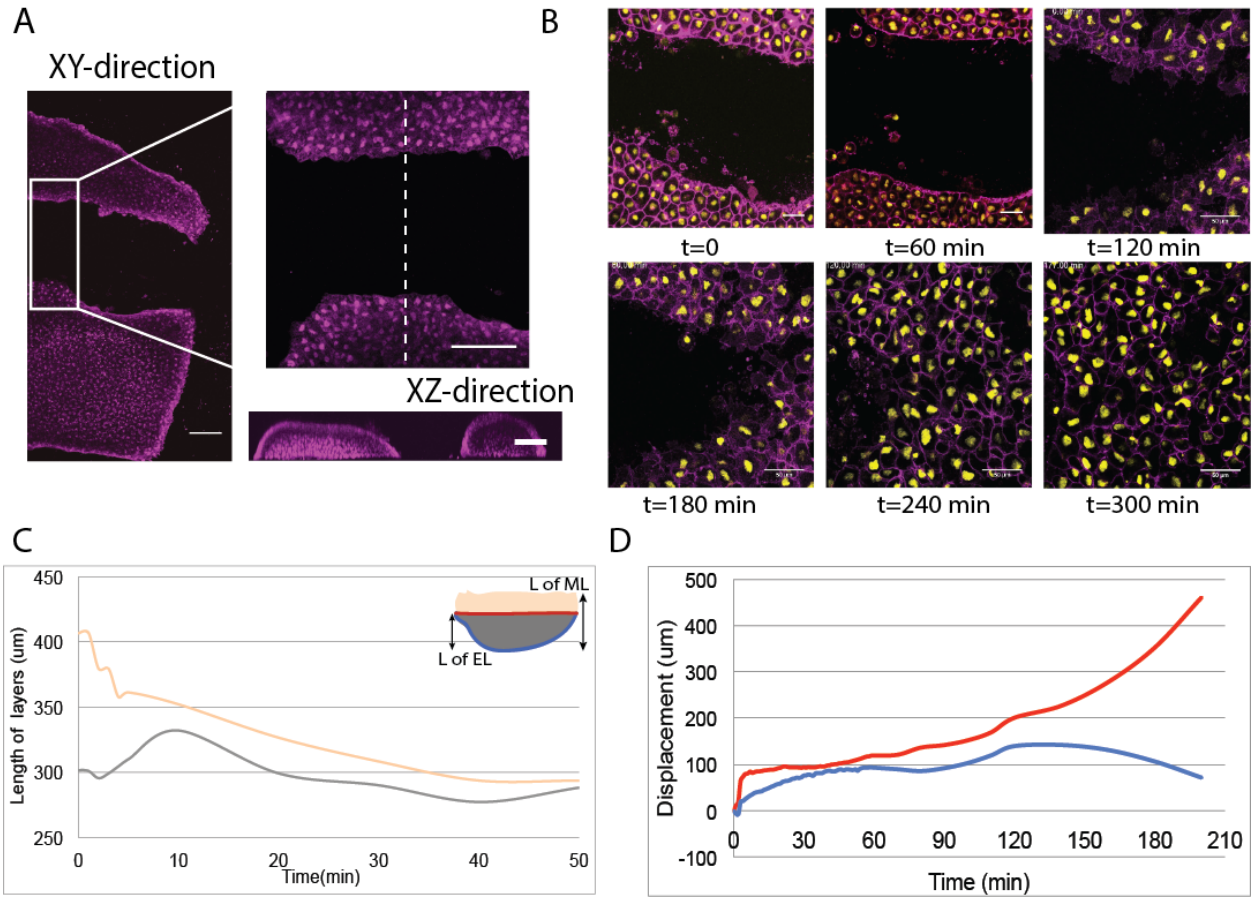

Figure 4.11: Inverted confocal images of refined multilayer etched animal cap healing. a)Dextran injected, fixed animal cap explants. Top view(XY direction) and Side view(Z-cut XZ direction). Scale bar is 100μm. b) Time lapse of mRNA injected explant after multi layer refined etching. The differences between t=0 and t=60min shows the contraction in ML. Magenta: GFP- membrane, Yellow: H2B-nuclear mRNAs were injected prior. Scale bar is 50um. c) Vertical length changes of ML and EL. This graph shows that EL layer (grey line) spreads and extends while ML contracts and shrinks until EL covers ML. This graph supports the hypothesis of mechanical coupling between EL and ML. d) Displacement of free edge of EL (red) and free edge of two cell layer (blue). In 2 hours, EL layer and ML restore and start spreading.

in EL and ML with narrow single layer etching and refined double layer etching. Two cell layer other edges seemed to respond to narrow etching that was in the center of the explant. This suggested the communication and collectiveness between cells over a long distance as a result of the changed force fields and strain rate. The contribution of the ML helps the EL accelerate the healing migration speed to heal faster. This technique reveals an important information about other layers contribution to epithelial layer for migration. Monolayer

epithelial cell migration studies cannot carry out the crosstalk between layers.

In single layer removal, removal of EL on top of the ML caused the ML change its own fate from spreading to contracting and shrinking. Shrinking of cell volume has been studied and shown in chick cells in response wound healing, too. Some suggest that wound formation releases calcium ions into the nearby environment, and this immediately triggers the contraction of any actomyosin in the vicinity [130]. This might be how the ML contracts. Contraction of ML might be the first response of multi phase wound healing response. Even further, my hypothesis is that superficial cell provides cues that coordinate collective migration in deep cells. To test that this, I etched superficial layer layer completely and watch ML response to removal of EL (Figure 4.12). This experiment supported my hypothesis, ML did not spread when EL was removed. Mesenchymal layer showed contraction for 6 hours and started to spread. In 6 hours of etching, mesenchymal layer cells clustered and layer got thickened. After 6 hours, mesenchymal cells mostly probably went through mesenchymal-epithelial transition (MET) and epithelialized.

To gain a better understanding of the cellular mechanism between two layers in a collective rearrangements in response to removal of neighboring cells, I then set up another experiment where I cleaved the half of the EL leaving half of the ML uncovered (Figure 4.14). This set up is great tool to compare the ML migration itself and two-cell layer migration. Removing half of the EL provided bigger EL etched area thus bigger ML uncovered proving bigger size of ML underneath. Here, fluidic resistances were set to same resistance to have the same flow rate in both inlets thus have the same width in the channel. Half of the microfluidic channel was culture media (pink) whereas the other half was detergent (green) (Figure 4.14 b). Interface was kept in the middle of the channel until EL was cleaved, then detergent inlet valve was turn off. I acquired the time lapse movie every second when etching and every minute when healing to see the reopens of explant to removal of the half superficial layer (figure 4.14 b and c). Interface is not as clear in these figures because of the deficient dye in the detergent. The dotted line in the figure shows where the interface was. Etching duration

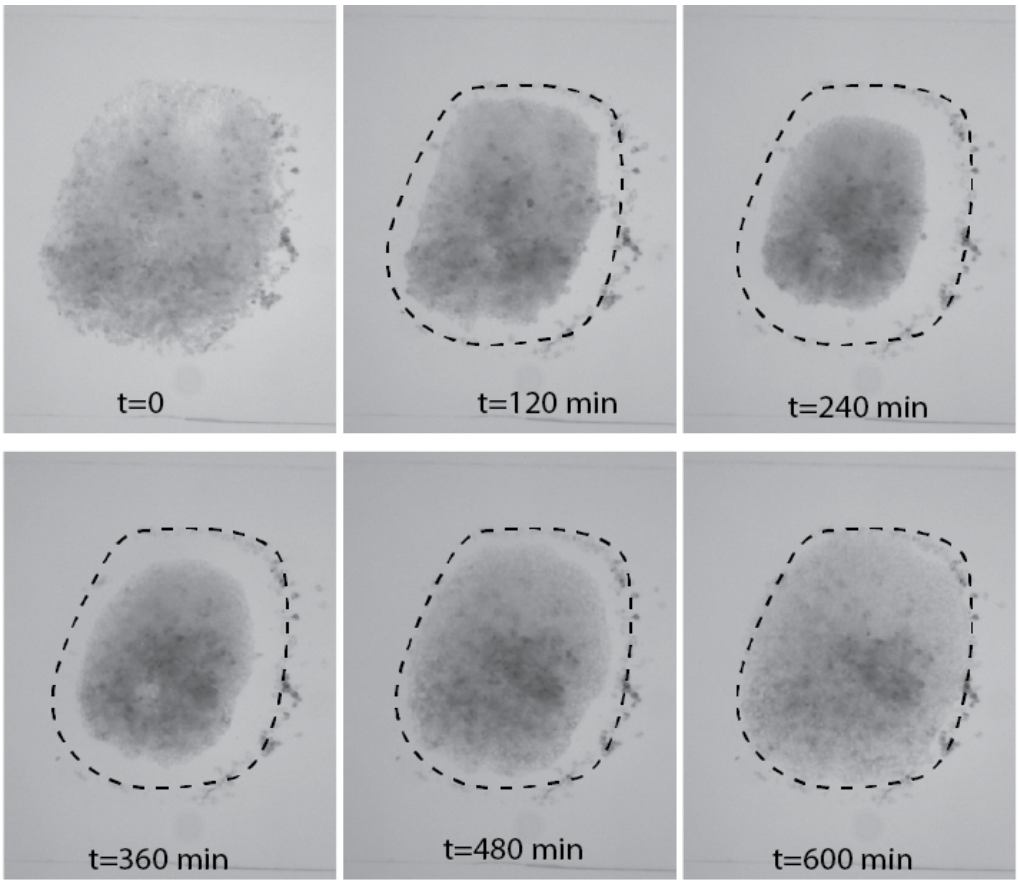

Figure 4.12: Mesenchymal layer response to whole epithelial layer etching. Left-over mesenchymal layer was observed for 10 hours.

was longer than previously because of the area to be etched. After etching was done, I turned off the valve of detergent and flow only DFA for 10 hours (Figure 4.14 c). Healing of half EL removed explant showed that ML did not migrate and spread without an EL on top. EL on the other hand, showed contraction before spreading. In contrast to other experiments, outer two-cell layer edge, started spreading and migrating before EL completely covers ML. In first 20 minutes of velocity profiles of these two edges (black: free de of EL and gold: free edge of two cell layer) showed no collective behavior. Etched edge showed a peak velocity in few minutes as in previous examples but this peak velocity duration was longer than previous ones (Figure 4.14 d). On the other hand, outer two-cell layer etched did not move to etched side and kept spreading. My explanation for this is the distance from etched side. Outer edge was too far to received the transmit forces and signals. To see where the transmission

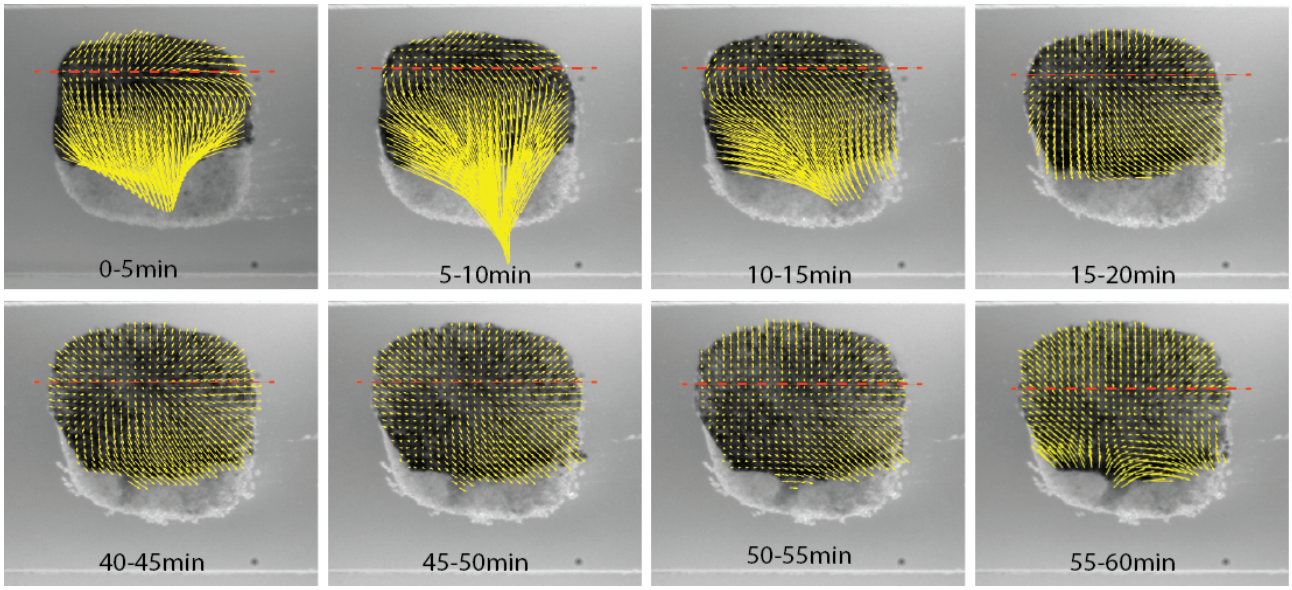

Figure 4.13: Displacement vectors during left-over epithelial layer re-epithelization over mesenchymal layer. Red dotted line shows the boundary of transmited broken tissue integrity

boundary, I used displacement vectors (Figure 4.13). Displacement vectors were generated by custom written macro in Fiji. It uses the displacement of each pixel points and generates vectors that shows the direction and magnitude of displacement.

Eventually all tissues recovered with a scar and re-epithelialized, started to spread in all direction. I was able to demonstrate the fact that the ML does not migrate until the EL completely covers it. EL showed a different velocity profile indicating that cell migration speed of layers might be depended on the free area or left over EL size. To highlight the differences in these three different responses in term of the migration speed, I put all displacement data in the same graph. Displacements were calculated at the peak velocity part of the explant for an hour (Figure 4.15). This graph pointed out that the half removed EL migrated the most. Although peak velocity is the highest in multi-layer etching, half EL removal migrated more than multi-layer etching. This also supports the hypothesis of mesenchymal layer contribution to epithelial movement since there is more ML area in half removed then multi-layer etching.

Manipulating the architecture of a tissue means changing the strain profiles of the cellular

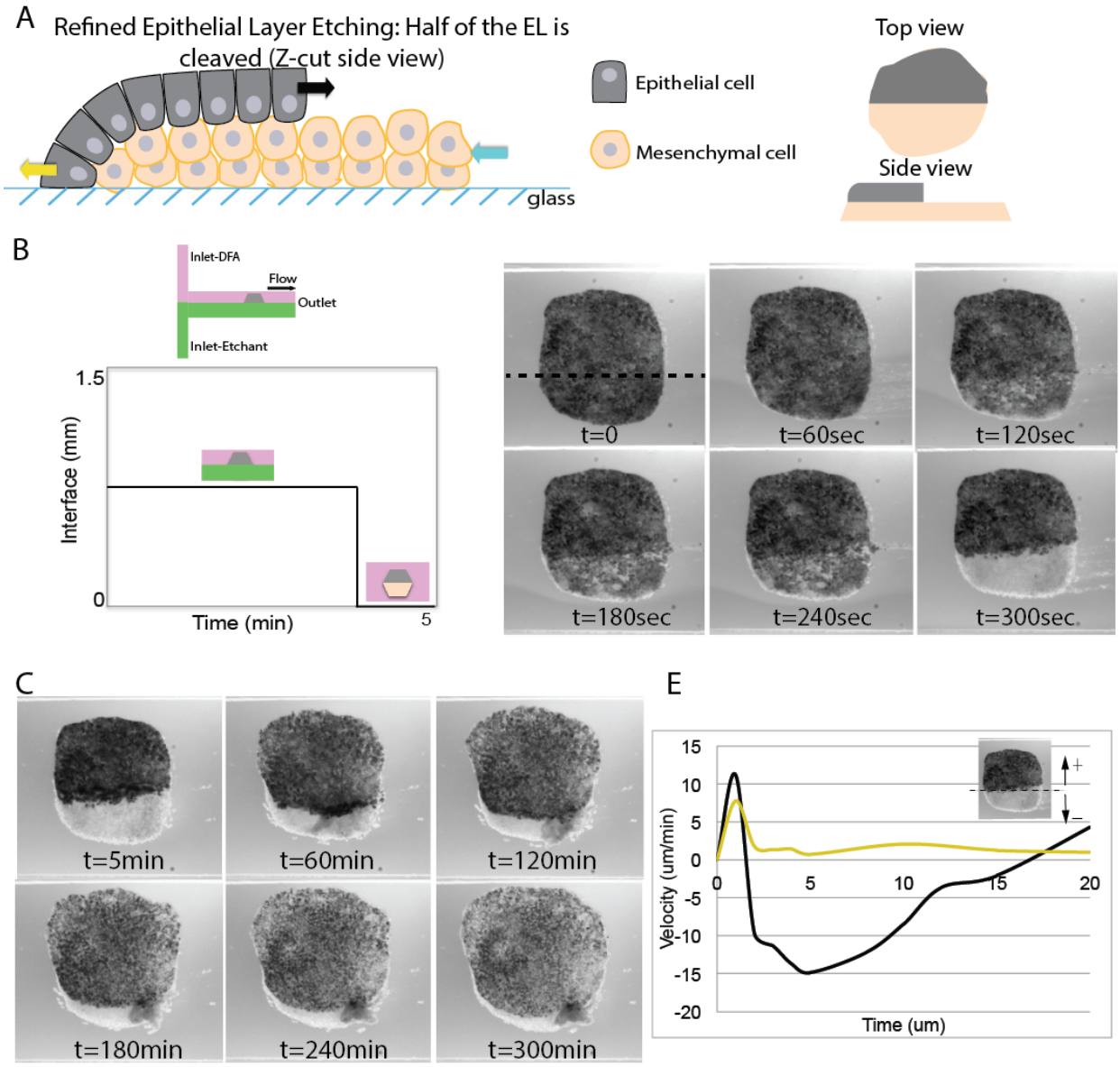

Figure 4.14: Removing half of the epithelial layer by Refined Bio-etching. a) Schematic of refined etched multilayer animal cap. b) Left: Schematic of microfluidic channel with animal cap explant housed in with interface control graph. Green: Etchant (Detergent) Pink: Culture Media (DFA). Right: Time lapse images of half of the superficial (epithelial) layer removal using stereomicroscopy. Dotted line indicates the interface. c) Time lapse images of healing explant. In an hour, epithelial layer covered most of the mesenchymal layer and outer edge started to migrate outwards. d) Velocity differences between free edge of epithelial layer and free of two cell layer when healing. Black:free edge of EL. Gold: free edge of two-cell layer. In first few minutes, left over EL part showed contraction. Right after contraction EL started to show a peak velocity whereas two-cell layer edge did not show any response to healing.

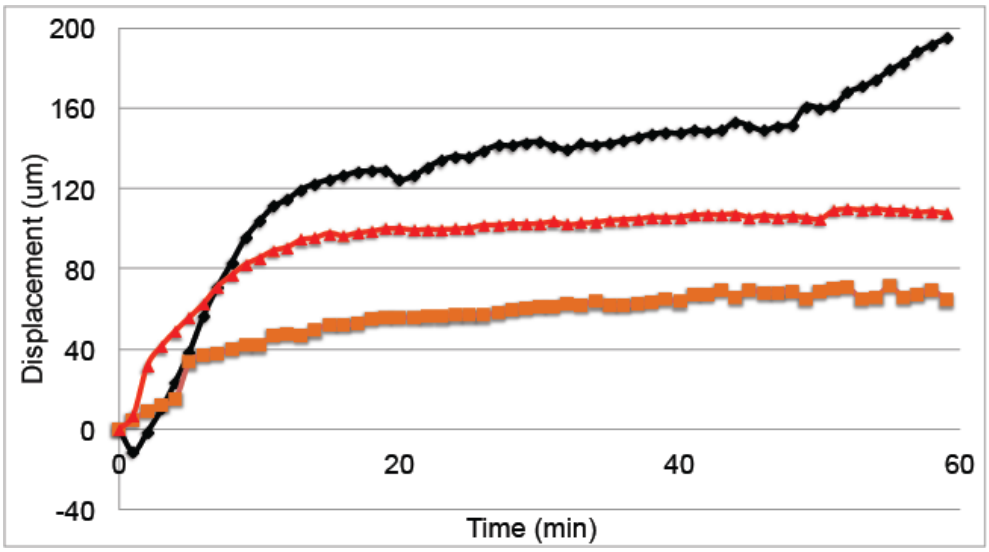

Figure 4.15: Displacement comparison between half EL removal(black), narrow EL removal(orange) and refined multi layer etching (red). Overall, half of EL removal migrated the most in response to etching. This indicates that there is a correlation between left over EL area, remaining ML area and displacement rate.

layers. By cleaving the part of the layer releases the strain in that specific layer. I used custom written macros to calculate the strain that tissue experiences after the etching. These macros were written based on a free code plug in (bUnwarpJ), and it uses simultaneous registration of two images based on elastic deformations represented by B-splines. It calculates the changes of a distance between two pixels from one image to another and elastically deforms the first image to make it look like the second one. It uses similarity term and the consistency term of the energy function. Strain profiles are generated using color-coded (red:contraction blue:relaxation) strain profile maps. I calculated strain profiles of left-over EL in response to removal of the other half (Figure 4.16). Strain profiles provide the individual pixel movement information in entire left over tissue thus let us to see the response globally rather than at the edges. Strain profiles can be calculated in any frame rate. Here, I showed change in strain in five minutes time intervals since the biggest rearrangement occurred in first 20 minutes. I also showed the last twenty minutes of an hour time period to highlight the difference in strain values. First 10 minutes, tissue experienced very significant strain values whereas after 20 minutes, it recovers and shows wild type strain values. In first 0-5 minutes strain

profile, tug-of-a-war effect can be seen. Cell uses tug-of-war mechanism [133] to transmit the forces in long ranges when moving together. The first 5 minutes interval showed the highest positive strain (blue) in the center of the left-over EL and the highest negative strain (red) at the edges. Especially the edge that neighboring cells removed experienced the highest negative strain because of the initial contraction. This data indicated that healing of the EL on the ML is composed of four phases. In the first phase, the remaining EL recoils and retracts. This first simultaneous response of removal of neighboring cells occurs within few minutes. The second phase is where remaining tissue stabilizes itself. Depending on the left over EL area size, the healing speed changes the more area etched the faster to heal. In the third phase, healing starts, and the EL starts to spread over ML. At this phase ML contracts and keep retracting until EL covers ML completely. Starting speed at this phase is the fastest known cell speed alive. At this phase, cells show a peak velocity. The fourth phase is restoration, where EL resumes back to its normal speed and after EL completely covers ML, AC tissue starts to spread normally.

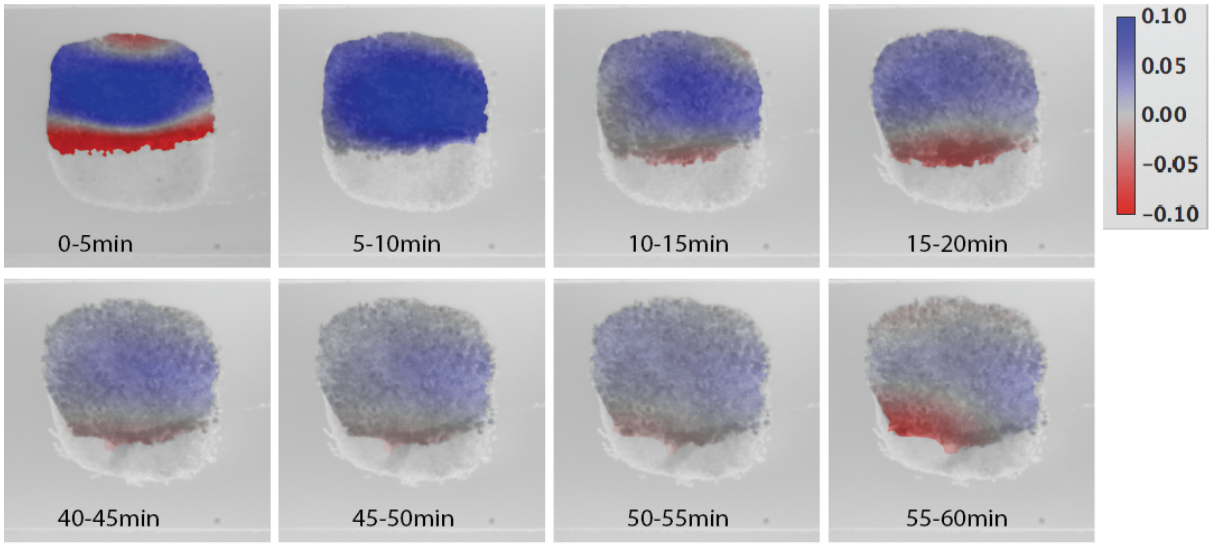

Figure 4.16: Strain profile changes in re-epithelization of half-epithelial-removed tissue.

These results support the hypothesis of mechanical coupling between cell layers to ensure efficient collective rearrangement. Epithelial layer migration rate goes up to 1500um

per hour, which seems impossible without mesenchymal layer contribution. Mesenchymal cells contraction seems to be accelerating the epithelial layer healing response. Mesenchymal cells might be using "conveyer belt" type of behavior to help epithelial layer to cover mesenchymal layer. Using this method, I created a 3D platform within a multilayer system to study different cell types' responses to bio-etching which was similar to a wound-healing response. Bio-etching technique will reveal useful information about collective behavior during development, wound healing and tumor growth. Furthermore, this assay might elucidate mechanisms used by both epithelial and mesenchymal cells to coordinate their movements during morphogenesis. The ability to control the form of multicellular tissues potentially will have high impact in tissue engineering and regeneration applications in bioengineering and medicine. Likewise, my custom microfluidic system can be configured to test a range of hypotheses concerning the control and regulation of development and cell differentiation with additional applications in tissue engineering. The ability to investigate complex developmental systems will provide great opportunities for increasing the understanding multicellular interactions in more evolving spatiotemporal environments than in vitro cell monolayer studies. The ability to control the chemical environments and then monitor the overall response of these systems such as AC explants provides a way to study complex and emergent behaviors in time and space. My integrated system combining long-term and high-speed dynamic pressure and flow control with microfluidics will be useful to investigate the dynamics of embryonic development at a molecular, cellular, and tissue levels with high spatial and temporal resolution. I believe this technique will enable development biologists to utilize spatiotemporal stimulation of growth factors (e.g. FGF or Activin) to stimulate specific sections of a tissue and potentially drive the development toward non-regular, but favorable phenotypes. This approach also can be extended to study other areas in developmental biology including cell motility, intercalation, and differentiation toward dictating overall explant system-wide responses. This work will be of interest to researchers in areas including developmental biology, engineering, physics, and chemistry.

Chapter 5

Conclusion

5.1 Conclusion

I have developed a novel microfluidic technique that demonstrated the ability to create and shape 3D tissues with subtractive manufacturing "bio-etching". While many approaches use 2D environments with monolayers, my unique microfluidic technique provided the ability to control the 3D environment and study the interactions of individual epithelial and mesenchymal layers. I used the animal cap ectoderm of the *Xenopus laevis* embryo as a model system for the study of tissue bio-etching since these tissues are multi-layered with both an epithelial and a mesenchymal layer, and are well suited to real-time analysis. My method introduced a new chemical bio-etching method with a precise spatial and temporal control of the etched area. This precise positioning allowed me to construct novel epithelial and mesenchymal tissue architectures. I was able to remove single cell layers or multiple layers with tremendous precision allowing me to shape 3D tissues.

Integration of methods for controlling cells within a bioengineering breadboard helped me pursue extremely challenging goals to generate and pattern at the fine scale distinct cell and tissue types (e.g. muscle versus bone); the breadboard combined microfluidic control with

cellular engineering to control a subset of morphogenetic machines. Using spatiotemporally controlled microfluidic streams I was able to study multi-layer coordination of epithelial and mesenchymal cell layers and acute mechanical and behavioral response of intact epithelial and mesenchymal cell sheets to removal of neighboring or overlying tissues.

Using bio-etching technique, I tested the hypothesis mesenchymal and epithelial layer are mechanically coupled. I showed that epithelial layer provides cues to coordinate collective migration in deep mesenchymal cells. In addition, mesenchymal cell layer helped epithelial layer reepithelialized by contracting until the epithelial layer completely covers. As result, epithelial layer migration rate goes up to 1500um per hour which is impossible without mesenchymal layer contribution. Epithelial sheet migration over mesenchymal cells exposed by etching is two-fold faster than the fastest migratory cell suggesting they might be mechanically coupled. Healing of epithelial layer(EL) on mesenchymal layer(ML) was composed of four phases. In first phase, remaining EL recoiled and retracted. This first simultaneous response of removal of neighboring cells occurred within few minutes. Second phase is where remaining tissue stabilized itself. Depending on the left over EL area, the healing speed changed with the more area etched the faster to heal. At third phase,healing started and EL started to spread over ML. At this phase ML contracted and keep retracting until EL covered ML completely. Starting speed at this phase is the fastest known cell speed alive. At this phase, cells showed a peak velocity. Fourth phase was restoration where EL restored back to its normal speed and after EL completely covered ML , AC tissue started to spread as normal. The explant recovered without a scar.

With the bio-etching technique, one can precisely manipulate distinct spatial regions of a single cell by delivering different fluids to different subcellular domains. This approach extends our ability to control chemical stimulation in biological systems beyond only 2D. I applied detergent to the epithelial layer of the *Xenopus* but only over one-half of the explant. To create a single layer of cells over half of the explant. I then captured images of cell migration occurring over time. I specifically focused on the cell migration in the top

layer, as the epithelial cells moved to heal through collective migration over the mesenchymal cell layer. By plotting the distance with respect to time, it was possible to examine the velocity of the cell movement at different locations along the length of the AC. Repeating the experiments and delivering the detergent at different locations, control the amount of the left-over epithelial cells. For example, delivering the detergent to the apical side where the stream covers most of the AC (e.g. 75% of the surface), caused most of the AC becomes only the mesenchymal cell layer. I plotted the recovery time and collective cell migration speed of the epithelial cell layer for different amounts of detergent subtraction of epithelial cell layers. I might need to look at the mesenchymal cell layer more in depth for a journal publication. Using confocal microscopy, I can reveal the mechanism in the deep cell layer. Using mechanical coupling inhibitors like heptagonal or Y-compounds I can test further my hypothesis about layers being coupled.

5.2 Future work

5.2.1 Creating Embryonic Bridges Using 3D Microfludics

Long-term studies of localized responses of cells and tissues to chemical stimuli are critical in numerous areas including developmental biology. Recent advances in development and stem cell biology have identified signaling and gene regulatory networks that control cell-identity and tissue assembly. However, these studies are all conducted en-mass, providing population-level analyses of the processes controlling identities. Missing from these studies are details of cell-level changes in cell identity and subsequent cell movements and rearrangements that accompany these changes. It is these processes that direct cells into their proper location within forming organs and prevent cells from adopting invasive pre-cancerous behaviors. To understand these events we need quantitative information on the life-history of stem cell-like embryonic cells as they receive chemical stimuli from their microenviron-

ment, change gene expression, adopt new cell behaviors, and assemble into tissues from a mechanics point of view. Furthermore, the ability to have spatiotemporal control extends researchers capabilities and enables the more sophisticated control needed to produce organs *ex vivo*, which is especially poignant in wound healing. One area of wound healing is particularly important when understanding 3D tissues. The coordinated responses of different cells types in developed tissues have been shown to have important geometrical constraints on collective cell migration. The collective behavior of the different cells has shown to create unique migration patterns that are directly related to wound healing. One response that has recently gained much attention is cellular bridging (Figure 5.1). Cellular bridging involves that ability of single cells and cell clusters to spatially span distances such as epithelia bridging [14], cytonemes [134], and tunneling nanotubes [135]. The recent work in epithelial bridging has been shown to be related to the mechanics of the system through tension with actomyosin contractility as well as being related to mechanically governed structures including actin bundles, adhesion sites of adherent junctions. Since the embryonic tissue is much more three-dimensional than single monolayers of cells that are essentially flat on the bottom of the microfluidic channel, dynamic control of 3D chemical patterns with both high precision and high speed is critical here. The lack of techniques to provide inputs and measure biological responses with sufficient temporal and spatial resolution has hampered the advance of quantitative approaches to understanding development and tissue engineering. To observe both high-speed and protracted tissue and cellular responses, 3D experimental apparatus is needed.

The ability of cells to sense and respond to mechanical cues is critical to their function within complex 3D microenvironments. While single cell studies are commonly used to investigate these abilities, extending these studies to naturally occurring integrated 3D multi-cellular tissues would provide tremendous advances in understanding mechanobiology responses. Model tissues such as those found in the developing frog *Xenopus laevis* are naturally three-dimensional and also allow for detailed cellular and molecular responses to be

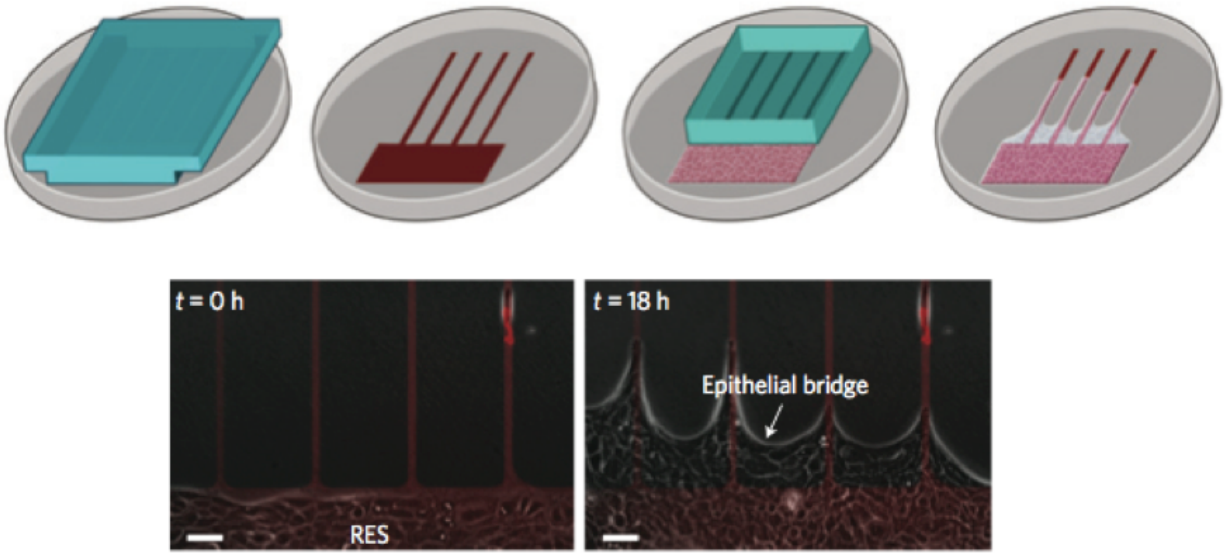

Figure 5.1: Monolayer keratinocytes migrating on microcontact-printed fibronectin patterns form multicellular suspended epithelial bridges [14].

assessed. These model tissues also are extremely important in exploring the mechanics of collective migration, which is important in wound healing. The ability to develop novel technologies for these model tissues is challenging though. Microfabrication technologies allow the development of tools to control and assay spatiotemporal responses of cellular systems. Here, I developed new 3D fabrication approaches for understanding the role of mechanics in terms of collective migration and cellular bridging, which will have implications in a diversity of fields including mechanotransduction. To understand the mechanics of collective migration, I developed a 3D microfluidic system, which will allow both mechanical stimulation and shaping of the *Xenopus* animal cap. The principles of collective migration exposed with these tools will lead to greater insights into tissue scale processes such as wound healing, tissue remodeling, and regeneration.

To probe the role of controlled chemical stimuli in differentiation and patterning of cell behaviors within vertebrate embryonic tissue in 3D, I built a microfluidic system capable of providing precise 3D spatial and temporal chemical stimuli to cultured tissues over long time

frames and dynamically control the apical and basal chemical environment while guiding the assembly of tissue functional units. This 3D microfluidics system is capable of manipulating streams in complex patterns in the main chamber, but also to capable of independently manipulating streams beneath the tissue nearer to the mesenchymal cell adhesion complexes. Using 3D streams and complex 3D tissues, one can generate complex chemical and architectural microenvironments with the goal of controlling the tissue mechanics, cell motility, and wound healing. This study offers tissue formation and remodeling in a vertebrate developmental model system to advance areas including engineering tissues, stem cell response, and developing new targets for diseases. This approach allows to detect spatiotemporal dynamic responses of apical and basal regions of living embryonic tissues. We can investigate: (1) distinct cytoskeletal dynamics in different chemical conditions of apical and basal parts of embryonic cells such as dynamics of F-actin (e.g. polymerization and depolymerization) when embryonic cells migrate during development; (2) membrane receptor based growth factor induced multicellular dynamics; and (3) induction of localized differentiation of the progenitors in Animal Cap tissue explants during living *Xenopus laevis* embryonic development

5.2.1.1 Transition from 2D to 3D-Molding of Microfluidic Devices

Animals are complex, dynamic, multicellular systems responsive to an set of physical and chemical inputs. At an early stage in development, cells and tissues receive spatiotemporal stimulation from a variety of inputs. One of the most important stimuli is the chemical environment, which profoundly influences developmental progression. Developing and implementing a system that can be integrated with developing multicellular systems and dynamically control their 3D chemical environment to guide the assembly of tissue functional units is essential to understand complex cellular systems.

Microfluidics has mainly been used in 2D systems such as laminar flow separation. Considering tissues and organs are three-dimensional, two-dimensional (2D) approaches may re-

spond differently than those in more physiologically relevant 3D environments [72, 116–118]. Traditional 2D cell culture studies lack important features necessary to accurately replicate cell function and formation. There is wide range of tools available to fabricate layers, molds or whole microfluidics devices including photolithography, solid object printing, mechanical or laser machining [136]. Thus, a number of 3D microfluidics approaches have been previously implemented including layered fabrication, direct 3D fabrication, and 3D molding. For example, Jo *et al.* fabricated 3D microchannels in PDMS by stacking 2D layers [137]. Also, Whitesides' group showed that with right aspect ratio, laminar flow in multi-layered 3D microstructures was achievable (Figure 5.2) [15].

5.2.2 Layered fabrication

Three dimensional microfluidic channel fabrication can be achieved by layered fabrication where two or more 2D microfluidic channel layers are bonded to together to form 3D channel as shown in Figure (5.2). Individual layer can be fabricated through any preferred method and they can be stacked with on top of each other with precise alignment. This method provides the flexibility of 3D topography whereas time requirement for alignment and the determining the sturdy bonding are the two biggest pitfalls. Depending on the material used, there are option for bonding the layer. Traditional bonding techniques includes the use of glue which has the potential to clog the small feature channels, and also the ability to modify the surface chemistry with plasma cleaning which might not be ideal for some materials. However, in microfluidics PDMS is mainly used and with oxygen plasma cleaning, baked PDMS surface can be modified to make it bond covalently.

5.2.3 Direct 3D printing

When alignment and bonding are an issue, monolithic 3D printing is one the options. 3D printing might be subtractive like micro-machining or additive manufacturing like stere-

olithography or solid object printing. There are many machines that are capable of manufacturing with resolutions down to few microns even in nanometers. In stereolithography, photosensitive material is solidified with UV in an additive manufacturing manner. Though, automation of this technique to have mass production is costly.

5.2.4 3D molding

3D molding is similar to 3D printing. The difference is that mold replicates the negative of the structure and using other materials microfluidic channel can be fabricated from the mold. In this method, there is no material restriction like in stereolithography, many materials can be used to fabricate the mold but the channel device material must compatible with mold material. Micro machining is one of the most desirable technique to fabricate 3D molding because of its advantages in high resolution. Although, solid object printing using 3D printers seems to be the most attractive one because of it accessibility, roughness on the surface and poor resolutions do not make it best candidate for small dimension microfluidic channel fabrication.

Comparing these methods, layered fabrication is the most suitable technique to fabricate 3D microfluidic channels to study cellular mechanisms. To house a tissue or a cell in a microfluidic channel, the bottom of the channels needs to be coated with an ECM-like fibronectin, which is to what substrate cells adhere. Since multiple channels are needed per day for cellular experiments, other methods become incompatible because of the need of mass production.

Shortly after, combination of 3D microfluidics with cell biology was studied by fabricating a layered 3D microfluidic channel with a single cell housed in main channel where apical and basal surface of the cell together stimulated [16]. Previously, our group was able to demonstrate 3D microstructures with pressure driven laminar flow are great tool to study cell behaviors.In previous work, our group has focused on independently controlling the apical

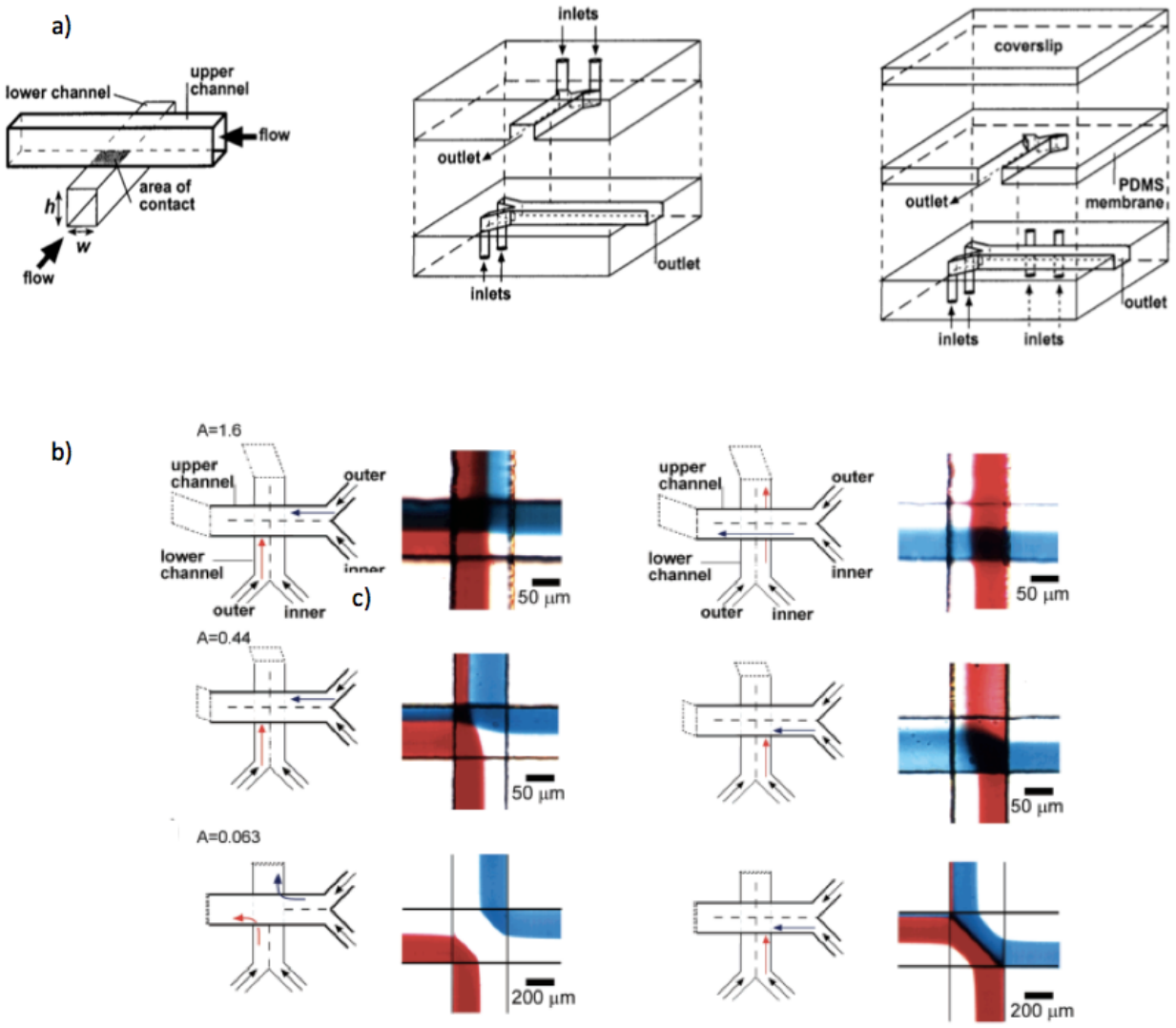

Figure 5.2: Pressure-Driven Laminar Flow in Tangential Microchannels a)Schematic drawing of the tangential microchannels fabrication. b)Two-stream laminar flow at Re=10 with different aspect ratios. A=h/w [15].

and basal environments in single living cells through vertical aqueous-phase separation under laminar flow (Figure 5.3). Using the ability to control the flow-rate within the two distinct layers of microchannels, simultaneous apical and basal stimulation was applied. Now my goal is to implement previous work to tissue level.

I developed a new technique of high-precision 3-D differential apical basal microfluidics for probing long-term embryonic development that allows precise control of differential api-

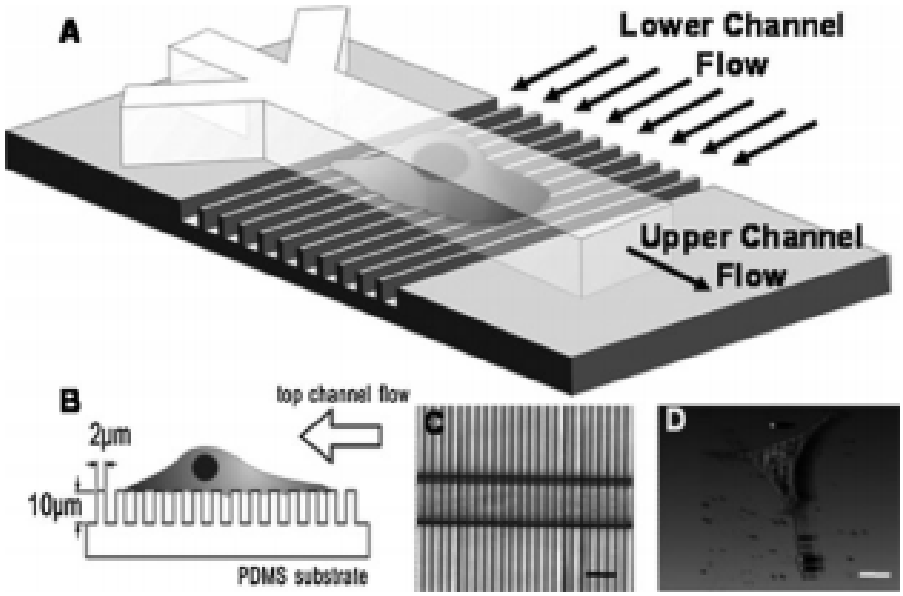

Figure 5.3: Schematic image of the apical-to-basal microfluidic device. [16].

cal and basal chemical stimulation and assaying. This contribution is significant because it enables 3D control and assaying of spatiotemporal cues over large tissues or over entire organisms. I constructed this new microfluidic system based on a previously constructed multi-layered microfluidic platform that had two independent microfluidic channels vertically aligned above each other and I could deliver vertically separated chemicals in solution. I first constructed this multi-layered microfluidic platform with two independent sets of channels. The design has the upper layer of the microfluidic systems having one large main chamber with inlet channels for both the apical and basal layers and with the lower layer having multiple narrow channels. I fabricated these two separate microfluidic slabs using conventional soft lithography and they were combined together to form one integrated device. This device has the characteristics of: (1) a multi-inlet PDMS slab for the apical stimulation with channels that are 0.3 mm tall and 1.5 mm wide for the embryonic tissue explants; (2) one PDMS slab with multiple narrow lanes that are 10μm tall and 5μm wide separated by 2μm (for a width of 55μm wide there are 6 narrow channels). I then vertically aligned and adhered these two slabs with the channels on the upper and lower slabs placed in directions running

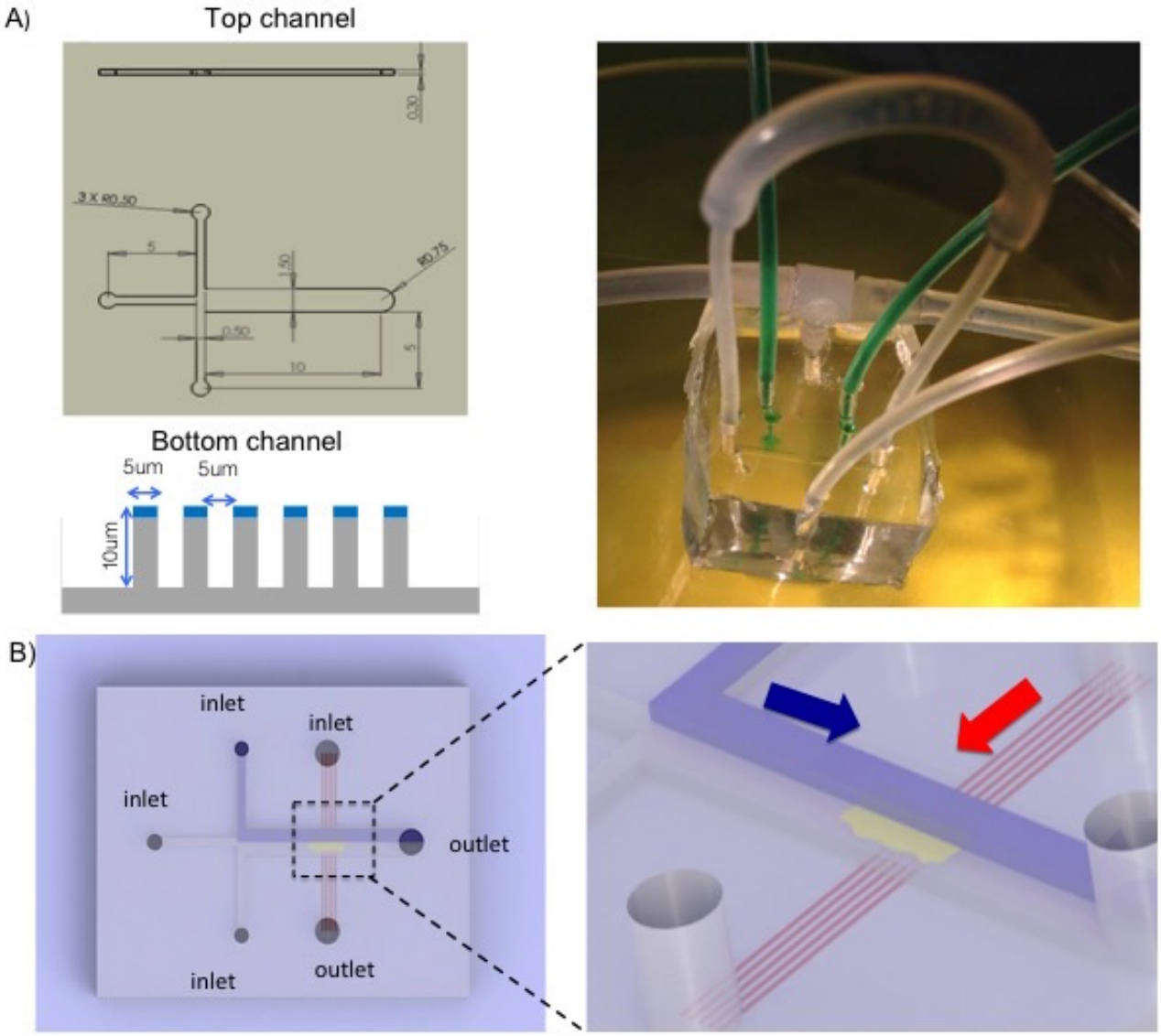

Figure 5.4: 3D apical-basal *Xenopus* stimulation approach through multilayered microfluidics. The narrow channels are to a) Top and bottom channel dimensions b) Schematic of 3D microfluidic channel with embryonic AC tissue housed in. The *Xenopus* tissue will be positioned in the main channel where its apical side can be stimulated fully or in local domains. The entire basal domain or local subregions can be stimulated through the multiple small channels running beneath the spread embryo.c) Two steps apical and basal chemical stimulations. Lower narrow channels are not drawn to scale to enhance visualization.

perpendicular to each other (Figure 5.4).

Since flows from the upper and lower channels of the two-layer microfluidic platform intersect each other in the middle of downstream although it is laminar, it is difficult to

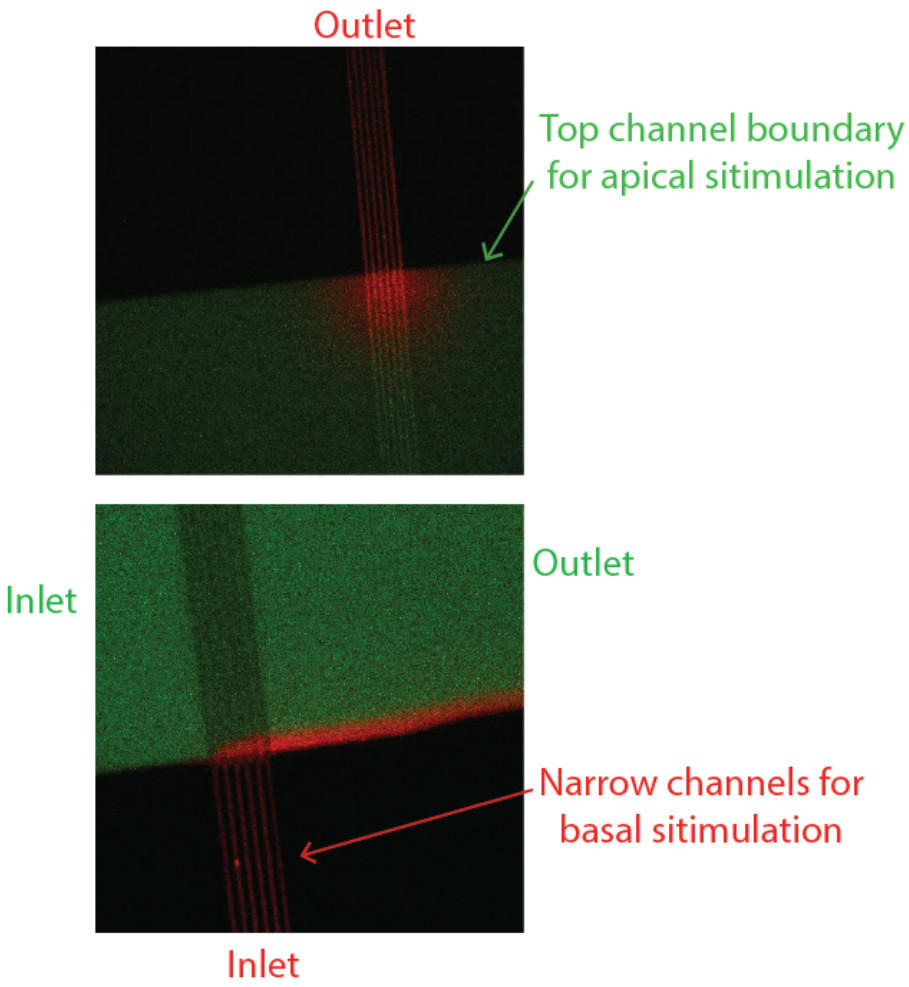

Figure 5.5: Confocal images of 3D microfluidic channel. Due to high resistance in narrow channel and lower resistance in the top channel, fluids get mixed at the intersection.

regulate each flow precisely because of the sensitivity of the flow caused by the large difference in sizes of the two channels. The challenge here is both channels have to have exactly the same pressure to be able to maintain laminar flow. In particular, an increase of the flow rate in the lower channel causes the flow to be mixed at the intersection and move to the upper channel outlet because the fluidic resistance in the lower channel is relatively very high (Figure 5.5). Since bottom narrow channel is so narrow compared to main channel that hydraulic resistance is higher which causes a low flow rate. Predicting flow patterns and determinig the exploitable range of flow rates is possible via computation flow analysis. Also, the lower channel size should be optimized to avoid a couple of unnecessary experimental

variations that might affect on the result such as tissue attachment variation due to shear flow underneath the tissue. 3D channel has been fabricated but still needs development to improve laminar flow and interface control in the channel. After characterization of the channel, I will grow *Xenopus* animal cap tissue in 3D channel. I do not anticipate any issue with this since AC tissues are shown to grow on posts. This is still on going part of the work.

5.2.5 Studying Tissue Integrity During Collective Migration Using 3D Microfluidics

My long term goal is to understand integrated mechanochemical responses of complex 3D tissues through novel 3D microfluidic approaches. I first want to approach this through "subtractive manufacturing" which I was able to do with the *Xenopus* animal cap and the ability to control the application of the etching chemicals using bio-etching. Before, I demonstrated that simultaneous control of the subcellular environment at both domains can be achieved with different chemical agents. Next, I will implement similar detergent extraction over the epithelial cell layer, but before the migration occurs, I will deliver a stream perpendicularly to the bottom mesenchymal cell layer from the lower layer of the 3D microfluidics. I will apply inhibitors of the mechanical connections such as blebbistatin, Y27632 etc. to examine the bridging response of the epithelial cells when local mechanical connections are inhibited in the mesenchymal layer. I will then track the collective migration as previously described in terms of motility and speed of motility. I will use as a control the delivery of the same inhibitors over the entire tissue and track the motility and speed of motility. I also will vary the concentration of the inhibitors to investigate the effects of amount of inhibition linked to the collective motility. This approach will allow me to elicit the effect of local tracks of mechanically inhibited mesenchymal cells, which adjacent mesenchymal cells are mechanically intact. Questions about the collective migration of the cells near and away from the area of local inhibition relative to the epithelial cell migration

will elucidate mechanical connectivity questions. In addition, instead of using mechanical inhibitors, I will use chemical inhibitors such as hepthanol, which is a gap junction inhibitor. This approach will allow me to investigate chemical versus mechanical connections and how these bridges are linked to collective cell migration from a mechanochemical standpoint. I expect that the cell motility of the epithelial cells is inhibited in the areas above the local application of the inhibitor on the mesenchymal cells due to the mechanical connections being disrupted (Figure 5.6). I expect that the further away from the locally inhibited cells, the epithelial cells will collectively migrate at speeds approaching those of the uninhibited collective migration. One potential limitation may be in the visualization of the individual cells using stereomicroscopy as imaging their characteristics such as their podia extensions could provide additional insight. If this is a limitation, I will express live cell reporters such as plasma membrane targeted mCherry, histone labeled mPlum, and the actomyosin reporter utrophin-GFP and use real time confocal microscopy to reveal fine scale cellular responses to micro-environmental features and regulated levels of contractility.

Once the *Xenopus* embryonic tissues is positioned, apical side of the tissue faces the main channel with the basal surface directly above the narrow lower channels. The narrow channels enable a support of the tissue for attachment and spreading- tissue will spread over rather than penetrating into the channels, but also allow flow to pass beneath the embryo to stimulate its basal domains (Figure 5.4b). The top channel is a T-shaped channel and consist of three inlets and one outlet. Bottom channel has 5mm long six straight channels (5μm width and 10μm height with 5μm spacing) and is bonded perpendicular to T-shaped channel's outlet (width 1500μm) (Figure 5.4a). These multiple narrow channels in the bottom layer then provide access for stably controlled localized chemical patterns to the tissues. In addition, these channels are 10 microns tall so that high-resolution imaging can be accomplished. These two channels were bonded to each other by using plasma cleaning technique. I anticipate that the *Xenopus* ACs easily cover the intersection of the apical and basal stimulation networks in the 3D microfluidic system (Figure 5.4b). It is important to note that the

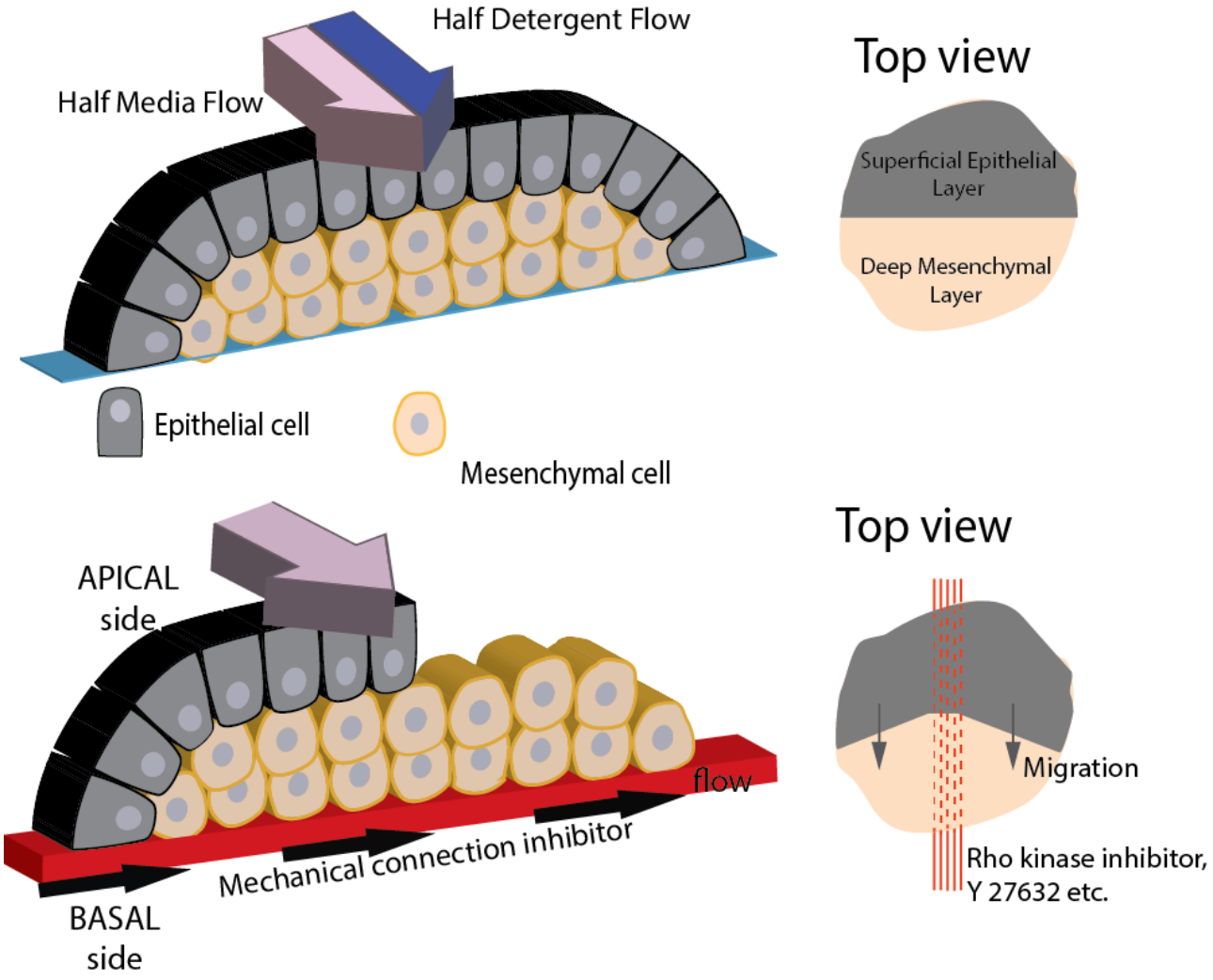

Figure 5.6: Schematic of apical and basal chemical stimulations response. Lower narrow channels are not drawn to scale to enhance visualization.

stimulation of the basal surface is really distributing a signal to the interstitial media that bathes the basolateral surfaces of cells (Figure 5.6). For example, the use of microfluidics to deliver chemicals to the apical surface of epithelial cells does not modify their interstitial microenvironment yet our "basal" delivery has the ability to accomplish just that, which is unexampled before. Thus, this design is capable of stimulating the basal and apical part of the animal cap tissue of *Xenopus* embryonic tissue simultaneously with different chemical reagent.

The cells of *Xenopus* embryonic animal cap share many features with mammalian embryonic stem cells, and may provide insights into stem cell response in the future studies. This will advance the field by developing a differential apical basal stimulation system and using a control-feedback approach to building a microfluidics device to probe and then control long term stimulation and response of 3D embryonic tissues by integrating these tools with synthetic cell biology approaches drawn for developmental biology studies. This project will be transformative by providing a unique apical-basal and controls-based approach to probe the role of spatiotemporal stimuli in 3D multi-cellular development as cells use maternal pre-patterning, gene regulatory networks, and input from external stimulus to guide development of future tissue replacements. Furthermore, our developed approaches will be extremely important in wound healing and could be extended to other medically important areas such as tumor biology. This contribution is significant because it enables 3D control and assaying of spatiotemporal cues over large tissues or over entire organisms. This ability will affect their single cell response toward physiologically functional tissues, and also may serve as a potential targets for therapeutic intervention as well as furthering tissue engineering and regenerative medicine. This project both develops new approaches for controlling 3D tissues and investigates important scientific questions involving wound healing. This project is transformative through understanding the basis of cell mechanical responses in 3D tissues, which is relevant to a number of physiological conditions, but is not conventionally explored in mechanotransduction. While investigating single cell migration is more commonly studied, the ability to exercise 3D control over cells that are integrated within a naturally occurring complex 3D embryonic tissue will enable a range of new experiments to shed light on mechanotransduction and cell interactions within complex physiologically relevant tissues. Unlike conventional decellularization approaches, this technique leaves remaining tissues viable. Thus, this 3D tissue-etching assay will be useful in the future to study mechanical responses, collective cell sheet migration, and explore processes that coordinate composite tissues movements during morphogenesis. The ability to control the form

of multicellular 3D tissues will have high impact in the allied fields of tissue engineering and regeneration medicine and provide insights into cancer and stem cell biology. This project will produce important findings in diverse areas including mechanics, engineering, biology, and biophysics, and will advance fields such as mechanotransduction, biotechnology, and cell migration.

Bibliography

[1] R. Field, Life cycle of the african claw-toed frog xenopus laevis @MISC (Jun. 2009).
URL http://www.uea.ac.uk/

[2] K. C. Bhargava, B. Thompson, N. Malmstadt, Discrete elements for 3d microfluidics, Proceedings of the National Academy of Sciences 111 (42) (2014) 15013–15018.

[3] Y. Xia, G. M. Whitesides, Soft lithography, Annual review of materials science 28 (1) (1998) 153–184.

[4] A. Author, Flow control in microfluidics: are the workhorse flows adequate?, Lab on a Chip 8 (3) (2008) 383–387.

[5] J. Atencia, D. J. Beebe, Controlled microfluidic interfaces, Nature 437 (7059) (2005) 648–655.

[6] Y. Kim, S. D. Joshi, L. A. Davidson, P. R. LeDuc, W. C. Messner, Dynamic control of 3d chemical profiles with a single 2d microfluidic platform, Lab on a Chip 11 (13) (2011) 2182–2188.

[7] H. A. Stone, Introduction to fluid dynamics for microfluidic flows, in: CMOS Biotechnology, Springer, 2007, pp. 5–30.

[8] J. Heasman, Patterning the early xenopus embryo, Development 133 (7) (2006) 1205–1217.

[9] D. B. E. Staveley, Vertebrate Development I: Life Cycles and Experimental Techniques.
URL http://www.mun.ca/biology/desmid/brian/BIOL3530/DEVO_03/devo_03.html

[10] T. Ariizumi, S. Takahashi, T.-c. Chan, Y. Ito, T. Michiue, M. Asashima, Isolation and differentiation of xenopus animal cap cells (2007). doi:10.1002/9780470151808.sc01d05s9.
URL http://dx.doi.org/10.1002/9780470151808.sc01d05s9

[11] D. Longo, S. M. Peirce, T. C. Skalak, L. Davidson, M. Marsden, B. Dzamba, D. W. DeSimone, Multicellular computer simulation of morphogenesis: blastocoel roof thinning and matrix assembly in< i> xenopus laevis</i>, Developmental Biology 271 (1) (2004) 210–222.

[12] F.-Q. Nie, M. Yamada, J. Kobayashi, M. Yamato, A. Kikuchi, T. Okano, On-chip cell migration assay using microfluidic channels, Biomaterials 28 (27) (2007) 4017–4022.

[13] L. A. Davidson, A. M. Ezin, R. Keller, Embryonic wound healing by apical contraction and ingression in xenopus laevis, Cell motility and the cytoskeleton 53 (3) (2002) 163–176.

[14] X. Trepat, C. T. Lim, B. Ladoux, Epithelial bridges maintain tissue integrity during collective cell migration.

[15] R. F. Ismagilov, D. Rosmarin, P. J. Kenis, D. T. Chiu, W. Zhang, H. A. Stone, G. M. Whitesides, Pressure-driven laminar flow in tangential microchannels: an elastomeric microfluidic switch, Analytical chemistry 73 (19) (2001) 4682–4687.

[16] J.-M. Yang, J. E. Didier, T. R. Cassino, P. R. LeDuc, Spatiotemporal control of apical and basal living subcellular chemical environments through vertical phase separation, Small 5 (17) (2009) 1984–1989.

[17] B. Alberts, A. Johnson, J. Lewis, M. Raff, K. Roberts, P. Walter, et al., Development of multicellular organisms.

[18] R. Keller, Shaping the vertebrate body plan by polarized embryonic cell movements, Science 298 (5600) (2002) 1950–1954.

[19] R. Keller, Cell migration during gastrulation, Current opinion in cell biology 17 (5) (2005) 533–541.

[20] M. Leptin, Gastrulation movements: the logic and the nuts and bolts, Developmental cell 8 (3) (2005) 305–320.

[21] L. A. Davidson, R. Keller, D. DeSimone, Patterning and tissue movements in a novel explant preparation of the marginal zone of xenopus laevis, Gene Expression Patterns 4 (4) (2004) 457 – 466. doi:http://dx.doi.org/10.1016/j.modgep.2004.01.001.
URL http://www.sciencedirect.com/science/article/pii/S1567133X0400002X

[22] P. N. Adler, Planar signaling and morphogenesis in drosophila, Developmental Cell 2 (5) (2002) 525 – 535. doi:http://dx.doi.org/10.1016/S1534-5807(02)00176-4.
URL http://www.sciencedirect.com/science/article/pii/S1534580702001764

[23] J. T. Bennett, H. L. Stickney, W.-Y. Choi, B. Ciruna, W. S. Talbot, A. F. Schier, Maternal nodal and zebrafish embryogenesis, Nature 450 (7167) (2007) E1–E2.

[24] L. A. Davidson, B. G. Hoffstrom, R. Keller, D. W. DeSimone, Mesendoderm extension and mantle closure in< i> xenopus laevis</i> gastrulation: Combined roles for integrin α< sub> 5</sub> β< sub> 1</sub>, fibronectin, and tissue geometry, Developmental biology 242 (2) (2002) 109–129.

[25] S. R. Singh, Cell signaling and growth factors in development: From molecules to organogenesis, Annals of Biomedical Engineering 37 (12) (2009) 2660–2660.

[26] P. Haas, D. Gilmour, Chemokine signaling mediates self-organizing tissue migration in the zebrafish lateral line, Developmental cell 10 (5) (2006) 673–680.

[27] J. Lewis, From signals to patterns: space, time, and mathematics in developmental biology, Science 322 (5900) (2008) 399–403.

[28] P. Rørth, Collective cell migration, Annual Review of Cell and Developmental 25 (2009) 407–429.

[29] M. Bindschadler, J. L. McGrath, Sheet migration by wounded monolayers as an emergent property of single-cell dynamics, Journal of cell science 120 (5) (2007) 876–884.

[30] T. E. Angelini, E. Hannezo, X. Trepat, M. Marquez, J. J. Fredberg, D. A. Weitz, Glass-like dynamics of collective cell migration, Proceedings of the National Academy of Sciences 108 (12) (2011) 4714–4719.

[31] M. Poujade, E. Grasland-Mongrain, A. Hertzog, J. Jouanneau, P. Chavrier, B. Ladoux, A. Buguin, P. Silberzan, Collective migration of an epithelial monolayer in response to a model wound, Proceedings of the National Academy of Sciences 104 (41) (2007) 15988–15993.

[32] J. B. Gurdon, N. Hopwood, The introduction of xenopus laevis into developmental biology: of empire, pregnancy testing and ribosomal genes, International Journal of Developmental Biology 44 (1) (2000) 43–50.

[33] P. Hausen, M. Riebesell, The early development of Xenopus laevis: an atlas of the histology, Verlag der Zeitschrift für Naturforschung, 1991.
URL `http://books.google.com/books?id=XLUoAAAAYAAJ`

[34] J. C. Smith, Forming and interpreting gradients in the early xenopus embryo, Cold Spring Harbor perspectives in biology 1 (1) (2009) a002477.

[35] M. Nemer, Genetic insights into normal and abnormal heart development, Cardiovascular Pathology 17 (1) (2008) 48–54.

[36] K. L. Moore, T. V. N. Persaud, M. G. Torchia, Before We Are Born: Essentials of Embryology and Birth Defects (with Student Consult Online Access), Elsevier Health Sciences, 2007.

[37] N. J. Waitzman, P. S. Romano, R. M. Scheffler, Estimates of the economic costs of birth defects, Inquiry (1994) 188–205.

[38] I. E. Zohn, K. V. Anderson, L. Niswander, Using genomewide mutagenesis screens to identify the genes required for neural tube closure in the mouse, Birth Defects Research Part A: Clinical and Molecular Teratology 73 (9) (2005) 583–590.

[39] M. Marí-Beffa, J. Knight, Key experiments in practical developmental biology, Cambridge University Press, 2005.

[40] T. Ariizumi, M. Asashima, et al., In vitro induction systems for analyses of amphibian organogenesis and body patterning, INTERNATIONAL JOURNAL OF DEVELOPMENTAL BIOLOGY 45 (1; SPI) (2001) 273–280.

[41] T. Ariizumi, M. Kinoshita, C. Yokota, K. Takano, K. Fukuda, N. Moriyama, G. M. Malacinski, M. Asashima, Amphibian in vitro heart induction: a simple and reliable model for the study of vertebrate cardiac development, International Journal of Developmental Biology 47 (6) (2003) 405–410.

[42] P. J. Kenis, R. F. Ismagilov, G. M. Whitesides, Microfabrication inside capillaries using multiphase laminar flow patterning, Science 285 (5424) (1999) 83–85.

[43] J. Atencia, D. J. Beebe, Controlled microfluidic interfaces, Nature 437 (7059) (2005) 648–655.

[44] N. Klauke, G. L. Smith, J. Cooper, Stimulation of single isolated adult ventricular myocytes within a low volume using a planar microelectrode array, Biophysical journal 85 (3) (2003) 1766–1774.

[45] J. Santos-Sacchi, L. Song, J. Zheng, A. L. Nuttall, Control of mammalian cochlear amplification by chloride anions, The Journal of neuroscience 26 (15) (2006) 3992–3998.

[46] Y.-W. Lin, C.-M. Cheng, P. R. LeDuc, C.-C. Chen, Understanding sensory nerve mechanotransduction through localized elastomeric matrix control, PLoS One 4 (1) (2009) e4293.

[47] S. I. Santos, M. Mathew, P. Loza-Alvarez, Real time imaging of femtosecond laser induced nano-neurosurgery dynamics in c. elegans, Optics express 18 (1) (2010) 364–377.

[48] D. J. Beebe, G. A. Mensing, G. M. Walker, Physics and applications of microfluidics in biology, Annual review of biomedical engineering 4 (1) (2002) 261–286.

[49] A. Folch, A. Ayon, O. Hurtado, M. Schmidt, M. Toner, Molding of deep polydimethylsiloxane microstructures for microfluidics and biological applications, Journal of Biomechanical Engineering 121 (1) (1999) 28–34.

[50] D. T. Chiu, A microfluidics platform for cell fusion, Current opinion in chemical biology 5 (5) (2001) 609–612.

[51] J. Gao, J. Xu, L. E. Locascio, C. S. Lee, Integrated microfluidic system enabling protein digestion, peptide separation, and protein identification, Analytical Chemistry 73 (11) (2001) 2648–2655.

[52] J. El-Ali, P. K. Sorger, K. F. Jensen, Cells on chips, Nature 442 (7101) (2006) 403–411.

[53] H. Stone, S. Kim, Microfluidics: basic issues, applications, and challenges, AIChE Journal 47 (6) (2001) 1250–1254.

[54] B. Kuczenski, P. R. LeDuc, W. C. Messner, Pressure-driven spatiotemporal control of the laminar flow interface in a microfluidic network, Lab on a Chip 7 (5) (2007) 647–649.

[55] J. Olofsson, H. Bridle, J. Sinclair, D. Granfeldt, E. Sahlin, O. Orwar, A chemical waveform synthesizer, Proceedings of the National Academy of Sciences of the United States of America 102 (23) (2005) 8097–8102.

[56] R. Karnik, F. Gu, P. Basto, C. Cannizzaro, L. Dean, W. Kyei-Manu, R. Langer, O. C. Farokhzad, Microfluidic platform for controlled synthesis of polymeric nanoparticles, Nano letters 8 (9) (2008) 2906–2912.

[57] D. Psaltis, S. R. Quake, C. Yang, Developing optofluidic technology through the fusion of microfluidics and optics, Nature 442 (7101) (2006) 381–386.

[58] A. Terray, J. Oakey, D. W. Marr, Microfluidic control using colloidal devices, Science 296 (5574) (2002) 1841–1844.

[59] E. Kjeang, A. G. Brolo, D. A. Harrington, N. Djilali, D. Sinton, Hydrogen peroxide as an oxidant for microfluidic fuel cells, Journal of the Electrochemical Society 154 (12) (2007) B1220–B1226.

[60] M. Sun, G. Velve Casquillas, S. Guo, J. Shi, H. Ji, Q. Ouyang, Y. Chen, Characterization of microfluidic fuel cell based on multiple laminar flow, Microelectronic Engineering 84 (5) (2007) 1182–1185.

[61] S. Takayama, J. C. McDonald, E. Ostuni, M. N. Liang, P. J. Kenis, R. F. Ismagilov, G. M. Whitesides, Patterning cells and their environments using multiple laminar fluid flows in capillary networks, Proceedings of the National Academy of Sciences 96 (10) (1999) 5545–5548.

[62] A. E. Kamholz, P. Yager, Theoretical analysis of molecular diffusion in pressure-driven laminar flow in microfluidic channels, Biophysical Journal 80 (1) (2001) 155–160.

[63] I. K. Glasgow, H. C. Zeringue, D. J. Beebe, S.-J. Choi, J. T. Lyman, N. G. Chan, M. B. Wheeler, Handling individual mammalian embryos using microfluidics, Biomedical Engineering, IEEE Transactions on 48 (5) (2001) 570–578.

[64] S. K. Dertinger, D. T. Chiu, N. L. Jeon, G. M. Whitesides, Generation of gradients having complex shapes using microfluidic networks, Analytical Chemistry 73 (6) (2001) 1240–1246.

[65] E. M. Lucchetta, M. S. Munson, R. F. Ismagilov, Characterization of the local temperature in space and time around a developing drosophila embryo in a microfluidic device, Lab on a Chip 6 (2) (2006) 185–190.

[66] G. M. Whitesides, The origins and the future of microfluidics, Nature 442 (7101) (2006) 368–373.

[67] G. Velve-Casquillas, M. Le Berre, M. Piel, P. T. Tran, Microfluidic tools for cell biological research, Nano Today 5 (1) (2010) 28–47.

[68] S. Takayama, E. Ostuni, P. LeDuc, K. Naruse, D. E. Ingber, G. M. Whitesides, et al., Subcellular positioning of small molecules, Nature 411 (6841) (2001) 1016.

[69] A. Sawano, S. Takayama, M. Matsuda, A. Miyawaki, Lateral propagation of egf signaling after local stimulation is dependent on receptor density, Developmental cell 3 (2) (2002) 245–257.

[70] E. M. Lucchetta, J. H. Lee, L. A. Fu, N. H. Patel, R. F. Ismagilov, Dynamics of drosophila embryonic patterning network perturbed in space and time using microfluidics, Nature 434 (7037) (2005) 1134–1138.

[71] D. Navajas, Probing mechanical properties of living cells with afm.

[72] L. G. Griffith, M. A. Swartz, Capturing complex 3d tissue physiology in vitro, Nature Reviews Molecular Cell Biology 7 (3) (2006) 211–224.

[73] Y. Kim, M. Hazar, D. S. Vijayraghavan, J. Song, T. R. Jackson, S. D. Joshi, W. C. Messner, L. A. Davidson, P. R. LeDuc, Mechanochemical actuators of embryonic epithelial contractility, Proceedings of the National Academy of Sciences 111 (40) (2014) 14366–14371.

[74] O. BurakáOzdoganlar, et al., Fabrication of circular microfluidic channels by combining mechanical micromilling and soft lithography, Lab on a Chip 11 (8) (2011) 1550–1555.

[75] Y. Kim, B. Kuczenski, P. R. LeDuc, W. C. Messner, Modulation of fluidic resistance and capacitance for long-term, high-speed feedback control of a microfluidic interface, Lab on a Chip 9 (17) (2009) 2603–2609.

[76] E. Berthier, D. J. Beebe, Flow rate analysis of a surface tension driven passive micropump, Lab on a Chip 7 (11) (2007) 1475–1478.

[77] Z. Guttenberg, A. Rathgeber, S. Keller, J. Rädler, A. Wixforth, M. Kostur, M. Schindler, P. Talkner, Flow profiling of a surface-acoustic-wave nanopump, Physical Review E 70 (5) (2004) 056311.

[78] K. Horiuchi, P. Dutta, Electrokinetic flow control in microfluidic chips using a field-effect transistor, Lab on a Chip 6 (6) (2006) 714–723.

[79] J. P. Brody, P. Yager, R. E. Goldstein, R. H. Austin, Biotechnology at low reynolds numbers, Biophysical journal 71 (6) (1996) 3430–3441.

[80] T. M. Squires, S. R. Quake, Microfluidics: Fluid physics at the nanoliter scale, Reviews of modern physics 77 (3) (2005) 977.

[81] K. V. Sharp, R. J. Adrian, Transition from laminar to turbulent flow in liquid filled microtubes, Experiments in fluids 36 (5) (2004) 741–747.

[82] Y. Kim, Closed-loop microfluidic control for probing multicellular dynamics, Ph.D. thesis, CARNEGIE MELLON UNIVERSITY (2011).

[83] H. Qiu, X. Wang, F. Hong, Measurements of interfacial film thickness for immiscible liquid–liquid slug/droplet flows, Measurement Science and Technology 16 (6) (2005) 1374.

[84] S. T. Chang, O. D. Velev, Evaporation-induced particle microseparations inside droplets floating on a chip, Langmuir 22 (4) (2006) 1459–1468.

[85] M. Srisa-Art, J. B. Edel, et al., Fluorescence lifetime imaging of mixing dynamics in continuous-flow microdroplet reactors, Physical review letters 101 (1) (2008) 014502.

[86] B. J. Kirby, Micro-and nanoscale fluid mechanics: transport in microfluidic devices, Cambridge University Press, 2010.

[87] A. E. Kamholz, P. Yager, Theoretical analysis of molecular diffusion in pressure-driven laminar flow in microfluidic channels, Biophysical Journal 80 (1) (2001) 155–160.

[88] Z. Wu, N.-T. Nguyen, Hydrodynamic focusing in microchannels under consideration of diffusive dispersion: theories and experiments, Sensors and Actuators B: Chemical 107 (2) (2005) 965–974.

[89] Y. Kim, S. D. Joshi, W. C. Messner, P. R. LeDuc, L. A. Davidson, Detection of dynamic spatiotemporal response to periodic chemical stimulation in a xenopus embryonic tissue, PloS one 6 (1) (2011) e14624.

[90] B. Kuczenski, W. C. Ruder, W. C. Messner, P. R. LeDuc, Probing cellular dynamics with a chemical signal generator, PLoS One 4 (3) (2009) e4847.

[91] T. Vestad, D. W. Marr, T. Munakata, Flow resistance for microfluidic logic operations, Applied Physics Letters 84 (25) (2004) 5074–5075.

[92] D. Kim, N. C. Chesler, D. J. Beebe, A method for dynamic system characterization using hydraulic series resistance, Lab on a Chip 6 (5) (2006) 639–644.

[93] S.-J. Kim, Y. T. Lim, H. Yang, Y. B. Shin, K. Kim, D.-S. Lee, S. H. Park, Y. T. Kim, Passive microfluidic control of two merging streams by capillarity and relative flow resistance, Analytical chemistry 77 (19) (2005) 6494–6499.

[94] Y. Kim, K. Pekkan, W. C. Messner, P. R. LeDuc, Three-dimensional chemical profile manipulation using two-dimensional autonomous microfluidic control, Journal of the American Chemical Society 132 (4) (2010) 1339–1347.

[95] B. K. Kay, H. B. Peng, Xenopus laevis: practical uses in cell and molecular biology, Vol. 36, Academic press, 1992.

[96] H. L. Sive, R. M. Grainger, R. M. Harland, Dejellying xenopus laevis embryos., CSH protocols 2007 (2006) pdb–prot4731.

[97] P. Nieuwkoop, The ?organization centre?, Acta biotheoretica 17 (4) (1967) 178–194.

[98] D. E. INGBER, G. M. Wrm, P. EsrDEs, Soft lithography and microfluidics.

[99] G. M. Whitesides, E. Ostuni, S. Takayama, X. Jiang, D. E. Ingber, Soft lithography in biology and biochemistry, Annual review of biomedical engineering 3 (1) (2001) 335–373.

[100] S. Takayama, E. Ostuni, P. LeDuc, K. Naruse, D. E. Ingber, G. M. Whitesides, Selective chemical treatment of cellular microdomains using multiple laminar streams, Chemistry & biology 10 (2) (2003) 123–130.

[101] S. Takayama, E. Ostuni, P. LeDuc, K. Naruse, D. E. Ingber, G. M. Whitesides, Selective chemical treatment of cellular microdomains using multiple laminar streams, Chemistry & biology 10 (2) (2003) 123–130.

[102] M. Freeman, Feedback control of intercellular signalling in development, Nature 408 (6810) (2000) 313–319.

[103] H. C. Ott, T. S. Matthiesen, S.-K. Goh, L. D. Black, S. M. Kren, T. I. Netoff, D. A. Taylor, Perfusion-decellularized matrix: using nature's platform to engineer a bioartificial heart, Nature medicine 14 (2) (2008) 213–221.

[104] T. W. Gilbert, T. L. Sellaro, S. F. Badylak, Decellularization of tissues and organs, Biomaterials 27 (19) (2006) 3675–3683.

[105] P. J. Schaner, N. D. Martin, T. N. Tulenko, I. M. Shapiro, N. A. Tarola, R. F. Leichter, R. A. Carabasi, P. J. DiMuzio, Decellularized vein as a potential scaffold for vascular tissue engineering, Journal of vascular surgery 40 (1) (2004) 146–153.

[106] Y. Kim, M. Hazar, D. S. Vijayraghavan, J. Song, T. R. Jackson, S. D. Joshi, W. C. Messner, L. A. Davidson, P. R. LeDuc, Mechanochemical actuators of embryonic epithelial contractility, Proceedings of the National Academy of Sciences 111 (40) (2014) 14366–14371.

[107] J. Hancock, Cell signalling, Oxford University Press, 2010.

[108] F. Marks, U. Klingmüller, K. Müller-Decker, Cellular signal processing: an introduction to the molecular mechanisms of signal transduction, Garland Science New York, NY, USA, 2009.

[109] P. J. Sammak, L. E. Hinman, P. Tran, M. D. Sjaastad, T. E. Machen, How do injured cells communicate with the surviving cell monolayer?, Journal of cell science 110 (4) (1997) 465–475.

[110] K. I. Hulkower, R. L. Herber, Cell migration and invasion assays as tools for drug discovery, Pharmaceutics 3 (1) (2011) 107–124.

[111] P. Friedl, D. Gilmour, Collective cell migration in morphogenesis, regeneration and cancer, Nature reviews Molecular cell biology 10 (7) (2009) 445–457.

[112] G. Fenteany, P. A. Janmey, T. P. Stossel, Signaling pathways and cell mechanics involved in wound closure by epithelial cell sheets, Current biology 10 (14) (2000) 831–838.

[113] C.-C. Liang, A. Y. Park, J.-L. Guan, In vitro scratch assay: a convenient and inexpensive method for analysis of cell migration in vitro, Nature protocols 2 (2) (2007) 329–333.

[114] M. Poujade, E. Grasland-Mongrain, A. Hertzog, J. Jouanneau, P. Chavrier, B. Ladoux, A. Buguin, P. Silberzan, Collective migration of an epithelial monolayer in response to a model wound, Proceedings of the National Academy of Sciences 104 (41) (2007) 15988–15993.

[115] K. M. Yamada, E. Cukierman, Modeling tissue morphogenesis and cancer in 3d, Cell 130 (4) (2007) 601–610.

[116] A. Birgersdotter, R. Sandberg, I. Ernberg, Gene expression perturbation in vitro?a growing case for three-dimensional (3d) culture systems, in: Seminars in cancer biology, Vol. 15, Elsevier, 2005, pp. 405–412.

[117] E. Cukierman, R. Pankov, K. M. Yamada, Cell interactions with three-dimensional matrices, Current opinion in cell biology 14 (5) (2002) 633–640.

[118] C. M. Nelson, M. J. Bissell, Of extracellular matrix, scaffolds, and signaling: tissue architecture regulates development, homeostasis, and cancer, Annual review of cell and developmental biology 22 (2006) 287.

[119] P. M. Crapo, T. W. Gilbert, S. F. Badylak, An overview of tissue and whole organ decellularization processes, Biomaterials 32 (12) (2011) 3233–3243.

[120] J. Arenas-Herrera, I. Ko, A. Atala, J. Yoo, Decellularization for whole organ bioengineering, Biomedical Materials 8 (1) (2013) 014106.

[121] P. Friedl, D. Gilmour, Collective cell migration in morphogenesis, regeneration and cancer, Nature reviews Molecular cell biology 10 (7) (2009) 445–457.

[122]

[123] R. Vaughan, J. Trinkaus, Movements of epithelial cell sheets in vitro, Journal of cell science 1 (4) (1966) 407–413.

[124] P. Friedl, Prespecification and plasticity: shifting mechanisms of cell migration, Current opinion in cell biology 16 (1) (2004) 14–23.

[125] D. J. Montell, Morphogenetic cell movements: diversity from modular mechanical properties, Science 322 (5907) (2008) 1502–1505.

[126] C. M. Jones, J. C. Smith, An overview of xenopus development, in: Molecular Embryology, Springer, 1999, pp. 331–340.

[127] R. Keller, The cellular basis of epiboly: an sem study of deep-cell rearrangement during gastrulation in xenopus laevis, Journal of embryology and experimental morphology 60 (1) (1980) 201–234.

[128] R. Keller, Time-lapse cinemicrographic analysis of superficial cell behavior during and prior to gastrulation in xenopus laevis, Journal of morphology 157 (2) (1978) 223–247.

[129] K. E. Degen, R. G. Gourdie, Embryonic wound healing: A primer for engineering novel therapies for tissue repair, Birth Defects Research Part C: Embryo Today: Reviews 96 (3) (2012) 258–270.

[130] M. A. Wyczalkowski, V. D. Varner, L. A. Taber, Computational and experimental study of the mechanics of embryonic wound healing, Journal of the mechanical behavior of biomedical materials 28 (2013) 125–146.

[131] D. A. Quint, Morphology and mechanics of the actin cytoskeleton.

[132] N. Gov, Cell mechanics: Moving under peer pressure, Nature materials 10 (6) (2011) 412–414.

[133] X. Trepat, J. J. Fredberg, Plithotaxis and emergent dynamics in collective cellular migration, Trends in cell biology 21 (11) (2011) 638–646.

[134] P. Rojas-Ríos, I. Guerrero, A. González-Reyes, Cytoneme-mediated delivery of hedgehog regulates the expression of bone morphogenetic proteins to maintain germline stem cells in drosophila, PLoS biology 10 (4) (2012) e1001298.

[135] N. M. Sherer, W. Mothes, Cytonemes and tunneling nanotubules in cell–cell communication and viral pathogenesis, Trends in cell biology 18 (9) (2008) 414–420.

[136] R. M. van Dam, Solvent-resistant elastomeric microfluidic devices and applications, Ph.D. thesis, California Institute of Technology (2006).

[137] B.-H. Jo, L. M. Van Lerberghe, K. M. Motsegood, D. J. Beebe, Three-dimensional micro-channel fabrication in polydimethylsiloxane (pdms) elastomer, Microelectromechanical Systems, Journal of 9 (1) (2000) 76–81.